INSTITUTE

FOR

AEROSPACE STUDIES

UNIVERSITY OF TORONTO

EXPLOSIVE-DRIVEN HEMISPHERICAL IMPLOSIONS FOR GENERATING FUSION PLASMAS

by

B. [illegible] and I. I. Glass

UNCLASSIFIED

SECURITY CLASSIFICATION OF THIS PAGE (When Data Entered)

REPORT DOCUMENTATION PAGE

READ INSTRUCTIONS BEFORE COMPLETING FORM

1. REPORT NUMBER: AFOSR-TR- 82-1014

2. GOVT ACCESSION NO.: [redacted]

3. RECIPIENT'S CATALOG NUMBER:

4. TITLE (and Subtitle): EXPLOSIVE-DRIVEN HEMISPHERICAL IMPLOSIONS FOR GENERATING FUSION PLASMAS

5. TYPE OF REPORT & PERIOD COVERED: Interim

6. PERFORMING ORG. REPORT NUMBER: UTIAS Tech. Note No. 233

7. AUTHOR(s): D. Sagie, I. I. Glass

8. CONTRACT OR GRANT NUMBER(s): AFOSR-82-0096

9. PERFORMING ORGANIZATION NAME AND ADDRESS: University of Toronto, Institute for Aerospace Studies, 4925 Dufferin Street, Downsview, Ontario, Canada, M3H 5T6

10. PROGRAM ELEMENT, PROJECT, TASK AREA & WORK UNIT NUMBERS: 61102F; 2307/A1

11. CONTROLLING OFFICE NAME AND ADDRESS: Air Force Office of Scientific Research/NA Bldg. 410, Bolling Air Force Base, DC 20332, U.S.A.

12. REPORT DATE: March, 1982

13. NUMBER OF PAGES: 60

14. MONITORING AGENCY NAME & ADDRESS (if different from Controlling Office):

15. SECURITY CLASS. (of this report): Unclassified

15a. DECLASSIFICATION DOWNGRADING SCHEDULE:

16. DISTRIBUTION STATEMENT (of this Report)

Approved for public release; distribution unlimited.

17. DISTRIBUTION STATEMENT (of the abstract entered in Block 20, if different from Report)

18. SUPPLEMENTARY NOTES

19. KEY WORDS (Continue on reverse side if necessary and identify by block number)

1. D-D fusion, 2. Implosion dynamics, 3. Explosion dynamics, 4. Neutrons and γ-rays.

20. ABSTRACT (Continue on reverse side if necessary and identify by block number)

The UTIAS explosive-driven-implosion facility was used to produce stable, centered and focussed hemispherical implosions to generate neutrons from D-D reactions. A high resolution scintillator-detection system measured the neutrons and γ-rays resulting from the fusion of deuterium. Several approaches were used to initiate fusion in deuterium. The simplest and most direct proved to be in a predetonated stoichiometric mixture of deuterium-oxygen.

Continued...

DD FORM 1 JAN 73 1473 EDITION OF 1 NOV 65 IS OBSOLETE

UNCLASSIFIED

SECURITY CLASSIFICATION OF THIS PAGE (When Data Entered)

The other successful method was a miniature Voitenko-type compressor where a plane diaphragm was driven by the implosion wave into a secondary small spherical cavity that contained pure deuterium gas at one atmosphere. A great deal of work still remains in order to measure accurately the neutron flux and its velocity distribution as well as the precise interactions of the neutrons with the steel chamber which produced the γ-rays. Nevertheless, this is the only known work where fusion neutrons were produced by chemical energy only in a direct and indirect manner.

Qualified requestors may obtain additional copies from the Defense Documentation Center, all others should apply to the National Technical Information Service.

Conditions of Reproduction:

Reproduction, translation, publication, use and disposal in whole or in part by or for the United States Government is permitted.

Approved for public release; distribution unlimited.

AIR FORCE OFFICE OF SCIENTIFIC RESEARCH (AFSC)
NOTICE OF [illegible] TO DTIC
This tech[illegible] and is
approved [illegible]-12.
Distribution [illegible].
MATTHEW J. [illegible]
Chief, Technical Information Division

EXPLOSIVE-DRIVEN HEMISPHERICAL IMPLOSIONS FOR GENERATING FUSION PLASMAS

by

D. Sagie and I. I. Glass

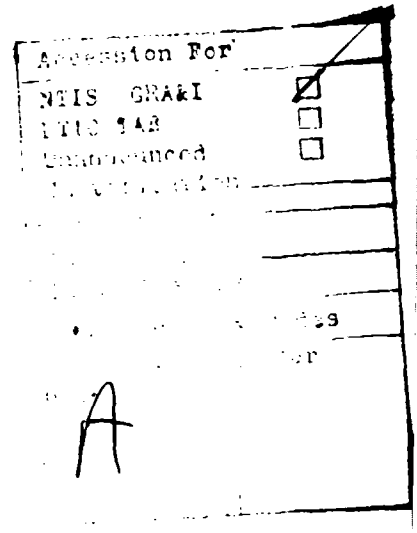

March, 1982

UTIAS Technical Note No. 233
CN ISSN 0082-5263

Acknowledgement

We wish to thank Dr. A. K. Kudian for his assistance in designing the detection and the deuterium capsule filling systems; Dr. Alan Entenberg of the Laboratory for Laser Energetics, University of Rochester, for calibrating the scintillator system; Prof. R. E. Jervis for a useful discussion; T. Saito for his assistance with some numerical calculations; and Laura Quintero and Ida Krauz for their help with the plates and figures.

The financial assistance received from the Natural Sciences and Engineering Research Council of Canada, the U.S. Air Force under Grant AFOSR-77-3303, and AFOSR-82-0096 the U.S. Army Research Office and the University of Toronto Connaught Fund is acknowledged with thanks.

Summary

The UTIAS explosive-driven-implosion facility was used to produce stable, centered and focussed hemispherical implosions to generate neutrons from D-D reactions. A high resolution scintillator-detection system measured the neutrons and γ-rays resulting from the fusion of deuterium. Several approaches were used to initiate fusion in deuterium. The simplest and most direct proved to be in a predetonated stoichiometric mixture of deuterium-oxygen. The other successful method was a miniature Voitenko-type compressor where a plane diaphragm was driven by the implosion wave into a secondary small spherical cavity that contained pure deuterium gas at one atmosphere. A great deal of work still remains in order to measure accurately the neutron flux and its velocity distribution as well as the precise interactions of the neutrons with the steel chamber which produced the γ-rays. Nevertheless, this is the only known work where fusion neutrons were produced by chemical energy only in a direct and indirect manner.

Contents

1. INTRODUCTION

The physics of thermonuclear reactions was studied intensively during and after World War II. During the last 40 years numerous papers were published giving the main parameters of several known thermonuclear reactions. Glasstone & Lovberg (1) gave a review of known results, which includes the collision cross-section of the fuel, by assuming a particle Maxwellian-energy distribution as a function of its temperature in a thermonuclear reaction. Collision cross-sections for D-D, D-T and D-He^3 are shown in Fig. 1.1. It is clear that up to a temperature of a few keV the reaction intensity would be a very strong function of temperature. Therefore, the first goal of the explosive-driven implosion project was to reach this range of temperatures, rather than any other thermodynamic parameter. Since the nuclear fuel cannot be confined for an unlimited time, the actual period of confinement has a great influence on the efficiency of fuel burn up. Two main approaches to fusion are under intensive study in the scientific community. In "magnetic confinement" (2) the plasma is held by magnetic fields in the desired configuration for reaction times large (up to 1 s) compared to its disassembly time at the speed of sound, or the particle thermal speed. In "inertial fusion" (3) the reaction confinement is essentially at the sound speed or thermal disassembly time (3×10^{-11} sec at T = 1keV for $p_1 = 10\mu$). The numerical expression of the confinement term is given by the "Lawson criterion" (4), which is the product of the particle density and confinement time required to achieve an energy balance at a specific temperature. For example $n_D\tau > 10^{15}$ sec/cm^{-3} at 100 keV (10^9K) for a D-D reaction.

The present report deals with an investigation of the application of explosive-driven implosions to produce thermonuclear reactions. This approach basically belongs to the inertial-confinement family. Most of the current scientific activity in this area is dedicated to laser fusion. Fortunately, this work also consists of spherical implosions, so that the principles of this method and explosive-driven implosions are quite similar. Important research on laser fusion is being conducted at the University of California, Lawrence Livermore Laboratory (5), the University of Rochester, Lasers Energetics Laboratory (6), and K.M.S. Fusion, Ann Arbor (7). Their reports were of great interest and assistance during the present study.

Spherical sectors rather than full spheres were frequently used by Russian researchers to produce fusion reactions. Bogolyubskii et al (8) accelerated a polyethylene diaphragm (10μ thick) up to 60 km/s by using a relativistic electron beam. They produced 3×10^6 neutrons with D_2 fuel contained in a conical lead capsule. Ziolkowski et al (9) used a solid explosive to implode a conical liner onto the surface of a copper cone. The generated shock wave was strong enough to accelerate a polyethylene layer up to a velocity of 50 km/s. The collapse of this layer in a gold cone filled with deuterium generated up to 3×10^7 neutrons. Recently, Anisomov et al. (10) reported that temperatures of 0.3 - 0.5 keV and a yield of 10^6 neutrons had been achieved by using an explosively accelerated metal liner (up to 5.4 km/s) striking deuterium fuel contained in a conical lead capsule. For the present work the UTIAS hemispherical implosion chamber (11 - 17) was used in several modes to produce implosions appropriate for fusion.

The spherical implosion chamber was conceived by Glass (12) in the 1950's. Since then it has proved to be a unique facility to generate stable implosions in a safe and reusable facility in order to provide a small region of extremely high pressures and temperatures (13-25). The implosion chamber had originally been used as a driver for a projectile launcher (15), for generating strong shock waves in a constant area shock tube (16), and for the production of diamonds from graphite (17). Recently it was applied to producing fusion reactions in deuterium, as reported herein.

The principle of operation of the UTIAS implosion chamber is described in detail in the above-mentioned reports. In brief, PETN solid explosive is used to form a hemispherical shell (3 mm to 6 mm thick) in a 20-cm diameter hemispherical cavity milled in a massive steel chamber (Fig. 1.2). The remaining volume is filled with a stoichiometric mixture of H_2 or D_2 and O_2. This mixture is detonated by a very short thin exploding wire located at the geometric centre (Fig. 1.3). The arrival of the detonation wave at the spherical surface instantly and simultaneously fires the explosive liner. The detonation wave in the explosive liner hits the metal cavity, reflects, and implodes on the preheated burnt gases, focusses at the centre of the hemisphere ($\sim$ 50 μsec after initiation of the exploding wire) and reflects, leaving behind a very small pocket (1 mm^3) of extremely high-temperature, high-pressure and high-density plasma. In the present study H_2 is replaced by D_2. For some other fusion experiments this focus takes place on top of a base of a small capsule containing D_2 at $\sim$ 1 atm (Fig. 1.4). The cavity in the capsule serves to produce a second compression and heating stage in order to produce extremely high temperatures, pressures and densities in the deuterium plasma.

In the second section the experimental set-up is explained. Special consideration is given to the neutron-detection system. The third section describes the experiments that were conducted and their results. The fourth section discusses the results and lists the main conclusions. In Appendix A1 consideration is given to several approaches for the application of explosive-driven implosions to fusion with advantages and disadvantages of each approach. In Appendix A2 a review is given of the neutron detection system. In Appendix A3 some consideration is given to the possibilities of scaling for better performance and neutron yield.

2. EXPERIMENTAL EQUIPMENT AND INSTRUMENTATION

2.1 Driver Description

Basically, the experimental facility consists of the UTIAS implosion chamber (Fig. 1.2). The principle of operation of the implosion chamber is as follows. The explosive material forms a hemispherical shell (3-6 mm thick) in the 20-cm diameter hemispherical cavity milled in a massive steel back plate. The explosive shell of PETN weighs up to 200g and has a total energy of up to 1.2 megajoules. The remaining volume is filled with a

stoichiometric mixture of H_2 and O_2 with a pressure of up to 70 atm and an energy of up to 1 megajoule. This mixture is detonated by a very short ($\sim$ 1 mm), thin (0.127 mm dia) exploding nickel wire located at the geometric centre. The arrival of the detonation wave at the spherical surface instantly and simultaneously fires the explosive liner. It reflects as an implosion wave. The detonation wave in the explosive liner hits the metal cavity, reflects, overtakes the first implosion wave and combines to form a final imploding shock wave in the preheated gases. It then focusses at the centre of the hemisphere. When the implosion reflects at the centre it leaves behind a zone of extremely high pressure and temperature. If the H_2 is replaced by D_2 then the stage is set for D-D fusion at this focus. Alternatively, a small hemispherical capsule containing D_2 at a few atm can be placed at the centre, with its base closed by a diaphragm and facing the focus (Fig. 1.4). This is a miniature Voitenko-type (36) compressor which brings the deuterium to extremely high pressures, temperatures and densities required to initiate a fusion reaction. Other set-ups using a small conical capsule or in combination with projectile compression have also been used but without successful results so far.

2.1.1 Implosion Chamber

The UTIAS implosion chamber was conceived by Glass (12) and has been used frequently for several applications in the last few years. It was used to drive projectiles to hypervelocities (15), to produce very strong shocks (16) and to convert graphite to diamond (17). The chamber itself was essentially the same for all these applications. The main modifications relate to a particular experiment. Briefly, the implosion driver consists of two halves, a rear plate and a front plate (Figs. 2.1 and 2.2). A 20-cm diameter, hemispherical cavity is machined in the rear plate and contains the explosive-liner package. The front plate consists of a cone which supports the barrel-capsule assembly and the liner plate. A 20-degree conical liner plate is placed on the top of the liner plate to give extra protection for the front plate section against any possible damage from an off-centred implosion (20). In the front plate, O-ring grooves are machined for pressure and vacuum sealing. Connections for the barrel, high-voltage feed-throughs for bringing in the ignition wires, and a pressure tube for venting and filling the chamber are installed in the front plate as well. The previous design was slightly modified to reduce possible damage during a run, and to ease disassembly afterwards.

2.1.2 Explosive Package

The explosive package that was used for the present experiments is described in detail by Saito (21). The preparation procedure is the final result of successive developments of the explosive-packaging technique which was studied by several researchers (15, 20, 22). Uniformity in thickness and especially in density is of prime importance to achieve centred, symmetrical implosions. The present scheme of initiating the explosive (superfine PETN) by a gaseous detonation wave in stoichiometric mixtures of hydrogen-oxygen or deuterium-oxygen at initial pressure of 1· to 70 atm, proved to be the most useful and was employed in all the runs in the present study. It was possible to

obtain nearly perfectly centred implosions from the reflected detonation of the gas mixture alone. This indicates that the original detonation wave was stable, symmetric, and well focussed with respect to the origin and therefore could provide a symmetric source for initiating the explosive liner.

To provide sufficient mechanical binding strength for the explosive to be self-sustained, the superfine PETN powder was mixed with 1.5% by weight of cotton fibers (linters) and water to form a slurry. A plastic honeycomb was glued to the accurately machined hemispherical copper liner (Fig. 2.3). Then the slurry was worked and pushed into the honeycomb to fill all air pockets. The cotton fibers serve as a binder providing the powdery PETN with very positive support, while the plastic honeycomb provides the support that allows the wet PETN slurry to dry while retaining the proper geometry. In this manner, the explosive package had sufficient strength to withstand handling and was also sufficiently homogeneous to ensure a stable, focussed implosion. The 20-cm diameter copper liner, with a 20-degree conical liner, and a 6-mm thick honeycomb, contained about 200g of explosive. The use of additional explosive was not advisable owing to possible chamber damage.

2.1.3 Ignition System

In order to induce a spherical detonation wave in a combustible mixture, sufficiently large amounts of energy must be released at a very high rate. The initiation point must be located exactly at the origin of the hemispherical explosive package to produce a symmetric implosion. For a given amount of stored energy of the ignition capacitors, this criterion could be satisfied by keeping the resistance of the exploding wire as high as possible, and the impedance of the rest of the ignition system as low as possible. The system as used by Roig (24) and Vasudevan (25) was adopted with minor modifications. A 0.127-mm (5-mil) diameter, 1-mm long nickel wire was used to ignite the explosive-gas mixture. The transmission line of the high-voltage circuit was a low inductance (16Ω) impedance) cable. The discharge system consisted of a spark gap and a 1.0 μfd, 30 kV capacitor, as shown in Fig. 2.4. The spark gap essentially consists of two brass electrodes, a Plexiglas tube and an automobile spark plug. The operating cycle of the system included dehumidifying the spark gap with compressed nitrogen and then charging the capacitor to 22 kV. A 5 kV trigger pulse to the spark plug was used to initiate the discharge.

While the exploding wire should be placed exactly at the focus, its own physical dimensions, with the terminals and insulation, practically eliminated that ideal position. Two designs were used as shown in Fig. 2.5. The exploding wire was located about 1 mm and 0.2 mm above the origin for the first and second design, respectively. Some other deviations from symmetry were introduced by the terminals and insulation but these undesired materials are all evaporated before the implosion arrival, causing some impurities to exist near the focus. A photograph showing the assembly over a deuterium capsule appears in Fig. 2.6.

2.1.4 Vacuum and Gas-Mixture-Inlet Systems

A schematic diagram of the pressure and vacuum manifolds to

the implosion chamber is given in Fig. 2.7, and the control panel is shown in Fig. 2.8. The control room has 12-inch concrete block walls, sand-filled and reinforced with steel rods. After assembly of the implosion chamber, the operation of the entire system, including the monitoring of pressures, vacuum pumps and the gas filling can be remotely controlled at the control panel in the control room. The control panel is designed for ease of operation and to eliminate accidents or damage to the instruments caused by following a wrong sequence of operation. The gases used were commercial bottles of compressed gas. They are shielded by heavy metal from direct damage through a failure of any connections. The H_2, O_2 or D_2 inlet is easily controlled by the operator who has just to open the appropriate valve.

2.2 Deuterium Capsule

As mentioned above some indirect approaches were tested as well. For those experiments pure deuterium was used, contained in a small capsule at the driver focus.

The main characteristics of the capsule were as follows: to contain the deuterium at the desired pressure, to maintain a good seal without a gas leak, to prevent impurities during assembly or the filling process, and to have the compression surface of the diaphragm located initially at the implosion focus. It must also provide a convenient way of filling the deuterium, maintain the desired geometry as long as possible during the gas-compression process, and reflect the "escaping" radiation back into the target. The design of the capsule was made in accordance with these requirements.

2.2.1 Capsule Design

A typical capsule design is shown in Fig. 2.9. Generally, the capsule was made of 440c stainless steel hardened up to 48R. For the design of a cone it was premachined with an apex radius of about 50 μm, and the diaphragm was of 0.005" cold-rolled stainless-steel sheet, plastically formed to get the spherical cap at its centre. The diaphragm circumferential flat area was indium coated to provide a soft medium which served to seal the diaphragm against the main capsule body when firmly pressed with the fastening nut. A standard capsule having a hemispherical or cone basic diameter of 3.2 mm dia was capable of maintaining an interior gas pressure of 70 atm. The diaphragm was strong enough to withstand the $2H_2+O_2$ detonation pressure without damage, as shown by primary experiments (3.1.2). Several experiments (3.1.3) also showed that this design was capable of containing the deuterium for at least 24 hours without a detectable leak. The capsule described above is easily modified to check the dominant parameters noted previously.

2.2.2 Preparation and Filling Procedure

The filling system for the capsules was developed, built and tested by Dr. A. K. Kudian. The system (Figs. 2.10 and 2.11) consists of a small vacuum chamber in which the open capsule is located. The fastening nut with the diaphragm inside are located in front of the capsule, fixed by two pins to a rotating shaft, and can be threaded in externally through a seal assembly without breaking the vacuum in

the chamber. The chamber itself is metal sealed and can be heated up to 400°C for degassing of all gaseous impurities that have penetrated into the capsule material. The organic seal of the rotating shaft is protected by a water cooling system. The chamber is evacuated by a primary rotating pump (Duo-Seal, Ref. 26) and secondary 2" diffusion pump (SpeediVac, Ref. 27). Two liquid nitrogen cold traps, between the rotary and diffusion pumps and between the diffusion pump and the chamber, provide further evacuation to less than 1μ. A deuterium cylinder (Matheson, 28) with a maximum impurities level of 0.5% is connected to the system by high-vacuum standard copper tubing. With the capsule components all located inside, the chamber is pumped down to about 1μ, then it is heated up to 200°C and maintained at that temperature for a few hours. After cooling down, the chamber is flushed by deuterium at 1 atmosphere and after a second evacuation is filled finally to the required pressure. The capsule is then closed firmly, the chamber is vented and then the capsule is taken out ready for use. McLeod and Pirani gages were used for precise vacuum measurements while gages installed on the deuterium-cylinder regulator were used to fill to the required pressure.

2.3 Neutron-Detection System

Among the few approaches that are available to detect a thermonuclear reaction, the detection of neutrons seems to be the most convenient. The neutrons being uncharged particles are the only particles that can penetrate the heavy-walled chamber that is required to confine the explosion inside. Their detection provides a positive unquestionable proof of a fusion reaction. Two independent neutron-detection systems were designed to be used simultaneously. The first is a scintillator-counting technique which is very sensitive and reliable. It makes it possible to detect both neutron intensity and their time of flight which is an indication of the neutron energy. As a second independent measurement, an indium activation technique was chosen to confirm the intensity of the neutron flux.

2.3.1 Scintillator Detection System

This system should cope with the following main constraints:

1. Neutrons are to be detected in a single pulse with a duration in the range of 10 nsec. This imposes on the electric circuit problems of transmitting and recording with low distortion, as well as very high reliability.

2. In order to record a signal shape with the above duration range, the oscilloscope is limited to a total detection time of about 1 μsec.

3. All the events in the combustion process previous to the neutron generation are not precisely fixed in time to provide a signal in advance that can trigger the detection system. Therefore, the system must be self-triggered by the neutron pulse itself.

4. The scintillator and the photomultiplier (PMT) constantly emit signals into the system. The scintillator is activated by high-energy particles moving around in the atmosphere (especially mesons) with a typical energy of 140 Mev. (Some cosmic particles carry energies of more than 1000 Mev.) The noise has a statistical voltage and flux distribution. Recalling that the neutrons

generated by D-D fusion have an energy of 2.45 MeV, the energies of the cosmic particles are much higher and, on average, would correspond to about 50 neutrons activating the scintillator at once. Shielding against these particles would be very heavy and expensive and therefore it was not practical to construct. The particles intersect with the scintillator at a rate of about 1 per second. In addition, electrical noise is an integral part of the operation of a photomultiplier (Fig. 2.12). The high potential that is maintained between the photocathode and the first anode attracts the electrons which are always "escaping" from the photocathode material. (This material is chosen a priori to have very loose electron bonds.) These electrons initiate the PMT amplification chain and in this way send a statistically distributed signal into the recording system. These dark current signals become less frequent for higher voltage levels (Fig. 2.12c). For our specific model of PMT, they are almost stable at a frequency of about 80 Hz, and a voltage level which is equivalent to a photon energy of about 1 MeV interacting with the scintillator material. The frequency of this noise as a function of its voltage is given in Table 2.1.

5. The ignition system that initiated the detonation-implosion cycle, radiates very high intensity electromagnetic waves. False triggering of the system by this noise must be eliminated.

The system is schematically shown in Fig. 2.13, while pictures of the main components are shown in Figs. 2.14 and 2.15. Technical specifications of the components are represented in Appendix A2. Two scintillator-photomultiplier assemblies are located in front of the implosion chamber. The first one is 30 cm from the neutron source. It provides for a low-speed sweep and a means of triggering the system. The second assembly is 80 cm from the source right behind the first one. The implosion chamber provides 10 cm of steel protection around the implosion space and has a steel window 2.5-cm thick thereby making a reasonable path for the neutrons (see Fig. 2.13). Both detectors are located within the solid angle emerging from this window. The short distance of the scintillators from the chamber increases the detection sensitivity. However, the close proximitry may distort the signal This short distance makes it possible for scattered neutrons and neutron-activated products from the steel chamber to reach the detectors. If a large enough signal could be obtained the detectors could be shifted further away from the chamber.

The recording system is based on two Hewlett-Packard Model 1744A single beam storage scopes, with a maximum frequency of 100 MHz and a sweep rate up to 5 nsec/div. Due to a special feature in the scope, it displays the entire triggering pulse with a 50 nsec backview. With a nominal writing speed of 1800cm/μs, the oscilloscopes are capable of storing a 10nsec single-shot sine wave with an amplitude of eight major divisions (full scale). The concept of the circuit operation is illustrated in Fig. 2.13. The recording system is armed and then it is ready to record and store a single signal. The detector assemblies are in an operating state. The ignition pushbutton, boosted by an amplifier, triggers scope I, the adjustale delay unit, and the counter simultaneously with the ignition of the chamber detonating-imploding cycle. The sweep rate of scope I is 100 μsec for full scale, enough to cover the fusion event, which is expected at about 50 μsec. The adjustable delay unit opens the gate after 40 μsec and enables signals from detector I to trigger scope II, externally. (The signal passage is blocked by the gate up to this moment.) If a signal from detector I now shows up, it is recorded by scope I and also triggers scope II.

Scope II is connected to detector II and so displays signals from this detector during 500 nsec after it has been triggered (its total sweep time). If a sufficient flux of 2.45 MeV neutrons is generated, both detectors would be activated. The second detector would respond 15 nsec after the first one, owing to the longer distance from the neutron source. Another delay unit extends this time difference even farther, and together with the "back in time" view of the oscilloscope, we are able to see the output of detector II back to 85 nsec before the trigger signal. This is essential, as in this manner it is possible to display the complete signal and any X-rays if they exist. (The X-rays propagate at the speed of light and would arrive before the neutrons. However, the signal would be too small to trigger the system.) The second scope system is blocked by the gate from receiving any signal up to about 10μsec before the arrival of the expected neutron signal. However this is a drawback as several noise signals could trigger that system from this moment on. Therefore, the trigger level must be set high enough to reduce the chance of false triggering. For example, if we chose a point such that the noise frequency is about 100Hz, the probability of false triggering would be 1/1000. If the sensitivity were increased by lowering the trigger level, then the chance of false triggering would increase significantly; and vice versa, decreasing the sensitivity will reduce the probability of false triggering. Triggering by noise would eliminate some experimental data but it could not be mistaken for a neutron signal, since there is almost no chance for any two independent noise signals to stimulate both detectors simultaneously. Only neutrons with a short period and high flux could do that, and therefore the coincidence of the signals on both oscilloscopes is positive proof of a neutron flux. The counter starts to count with the ignition signal and stops with the triggering of the second scope, and strengthens the evidence of getting the signal at the right moment.

The scintillator-photomultiplier assemblies are identical in their mechanical design, but different in their internal electronic circuit (Appendix A2). The first detector serves both to trigger the system, and to record events through the whole process. Its signal is distributed into two main lines. Therefore, its circuit is built to provide a relatively high-voltage amplitude, but it is quickly saturated. The signal, being very nonlinear, can hardly provide an indication of the number of neutrons generated. The second detector has a more linear circuit. The signal is directly connected to the storage oscilloscope with no other components on the line, except the delay unit which is purely resistive and therefore transmits the high-frequency (100MHz) signal without any distortion. The area confined by this signal rather than its amplitude provides an accurate indication of the amount of energy transmitted to the scintillator, which in turn is proportional to the number of neutrons that passed through the scintillator material. However, for a low-neutron yield, while only a few neutrons intersect with the scintillators, both detectors provide a good estimate of the neutron yield (referring to the signal amplitude). If in future more neutrons can be generated in the chamber, the detectors circuit should be changed or preferably, the detectors can be moved away from the source. Then the scattering effect of neutrons and neutron products from the chamber hitting the detectors will be minimized, and the overlap of the two detectors will be eliminated.

In the present set-up the effective diameter of the first

generated by D-D fusion have an energy of 2.45 MeV, the energies of the cosmic particles are much higher and, on average, would correspond to about 50 neutrons activating the scintillator at once. Shielding against these particles would be very heavy and expensive and therefore it was not practical to construct. The particles intersect with the scintillator at a rate of about 1 per second. In addition, electrical noise is an integral part of the operation of a photomultiplier (Fig. 2.12). The high potential that is maintained between the photocathode and the first anode attracts the electrons which are always "escaping" from the photocathode material. (This material is chosen a priori to have very loose electron bonds.) These electrons initiate the PMT amplification chain and in this way send a statistically distributed signal into the recording system. These dark current signals become less frequent for higher voltage levels (Fig. 2.12c). For our specific model of PMT, they are almost stable at a frequency of about 80 Hz, and a voltage level which is equivalent to a photon energy of about 1 MeV interacting with the scintillator material. The frequency of this noise as a function of its voltage is given in Table 2.1.

5. The ignition system that initiated the detonation-implosion cycle, radiates very high intensity electromagnetic waves. False triggering of the system by this noise must be eliminated.

The system is schematically shown in Fig. 2.13, while pictures of the main components are shown in Figs. 2.14 and 2.15. Technical specifications of the components are represented in Appendix A2. Two scintillator-photomultiplier assemblies are located in front of the implosion chamber. The first one is 30 cm from the neutron source. It provides for a low-speed sweep and a means of triggering the system. The second assembly is 80 cm from the source right behind the first one. The implosion chamber provides 10 cm of steel protection around the implosion space and has a steel window 2.5-cm thick thereby making a reasonable path for the neutrons (see Fig. 2.13). Both detectors are located within the solid angle emerging from this window. The short distance of the scintillators from the chamber increases the detection sensitivity. However, the close proximitry may distort the signal This short distance makes it possible for scattered neutrons and neutron-activated products from the steel chamber to reach the detectors. If a large enough signal could be obtained the detectors could be shifted further away from the chamber.

The recording system is based on two Hewlett-Packard Model 1744A single beam storage scopes, with a maximum frequency of 100 MHz and a sweep rate up to 5 nsec/div. Due to a special feature in the scope, it displays the entire triggering pulse with a 50 nsec backview. With a nominal writing speed of 1800cm/μs, the oscilloscopes are capable of storing a 10nsec single-shot sine wave with an amplitude of eight major divisions (full scale). The concept of the circuit operation is illustrated in Fig. 2.13. The recording system is armed and then it is ready to record and store a single signal. The detector assemblies are in an operating state. The ignition pushbutton, boosted by an amplifier, triggers scope I, the adjustale delay unit, and the counter simultaneously with the ignition of the chamber detonating-imploding cycle. The sweep rate of scope I is 100 μsec for full scale, enough to cover the fusion event, which is expected at about 50 μsec. The adjustable delay unit opens the gate after 40 μsec and enables signals from detector I to trigger scope II, externally. (The signal passage is blocked by the gate up to this moment.) If a signal from detector I now shows up, it is recorded by scope I and also triggers scope II.

scintillator, taking only the solid angle emerging from the "window" into consideration, is 3cm, and the distance from the neutron source is 30 cm. For the second scintillator the effective diameter and distance are 7.5 cm and 80 cm, respectively. The scintillator material is 5cm thick and 10 cm in diameter, so that almost every intersecting neutron delivers some of its energy. A single neutron is equivalent to about 1650 neutron yield for the first detector and about 2960 neutron for the second one. However, even if a single neutron indicates that a fusion reaction has occurred, it cannot give a reasonable indication of the total yield, since the energy is delivered to the scintillator in a wide energy distribution. Considering 10 neutrons as the minimum-required flux for statistical estimation, then the minimum neutron yield that can be estimated is about 16,000 neutrons for the first detector and 30,000 for the second one. The lower limit of the system sensitivity is set by the electron-emission noise as was mentioned before since for too low a trigger level, this noise might trigger the system instead of the neutron signal. A very serious problem is presented by the giant electromagnetic noise generated by the discharge of the capacitor in order to explode the ignition wire. These electromagnetic waves propagate in the air and excite the detector to an amplitude which is equivalent to a few hundred neutrons intersecting the detector simultaneously. These electromagnetic waves oscillate and damp down (Fig. 2.16) and should diminish before the gate is open. Their damping rate is controlled by the ignition circuit conductors, and the oscillating period can be reduced to 35 μsec. Unfortunately, the ignition noise is so high that several gates were not able to block it from penetrating and triggering the system. The solution was found by introducing a discriminator unit, which has an output logic signal (constant voltage and shape), for every input signal in a wide range. Although the discriminator is not able to maintain the logic signal for the ignition noise, it reduces it significantly, enough to eliminate it from penetrating through the gate. At the same time low signals are transmitted with only small attenuation.

2.3.2 Neutron-Activation Technique

To get an independent indication of neutron production, and an estimation of the total number as well, a neutron activation technique is used simultaneously. Several approaches for our specific chamber set-up are shown in Fig. 2.17. They are all designed not to block the neutron path to the scintillator. The expected performance is listed in Table 2.2. Most of the suggested approaches are based on activation by the fast neutrons, while the activation cross-section for fast neutrons is considerably lower than that of thermal neutrons. We have found it more convenient and reliable to attenuate the fusion neutrons down to the thermal region and then to activate indium (Fig. 2.18). The attenuation is done by paraffin with a scattering cross-section of 45.3 barns per (CH_2) unit for fast neutrons (29). Through the 7cm path about 90% of the neutrons are attenuated, while the rest are attenuated by the paraffin at the back of the indium and are partially reflected back into the indium. The indium itself captures thermal neutrons by the reaction $In^{115}(n,\gamma)In^{116m}$ with a cross-section of 145 barns (30). For the thickness of 2mm, 65% of the crossing thermal neutrons are captured. Having an effective area ratio of 3×10^{-3} to the total space, 500 neutrons are required for every single reaction in the indium. The final detection sensitivity depends on the radioactive background in the laboratory. Assuming that a rate of 100 disintegration per hour is detectable, and for the activated In^{116m}

with a half-life of 54min, a minimum neutron yield of 10^5 can be detected. The activated indium can be drawn outside the chamber assembly within a minute, while the other approaches require an hour at least for the activated material to be taken out of the chamber, which makes materials with a half-life of minutes unreasonable to use. The indium is quickly cooled down and can be reused again for detection.

3. RESULTS AND DISCUSSIONS

3.1 Primary Functional Tests and Calibrations

3.1.1 Neutron Detection System Calibration

The neutron detection system was fully described in 2.3.1. The logics, main components and constraints were introduced. Here we will become familiar with the actual performance of the components and the integrated system. A typical signal of electron emission from the photomultiplier is shown in Fig. 3.1. A typical signal from a Co^{60} radioactive source which has γ-rays (photons) of 1.1 MeV is shown as well. The signals are similar and cannot be distinguished even by sophisticated electronic equipment. A Co^{60} radioactive source of 1μ Curie has been used to calibrate the detector. This source, when located at the front of the scintillator, stimulates it to about 10^4 signals per second. The display of the exposed detector on the storage screen shows the envelope of the whole spectrum, which corresponds to the photons that transmitted all their energy to the scintillator material (Fig. 3.1c). Hence the area surrounded by this envelope represents energy of 1.1 MeV, and is used as the basis to compare with the energy that any other process delivers to the scintillator material. For short duration signals (less than 20 nsec, like the inertial-confinement fusion), we refer to the amplitude, rather than the area under the curve. A Co^{60} photon, while completely delivering its energy of 1.1 MeV into the scintillator, produces a signal of amplitude A. A neutron of 2.45 MeV, when interacting with a scintillator made of "Pilot B" material (31) with diameter of 4" and thickness of 2", delivers on the average 0.295 MeV per interacting neutron, or 0.23 MeV per incident neutron (32). Hence $B = 0.23/1.1 \times A$ is the average amplitude for a single 2.45 MeV neutron and the total neutron yield is given by the ratio of the actual signal to B.

An estimate of the neutron yield as described above assumes a linear amplitude with energy delivered to the scintillator. This assumption might hold only for a low-neutron flux, while for a higher flux the PMT becomes saturated. Therefore, the detectors were calibrated directly with a neutron source (with assistance from the Laboratory for Laser Energetics, University of Rochester, N.Y.). Some calibration displays of detectors I and II are given in Figs. 3.2 and 3.3 respectively, and the amplitude as a function of distance is given in Table 3.1. The decay of the amplitude which is supposed to decrease like r^{-2} decreases actually like $r^{-0.2}$ for detector I and r^{-1} for detector II, owing to the high-saturation effect of the photomultiplier at that high level of radiation. The neutron source for the calibration (33) is a particle accelerator that accelerates deuterium ions into a static deuterium target. The total number of 5×10^5 neutrons are distributed in about 2μsec as shown in Fig. 3.4. (The total yield was measured by Dr. A. Entenberg using a silver activation technique.) For our specific PMT (RCA8575) we found the

largest electron-emission signals to be of about 80% of the Co^{60} highest signals. As to the signals from high-energy particles that are moving in the atmosphere (like a meson), they are displayed in Fig. 3.5 together with the electron emission and Co^{60} signals. The signals are distinguished by their energy. Typical frequencies are 100Hz for the electron emission in 10% of the upper-voltage range, 10^4Hz for the 1μ Curie Co^{60} source, and a few Hz for the atmospheric particles. As was mentioned before neither a commercial nor a laboratory-made gate was able to block the high-energy signal generated by the atmospheric particles and the ignition noise. The solution was found by introducing a discriminator unit which was supposed to produce a constant amplitude output signal for a wide range of input signals. The actual performance is shown in Fig. 3.6. While the discriminator does not succeed to keep high input voltages at the nominal output of 0.6v, it does cut it off considerably. The very rare input signal of 18v, which is the maximum expected from the detector, is transmitted as 1.6v and this is now low enough to be blocked by the closed gate. On the other hand, low-voltage signals are transmitted through the discriminator with low attenuation (0.8v input and 0.6v output) such that, when the gate is open, they can pass through and trigger the system.

The electron-emission frequency of the first detector becomes almost stable at a level of 80Hz, while the signal amplitude is about 1.2v (Table 2.1). After distribution and some decay this signal emerges from the discriminator at 0.5v. The 1.2v signal compared with the Co^{60} maximum signal of 1.5v corresponds to 1.2/1.5 x 1.1 MeV = 0.88 MeV of delivered energy. Since the 2.45 MeV neutrons deliver an average of 0.23 Mev per incident neutron (32), an output of 1.2v from the first detector is equivalent to 0.88/0.23 $\sim$ 4 neutrons. For the 80Hz frequency of electron emission and for an average gate opening period of 10μsec before the imploding wave collapses, the chance for a false triggering will be: $80sec^{-1} \times 10^{-5}sec = 1/1250$. Actually we chose to set up the level to trigger the second oscilloscope at 0.2v (0.5v at the first detector), which corresponds to 0.5/1.5 x 1.1 MeV = 0.367 MeV or 1.6 neutrons. In the present geometric set-up this is equivalent to a total yield of about 2560 neutrons. The electron emission for this level is 125Hz putting the chance of false triggering at 1:570. The frequency of the dark current is unstable and sometimes might be greater by a factor of up to three. Some effort was made to reduce the "noise-to-signal ratio". The P.M.T. was cooled down to -50^0 C but an improvement of about 30% was not enough to justify the inconvenience. A potentiometer was introduced to control the potential between the photocathode and the first anode (Fig. 2.16), and the noise-to-signal ratio was taken for several voltage difference in a wide range of total high-voltage inputs. An input voltage of 2000v was the optimum, and the first anode to photocathode potential made no significant effect on the noise-to-signal ratio. To summarize: the detection system was set up to trigger at a total yield of 2600 neutrons with a reliability of 99.8% for the electron-emission effect. As was mentioned before, a signal in that case will be definite proof of a fusion reaction, but for an accurate estimation of the neutron yield a statistical number of neutrons are required to intersect the detector. Ten neutrons at the first detector are equivalent to a total yield of 16,000 neutrons.

The neutron source of the Laboratory for Laser Energetics, mentioned above, was used to display the signals of single neutrons. Figure 3.7a shows the display of detector II when exposed to the neutron source at a distance of 30 ft. This same signal when taken at a faster sweep rate is shown in Fig. 3.7b. At this distance the number of neutrons is low enough that the contribution of single neutrons can be recognized. With careful adjustment, the tail of the last signal can be displayed (Fig. 3.7c). Here single neutron signals are clearly recognized. As for the higher flux of neutrons, the actual calibration with the neutron source (Fig. 3.3, 3.4 and Table 3.1) showed very quick deviation from linearity due to saturation. A testing of the components which compose the system showed that the "bottle neck" was in the PMT unit. To study the PMT range of linear operation in more detail, the scintillators were replaced by light-emitting diodes (LED) type MV2 of Litronix (34). The specifications of both the LED and the PMT are given in Appendix A2. The relevant character is that the LED emits a light with a wave-length of 572n meter at the peak (green light). At that wave-length the PMT relative response is 23%; or the photocathode emits 23% of the electrons which would be emitted for the same light intensity but at 380n meter, which is the PMT peak wave-length. The maximum emission of the scintillator is generated at a wave-length of 425n meter, where the PMT relative response is 94%. The chosen LED is the closest to the scintillator wave-length that is available, having $\eta = 0.244$ of the scintillator coupling efficiency to the PMT. Knowing the power output of the LED, the power-response character of the PMT can be derived experimentally. (Neutron-yield calibration would follow, since the energy delivered into the scintillator is known and the coupling to the PMT as well. However, for the duration of about 10 nsec expected in our case, this calibration cannot be carried out practically. The rise-times of the LED and its power source (pulse generator) are of 2 - 3 nsec duration each.)

Figure 3.8 shows typical PMT-outputs for several power inputs into the LED, while Fig. 3.9 shows the output signal for constant-power input but for different durations. Different results were received for the two PMTs. Although the PMT are identical, their electronic circuits are different. The results are listed in Tables 3.2 and 3.3. The saturation effect, especially of PMT of detector 1, is well seen. The PMT output is still lower with the voltage for a constant-emission duration. The parameters of the PMT electronic circuit can be modified to maintain linearity for higher light emission. However, at the present stage of the project, we found it more useful to keep the PMT linearity at the lowest intensity and, as was explained before, above some minimum level it is always preferable to move the detector a certain distance away than to reduce its sensitivity.

3.1.2 Diaphragm Strength*

The diaphragm used for several indirect designs must contain the deuterium gas through the ignition and detonation stages, up to the moment when the imploding shock wave reaches it. The exploding wire adds enough energy to the $2D_2+O_2$ to initiate a detonation wave with a pressure ratio of 22-fold the initial pressure (Chapman-Jouguet condition). The diaphragm, located close to the exploding wire,

---

* This set of experiments was carried out with the kind assistance of Mr. T. Saito, which is appreciated very much.

is exposed to unsteady pressures and its strength under dynamic conditions is not well known. Therefore, it is difficult to predict analytically its survival up to the imploding-wave arrival. The spectrograph with an eight-photomultiplier system (polychromator) (Ref. 21) was used to determine experimentally when the diaphragm collapses. After being detonated (Fig.3.10a) the gas reaches a temperature of about 5000 K, and radiates over the wavelength spectrum. Eight specific wavelength intensities as monitored by the photomultipliers and are recorded as a function of time. While the diaphragm blocks the light path, no signal is recorded by the system, but when the diaphragm breaks the light can be transmitted and signals appear. Typical results are shown in Fig. 5.3.10b and c. After the oscillations caused by the ignition noise light penetrates the broken 2-mil thick stainless-steel diaphragm, and is detected at 6 wave-lengths out of the 8 over the range of 4128A to 6328A. Then the imploding wave arrives, generating a much higher temperature which is recognized by a sharp negative peak. For the 5-mil thick stainless-steel diaphragm it can sustain the gaseous detonation and no light penetrates before the imploding wave arrives. With some safety margin taken into account, this is the minimum thickness for a stainless-steel diaphragm. The diaphragm experiments were carried out with a vacuum inside the capsule, but even for a 400 psi deuterium pressure, the deviation from the nominal thickness was small.

3.1.3 Capsule Functioning

Owing to the very high-diffusive character of deuterium gas, and the filling procedure of the capsule, which necessitates external fastening of the diaphragm, it was important to confirm that the capsule really can contain the deuterium for a few hours at least. In order to check this, the filling system described in Sec. 2.2 was used. The volume of the vacuum chamber was reduced artificially to a minimum, to increase the sensitivity of the measurement. The capsule was installed and the regular filling procedure followed. When the capsule was full and closed, the chamber was evacuated again and then the capsule was opened. The capsule cavity volume of $0.1 cm^3$ is only 1:38000 of the chamber and tubing volume. The initial pressure at the capsule (100, 400 and 1000 psi) was enough for the equilibrium pressure to be clearly detected by the vacuum gages. The capsule was first filled up to 100 psi and immediately released for calibration. Then the procedure was repeated with 400 psi and 1000 psi pressure with immediate release and 24 hours of waiting. The indium plating that provides the metal seal was a subject of some concern, since its melting point is 156°C, while the procedure inludes heating to 400°C for a few hours under high vacuum. At first we found indium traces inside the capsule. Therefore, the degassing temperature was reduced to 200°C and the indium was restricted to a narrow zone at the edge of diaphragm, with no indium plating on the capsule body. In all experiments, the capsule maintained its full pressure for 24 hours with no detectable change.

3.2 Fusion Experiments

A total number of 2 experiments were done during this study, as given in Fig. 3.4. The table includes a variety of designs, direct and indirect approaches as they were developed. The detailed design for each experiment is indicated by an appropriate figure in Figs. 3.11 to 3.17. Unfortunately, a completely reliable neutron detection

system was not available until December, 1980, owing to the necessity to develop electrical components capable of coping with large noise signals, and a lack of appropriate display equipment. Therefore, for some of the earlier experiments, the present results are not decisive and should be repeated.

Typical craters as produced by the imploding shock wave are shown in Figs. 3.18 to 3.25. The final shape and dimensions of the craters are a combination of several effects such as the pressure of the first imploding wave, melting of the steel due to primary heating by the shock wave and then heating by the very hot gases. A lot of material is also ejected. A detailed study of crater generation can be found in Ref. 35. The initial shape at the focus which is different for each design also plays an important role in the final shape of the crater. Therefore, the crater shape and dimensions cannot be used for quantifying the imploding shock strength and focus. Only a rough estimate can be made by referring to a deep, small diameter crater as resulting from a stronger and better focussed implosion. As can be seen in Table 3.4, only in two very different experiments did neutrons appear as randomly-distributed negative signals. One of these runs is a direct detonation of the deuterium-oxygen stoichiometric mixture with a 97g PETN shell, while the other made use of an indirect method using a capsule of a miniature Voitenko design (36). The detection system for the neutrons, and γ rays which were produced by fusion neutrons interacting with the steel implosion chamber, consisted of the two scintillator-photomultiplier assemblies previously described. The first detector was located at the outer front-plate surface, 30 cm from the implosion focus, while the second detector was 80 cm from the focus (Fig. 3.26). The first oscilloscope displays the entire ignition-detonation-implosion process lasting about 50 μsec as well as the subsequent events. The second oscilloscope was designed to display the full undisturbed shape of the first signal coming from the second detector with a sweep of 50 μsec/division. From its shape it would have been possible to obtain the neutron-velocity distribution and its flux. However, the second oscilloscope can only trigger if a large enough signal ($\sim$ 0.5v) is produced by the first detector. This requires more than one neutron to cross the scintillator within 10nsec. The threshold level is essential to prevent false triggering arising from the photomultipler dark current, cosmic rays and ignition noise.

Records of voltage vs time from the first detector for two runs without fusion a) and with fusion b) are shown in Fig. 3.27. Initially, there are large oscillations arising from the capacitor discharge to the exploding wire, which are damped out in about 35 μsec. In the case of no fusion when a stoichiometric mixture of $2H_2+O_2$ is detonated, no other signals appear. However, with a stoichiometric mixture of $2D_2+O_2$ when fusion occurs at about 50 μsec, about 20 negative signals appear in a random-time and amplitude distribution over a period of about 50 μsec. The maximum amplitude of about 0.2v corresponds to a single impact by a neutron or a γ photon in the MeV range, obtained from a calibration of the scintillators at the University of Rochester. In this case the second oscilloscope did not trigger as none of the events generated a large enough signal. We estimate that the total yield was a few thousand neutrons.

The distribution of events can be explained by the scattering of neutrons as they encountered the steel chamber walls (37,38). Iron

has a total cross-section of about 3.5 barns at 2.45 MeV (39,40), see Fig. 3.28 and Table 3.5 for details. Other components of the steel alloy like Mn and Co also contribute to the neutron scattering. Inelastic scattering by iron atoms produces mainly 0.85 MeV and 1.24 MeV γ rays. However, neutron capture by Fe^{56} produces metastable Fe^{57} with γ-ray energies up to 10 MeV. The total number of neutrons and photons generated per reacting neutron is about three. The coupling angle between the chamber and the detector is about tenfold greater for the scattered neutrons and γ rays than for the neutrons generated at the implosion focus. Consequently, the scintillator is far more efficient in detecting the indirect scattered neutrons and γ rays than the direct neutrons from the implosion focus. Owing to the large attenuation of the inelastically scattered neutrons, the phenomenon is spread out and delayed as recorded in Fig. 3.27. Figure 3.29 shows the display of the first detector for the case when a small hemispherical cavity, capsule containing D_2 was placed at the implosion focus (miniature Voitenko compressor, Fig. 3.16a and 3.16b). The display is nearly identical with the $2D_2+O_2$ stoichiometric mixture case.

4. DISCUSSIONS AND CONCLUSIONS

The compression of hydrogen isotopes by accelerated shells or shock waves in order to achieve a fusion reaction was studied in some detail in the last decade, especially in conjunction with laser applications to fusion (2-10, 41, 42). For planar shock heating, the final temperature can be readily calculated by assuming that all the kinetic energy that the shock has transmitted to the gas is turned into heat when the gas is suddenly stopped by the reflected shock. However, in the case of a spherical implosion this can also be done using numerical methods (Ref. 21) as long as one does not try to reach the discontinuity at the focus, where the continuum equations break down. If one uses these equations unlimited temperatures and pressures are reached at the origin. However, this would always be limited by the transport of energy through radiation and conduction. However, within a radius of a few microns from the origin very high pressures and temperatures are reached sufficient to obtain fusion reactions in deuterium. The Voitenko-type compressor is also capable of producing similar results.

For the direct approach a stoichiometric mixture of deuterium and oxygen must be used in the present experiments which introduces oxygen as an impurity and additional heat sink. This approach also uses a relatively large amount of deuterium to fill the hemispherical implosion chamber to pressures of tens of atmospheres. Yet, only a very small fraction at the origin can actually be used for fusion. Looking ahead for a possible commercial use of this process for energy production stimulated our study of the indirect approach where small amounts of pure deuterium could be confined right at the implosion origin. The challenge is to produce a secondary implosion to be extremely symmetrical. The stability characteristics of spherical implosions becomes very important at this stage. Several stability studies (43,44,45,46) disagree about the stability criterion for spherical implosions. Fong and Ahlborn (46) predicted stability for initial implosion conditions similar to our case. This was substantiated here experimentally by the generation of neutrons when the implosion takes place in a D_2-O_2 stoichiometric mixture. All the stability studies show significant reduction in implosion

stability as the rates of the radius of the perturbations to the radius of the shock wave increases. As a result a symmetrical collapse is all-important and is far more difficult to achieve for the indirect approach. From this point of view the projectile designs (Fig. 3.14 and 3.17) are preferred. In this case, the second implosion is not directly depended on the first implosion, but on its own initial geometry. Previous studies also showed (20) that by providing a proper entrance into the acceleration tube the projectile velocity is hardly reduced by small off-centering and defocussing effects. In some of the projectile experiments a multiple staging acceleration effect (47,48) was used to increase the final diaphragm velocity by a factor of two. In the final phase the shell velocity must be used to generate very strong shock waves to compress and heat the gas. This might be done by either a spherical implosion or a Voitenko compressor.

Although very encouraging results were obtained in generating neutrons and γ rays from D-D fusion reactions using our implosion chamber, its full potential for fusion has not been realized so far. The present facility was built for various types of research applications. The geometrical accuracy of the assembly after years of service could be improved. The uniformity of the present hand-made explosive shells certainly could stand a re-evaluation. Asymmetry also results from gravitational effects due to the difference in density of the detonating gas components. A new vertical oriented implosion chamber built recently for making diamonds from graphite produces much better centered implosions (49).

The type of PETN used is very important. New batches from different suppliers were found to have a very fine structure and therefore had a higher density in the final shell. Following the usual explosive-package-preparation procedure the shells ended up with a density above $1 g/cm^3$, while for the older experiments, the density was usually about $0.65 g/cm^3$. Steele (50) pointed out in a figure (Fig. 41) taken from a Lawrence Livermore report (51) which shows that PETN at higher density is very difficult to initiate by a $2H_2$ and O_2 detonation wave. However, the present results definitely show that we are approaching the thermodynamic conditions for fusion. Therefore any improvement in the implosion strength and symmetry might be significant. For commercial use the explosive package can be cast and even machined to obtain accurate sphericity, uniformity in thickness and density. This would contribute significantly to the final performance. Consequently, some experiments that failed to show any neutron yield might do so with the above improved initial conditions.

The major result is that we have obtained fusion neutrons and γ rays using chemical energy only. As far as we could determine it is the first time that this has been done. It would be gratifying for others to build an implosion chamber and improve on our initial results.

REFERENCES

1. Glasstone, S. Lovberg, R. H. — Controlled Thermonuclear Reactions, D. Van Nostrand Company, Inc., Princeton, New Jersey, 1960.

2. Ribe, F. L. — Fusion Reactor Systems, Reviews of Modern Physics, Vol. 47, No. 1. Jan. 1975.

3. Stickley, C. M. — Laser Fusion, Physics Today, Vol. 31, No. 5, May 1978.

4. Lawson, J. D. — Some Criteria for a Power Producing Thermonuclear Reactor, Proc. Phys. Soc. No. 70B, pp. 6-10, 1957.

5. Shay, H. D. Crawford, R. B. Staehle, J. T. — Energy and Technology Review. Lawrence Livermore Laboratory. UCRL -52000-77-8, August, 1977.

6. Lubin, M. et al. — Single and Multi-Beam Laser Pellet Fusion Experiments. Proceeding of the Fuji Seminar on Laser Interaction with Plasma, edited by Yamanaka, C. Nov. 1974., pp. 1-22.

7. Clayton, J. F. Mayer, F. J. — KMS Fusion, Inc., 1977 Annual Report on Laser Fusion Research.

8. Bogolyubskii, S. L. et al. — Thermonuclear-Neutron Yield from a Plasma Compressed by a Shell. JETP Letters, Vol. 24, No. 4, 20 August, 1976.

9. Ziolkowski, Z. Kaliski, S. Derentowicz, H. — Generation of Fusion Neutrons in a Deuterium Filled Cone by Means of Exp osive Implosion of Polyethylene Shell: Part 1. Theoretical Estimations, Journal of Technical Physics, Polish Academy of Science, 18, 4, 465-471, 1977.
Part 2: Experimental Results, Bulletin de L'Academie Polonaise Des Sciences, Vol. 25, No. 10, 1977.

10. Anisimov, S. I. — Generation of Neutrons as a Result of Explosive Initiation of the D-D Reactions in Conical Targets, JETP Letters, Vol. 31, No. 1, 5 Jan. 1980.

11. Glass, I. I. — Research Frontiers at Hypervelocities, Canadian Aeronautics and Space Journal, Vol. 13, Nos. 8 & 9, 348-366, 401-426, Oct. and Nov. 1967.

12. Glass, I. I. — Appraisal of UTIAS Implosion-Driven Hypervelocity Launchers and Shock Tubes. Progress in Aerospace Science, Vol. 13, edited by Kuchemann, D., 223-291, Pergamon Press, 1972.

13. Elsenaar, A. — A Numerical Model for a Combustion-Driven Spherical Implosion Wave, UTIAS Tech. Note, No. 144, 1969.

14. Brode, H. L. — Theoretical Description of the Performance of the UTIAS Hypervelocity Launcher. Proceeding of the Second International Colloquium on the Gasdynamics of Explosions and Reactive Systems, Astronautica Acta, Vol. 15, 301-309, 1970.

15. Flagg, R. F.
Glass, I. I.
Explosive-Driven Spherical Implosion Waves, Phys. Fluids, Vol. 11, No. 10, p. 2282; see also:

Flagg, R. F.
Application of Implosion Wave Dynamics to a Hypervelocity Launcher, UTIAS Report No. 125, June 1967.

16. Glass, I. I.
Brode, H. L.
Chan, S. K.
Strong Planar Shock Waves Generated by Explosively-Driven Spherical Implosions, AIAA J. Vol. 12, No. 3, 367-374, 1974; see also:

Chan, S. K.
An Analytical and Experimental Study of an Implosion-Driven Shock Tube, UTIAS Report No. 191, August 1973.

17. Glass, I. I.
Sharma, S. P.
Production of Diamonds from Graphite Using Explosive Driven Implosions, AIAA J., Vol. 14, No. 3, 402, 1976; see also:

Sharma, S. P.
Production of Diamonds from Graphite Using Explosive-Driven Implosions, UTIAS Tech. Note No. 196, Dec. 1975.

18. Sevray, P.
Performance Analysis of UTIAS Implosion-Driven Hypervelocity Launcher, UTIAS Technical Note No. 121, 1968.

19. Poinssot, J. C.
A Preliminary Investigation of a UTIAS Implosion-Driven Shock Tube, UTIAS Tech. Note No. 1969.

20. Chan, S. K.
Cappelli, G.
Graf, W. O.
Performance Trials of the Eight-Inch Diameter UTIAS Implosion-Driven Hypervelocity Launcher MKII and MKIII, UTIAS Tech. Note No. 161, 1971.

21. Saito, T.
An Experimental, Analytical and Numerical Study of Temperatures Near Hemispherical Implosion Foci, UTIAS Report No. 260, 1982.

22. Czerwinski, W.
Structural Design and Development of UTIAS Implosion-Driven Launchers, UTIAS Report No. 153, 1971.

23. Makomaski, A. H.
Preliminary One-Dimensional Investigation of the Initiation of Low-Density PETN by Hydrogen-Oxygen Detonation Waves, UTIAS Technical Note No. 83, 1965.

24. Roig, R. A.
A Spectroscopic Investigation of Combustion-Driven Implosions, UTIAS Report No. 214, 1977.

25. Vasudevan, B.
Pressure Measurements at the Focus of Combustion-Driven Implosions, UTIAS Technical Note No. 209, 1977.

26.
"Duo-Seal" Vacuum Pump Model 1452. The Welch Scientific Company.

27. "SpeediVac", Vapour Diffusion Pump, Model 203. Edwards, High Vacuum Ltd., Crawley, Sussex, England.

28. Matheson of Canada, P.O.B. 89, 530 Watson St. E., Whitby, Ont., L1N 5R9: Catalogue No. 30c, 1975.

29. Bolz, R. E.
Tuve, G. L. CRC Handbook of Tables for Applied Engineering Science, 2nd Edition, CRC Press, 1976.

30. Barschall, H. H. Detection of Neutrons; Handbuch der Physik, Vol. XVI: 1956.

31. Organic Scintillators, Plastic Scintillator NE102, Nuclear Enterprise.

32. Entenberg, Alan Laboratory for Laser Energetics, University of Rochester, N.Y. - Private communication.

33. Kaman Nuclear - Instruction Manual for Model A800/801 Neutron Generator.

34. Gallium Arsenide Phosphide LED (Green light), "Electrosonic", Industrial Electronic Components Catalogue No. 771, 136, 1980.

35. Kinslow, R. High-Velocity Impact Phenomena, Academic Press, New York, 1970.

36. Voitenko, A. E. Generation of High Speed Gas Jets, Soviet Physics, Doklady, Vol. 9, pp. 860-862, 1965.

37. Kiehn, R. M.
Goodman, C. Neutron Inelastic Scattering, Physical Review, Vol. 93, No. 1, pp. 177-180, Jan. 1954; see also

Kiehn, R. M.
Goodman, C. Neutron Inelastic Scattering, Physical Review, Vol. 95, No. 4, pp. 989-992, Aug. 1954.

38. Nuclear Data Sheets, U.S. National Bureau of Standards, Section B, 33-3, 4-44, Feb. 1966-.

39. Hughes, D. J.
Schwartz, R. D. Neutron Cross Sections, Brookhaven National Laboratory Report BNL-325, 1958.

40. NBS Special Publication 425, Vol. 1; Nuclear Cross-Sections and Technology. Proc. of a Conference, Washington, D.C., March 3-7, edited by Schrack, L. A. & Bowman, C. D., 1957.

41. Gross, R. A. The Physics of Strong Shock Waves in Gases, Physics of High Energy Density, Proceedings of the International School of Physics, "Enrico Fermi", edited by Caldirola P. and Knoepfel H., pp. 245-277, 1967.

42. Brueckner, K. A. Laser-Driven Fusion, Reviews of Modern Physics, Vol. 46, No. 2, pp. 325-368, 1974.

43. Zimmerman, B. — Hydrodynamic Instabilities in Laser Fusion Targets. Proceeding of the Fuji Seminar on Laser Interaction with Plasma, Edited by Yamanaka, C. Institute of Laser Engineering, Osaka, University, Nov. 1974.

44. McCracy, R. J. — Implosion, Stability and Burn of Multishell Fusion Pellets. Proceedings of the Fuji Seminar on Laser Interaction with Plasmas. Edited by Yamanaka, C., Institute of Laser Engineering, Osaka University, Nov. 1974.

45. Butler — The Stability of Converging Spherical and Cylindrical Shock Waves. ARDE Report (B), 18/56, Aug. 1956.

46. Fong, K.; Alborn, B. — Stability of Converging Shock Waves. Physics of Fluids. Vol. 22, No. 3, pp. 416-421, 1979

47. Fowles, G. R.; Leung, C.; Rabiz, R.; Shance, J. — Acceleration of Flat Plates by Multiple Staging, High Pressure Science and Technology. Edited by Timmerhaus and Barber, Vol. 2, 1974.

48. Laptev, V. I.; Trishin, Yu, A. — Increase of Initial Velocity and Pressure Upon Impact on an Inhomogeneous Target. Soviet Physics, Journal of Applied Mechanics and Technical Physics, No. 6, p. 128, 1974.

49. Glass, I. I. — Beyond Three Decades of Continuous Research at UTIAS on Shock Tubes and Waves, UTIAS Review No. 45, 1981.

50. Steele, R. D. — Los Alamos Scientific Laboratory. Private communication.

51. — Properties of Chemical Explosives and Explosive Simulants. Lawrence Livermore Laboratory, UCRL 51319, Rev. 1, 1974.

52. Glass, I. I.; Sagie, D. — Application of Explosive Driven Implosions to Fusion, Phys. Fluids Vol. 25, No. 2, 1982.

53. Cheng, D. Y. — Formation of a Fusionable Plasma in a High-Pressure Arc Channel, Nuclear Fusion (Austria), Vol. 13, pp. 129-133, 1973. (This is an interesting paper on an alternate electrical scheme to produce neutrons from fusion in deuterium reactions.)

Table 2.1

Electron emission frequency of RCA 8575 photomultiplier above several voltage levels.

Voltage Level of Discrimation	Signals Frequency H_z
0.22	1200
0.24	850
0.30	575
0.40	375
0.50	175
0.60	125
0.70	105
0.80	95
0.90	90
1.00	85
1.25	80
1.50	75

Table 2.2

Neutron activation detection

Description	Solid Angle	Relative Flux Density	Counts for Detection	Minimum Detectable Yield
1. Hemispherical envelope	2π	1/45	500/30 min.	5×10^{6}
2. Capsule envelope	$2/3\pi$	I	300/30 min.	10^{6}
3. Barrel envelope	$1/2\pi$	1/4	300/30 min.	10^{7}
4. Foil in barrel; fast neutrons	0.08π	1/7	250/30 min.	10^{7}
5. Makrofol G/U^{238} fission track foil	0.08π	1/7	10 sparks	10^{6}
6. Gold plated detector	0.08π	1/7	4/1st sec.	10^{5}
7. Foil in barrel; paraffin attenuated neutrons	$3\times10^{-3}\pi$	1/45	850/30 min.	10^{6}
8. Boron plated detector; paraffin attenuated neutrons	$3\times10^{-3}\pi$	1/45	34/1st sec.	10^{4}

Note: The activated foil is of In^{115}, if not specified.

$$In^{115}(n,\gamma)\ In^{116m} \xrightarrow[1.46\ eV]{\gamma} In^{116},\ T_{\frac{1}{2}} = 54\ min.$$

Table 3.1

Signal amplitude as a function of distance from D-D source of 3×10^5 neutrons

Detector I		Detector II	
Distance (ft)	Output (v)	Distance (ft)	Output (v)
0.65	2.7	0.6	3 (Double)
5	2.5	10	1.9
10	2.2	20	1
20	1.9	27	0.5

Table 3.2

Output of PMT for several voltage inputs with 20 nsec duration to the LED

Input to L.E.D. (v)	P.M.T. I		P.M.T. II	
	Output (v)	Output / Input	Output (v)	Output / Input
3	2.8	0.93	0.9	0.300
4	3.8	0.95	1.1	0.275
6	4.7	0.78	1.7	0.283
8	5.8	0.72	2.4	0.300

Table 3.3

Output of PMT for several durations

at constant voltage input of 4V to the LED

Input Duration (nsec)	P.M.T. I Output (v)	P.M.T. II Output (v)
20	3.8	1.1
30	4.2	1.5
40	4.9	2.2
50	5.1	2.8

TABLE 3.4 EXPERIMENTAL DATA

Run No. and Date	Explosive Weight (gr)	Gas Pressure (psi)	Target Design and Pressure (psi)	Diameter and Depth (mm)	Off Centre (mm)	Neutron Detection: Scope I Sweep Time and Resolution	Scope I Display I	Scope II Sweep Time and Resolution	Scope II Display II	Explosive Batch	Notes
A1 11/1/79	162	400	Cone, flat SS diaphragm, 400 psi Fig. 3.11	25x20	X	100 µsec LR	0.1V negative signal at 4.7 µsec				
A2 21/2/80	160	400	Cone, hemispherical SS diaphragm 1.0 psi Fig. 3.12	20x15	9	0.5 µsec LR	high negative	0.5 µsec HR	high frequency oscillations	I	
A3 28/2/80	171	400	Cone, hemispherical SS diaphragm 100 psi Fig. 3.12	21x18	X	0.5 µsec LR	high negative	0.5 µsec HR	high frequency oscillations with envelope	I	
A4 14/4/80	167	400	Cone, hemispherical SS diaphragm 100 psi Fig. 3.12		X	0.5 µsec HR	high frequency noise	0.5 µsec MR	very faint display probably like A3	I	
A5 23/4/80	170	400	Cone, hemispherical SS diaphragm 100 psi Fig. 3.12		X	0.5 µsec LR	high negative	0.5 µsec HR	no signal	I	
A6 5/5/80	163	400	Cone, hemispherical SS diaphragm 100 psi Fig. 3.12		X	0.5 µsec LR		0.5 µsec HR		I	
B1*		400	$2D_2+O_2$ gas run Fig. 3.13	Very small and defocussed		0.5 µsec MR	high negative	0.5 µsec HR	very light disturbances		
B2*		400	$2D_2+O_2$ gas run Fig. 3.13	Very small and defocussed		100 µsec MR	no signal	0.5 µsec HR	too much exposure		
B3*		600	$2D_2+O_2$ gas run	Very small and defocussed		100 µsec HR	no trace	0.5 µsec MR	high negative (at 0.22 sec)		The detection system failed to trigger in time.
B4*		1000	$2D_2+O_2$ gas run								Explosion in the main manifold; damage to the gas tubing.
C1 1/10/80	98	400	Projectile 1.2 atm, Fig. 3.14			0.5 µsec HR	ignition noise	0.5 µsec MR	ignition noise	II	Triggered from the ignition noise.
C2 23/10/80	111	400	Shallow cone 1.2 atm Fig. 3.15	15x20		100 µsec HR	straight trace	0.5 µsec MR	straight trace	II	
C3 30/11/80	132	400	Standard cone 1.2 atm Fig. 3.12	13x13		100 µsec HR	no signal	0.5 µsec MR	no signal	II	
Arrival of second high-frequency storage scope. Reconstruction of the detection system to the present design.											
D1 14/12/80	122	400	Projectile 1.2 atm, Fig. 3.14	Defocussed	20	100 µsec HR	no signal	0.5 µsec HR trig. level	no trigger	II	
*Study of the experimental procedure after this set of experiments was accomplished showed that the gas components were not sufficiently mixed up, since the deuterium was the first to be introduced into the chamber.											
D2 24/12/80	108	400	Shallow cone, 1.2 atm, Fig. 3.15	13x14	X	100 µsec HR	no signal	0.5 µsec HR trig. level	no trigger no trigger	II	
E1 16/2/81	113	400	Voitenko, 1.2 atm Fig. 3.16	19x15	X	100 µsec HR	distributed negative signals from 43 µsec	0.5 µsec HR trig. level 0.2V	no trigger	II	
E2 19/2/81	104	400	Projectile 1.2 atm Fig. 3.14		10	100 µsec HR	no signal	0.5 µsec trig. level 0.2V	no trigger	II	
F1 9/3/81	127	400	Projectile 1.2 atm Fig. 3.14	Defocussed	X	100 µsec HR	no signal	0.5 µsec HR trig. level 0.2V	no trigger		
F2 11/3/81	97	800	D_2+O_2 Fig. 3.13		X	100 µsec HR	distributed negative signals from 42 µsec	0.5 µsec HR trig. level 0.2V	no trigger		
F3 13/3/81	119	400	Voitenko, 1.2 atm Fig. 3.16		30	100 µsec HR	no signal	0.5 µsec HR trig. level 0.2V	no trigger		
G1 2/4/81	140	400	$2D_2+O_2$ Fig. 3.13	Diffused		100 µsec HR	no signal	0.5 µsec HR	no trigger	III	
G2 9/4/81	100.5	800	Voitenko, Fig. 3.16	16xg	X	100 µsec HR	no signal	0.5 µsec HR	no trigger	III	
G3 14/4/81	98	400	$1.33D_2+3O_2$	no print		100 µsec HR	no signal	0.5 µsec HR	no trigger	III	Nonstoichiometric gas mixture $+333+D_2$.
G4 15/4/81	104	800	Voitenko, Mylar diaphragm, Lan., Fig. 3.16	15x9	X	100 µsec HR	probably a very faint signal at 42 µsec	0.5 µsec HR	no trigger	III	
H1 2/6/81	97	400	$2D_2+O_2$ Fig. 3.13	Diffused	50	100 µsec HR	no signal	0.5 µsec HR	no trigger	III	Renewed explosive package.
H2 10/6/81	102	400	$2D_2+O_2$ Fig. 3.13	21x2	3	100 µsec HR	no signal	0.5 µsec HR	no trigger	III	Honeycomb 5/16"
H3 12/6/81	114	400	Commercial Fig. 3.17	flyer tilted	X	100 µsec HR	no signal	0.5 µsec HR	no trigger	III	Honeycomb 5/16

Abbreviations: HR - high resolution
MR - medium resolution
LR - low resolution

Table 3.5

Data on iron activation

Iron Activation

1. Possible Reactions (examples)

   1. Elastic scattering

   2. Inelastic scattering: $Fe^{56}(n,n')Fe^{56m} \xrightarrow[0.85]{\gamma} Fe^{56}$

      $Fe^{56}(n,n')Fe^{56m'} \xrightarrow[1.24]{\gamma} Fe^{56m} \xrightarrow[0.85]{\gamma} Fe^{56}$

   3. Absorption (capture): $Fe^{56}(n)\ Fe^{57m} \xrightarrow{\gamma} Fe^{57}$

   4. $_{26}Fe^{56}(n.p)_{25}Mn^{56}, \xrightarrow{\gamma} {}_{25}Mn^{56}$, $T_{\frac{1}{2}} = 2.58_h$

2. Cross Sections

Energy of n	σab	σsc	σt
2.45 Mev	∿ 1	∿ 1	3.5
thermal	2.62	11	13.6

3. γ Ray Spectra from thermal-neutron capture of Fe

Photon Energy Mev	0-1	1-4	2-3	3-5	5-7	7-9	>9
No. of Photons per 100 captures	>75	60	27	23	25	38	2.1

Highest energy γ-rays: 10.16 Mev

Average No. of photons per 100 captures >250

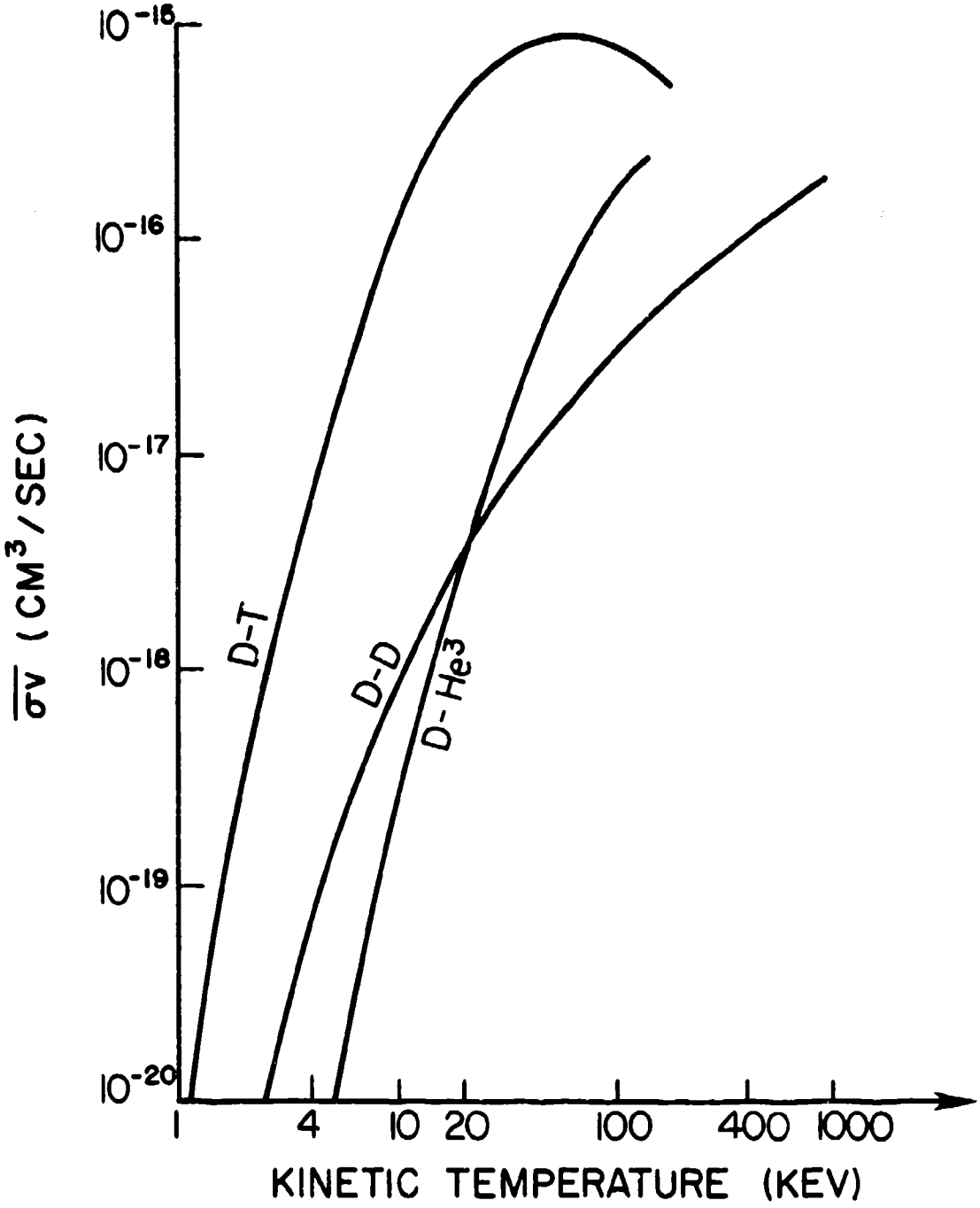

FIG. 1.1 PHYSICAL CONDITIONS FOR THERMONUCLEAR REACTIONS. VALUES OF $\overline{\sigma v}$ BASED ON MAXWELLIAN DISTRIBUTION FOR D-T, D-D (TOTAL), AND D-He^3 REACTIONS (REF. 1).

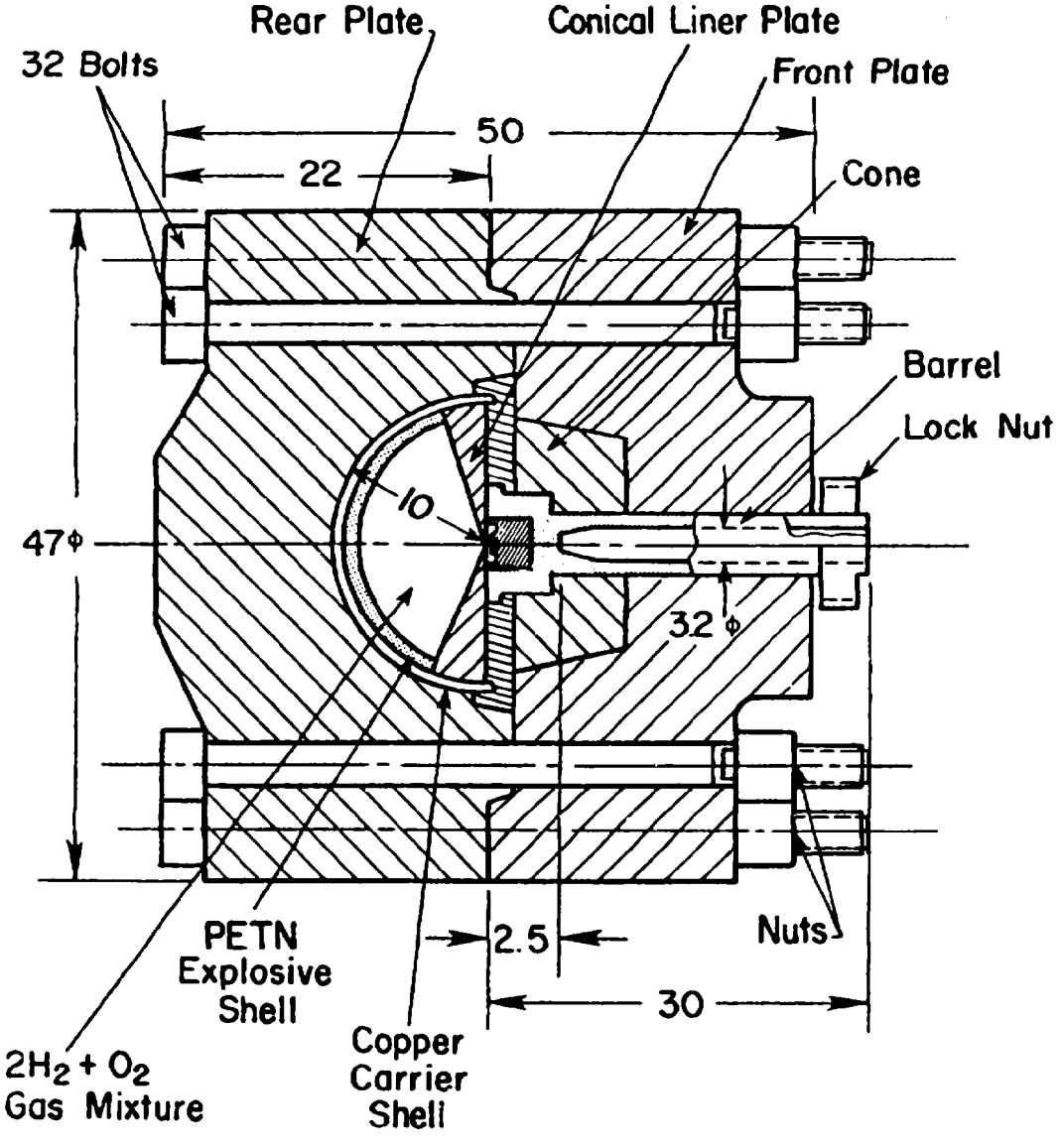

FIG. 1.2 UTIAS IMPLOSION CHAMBER FOR DIRECT $2D_2+O_2$ DETONATION PETN IMPLOSIONS.

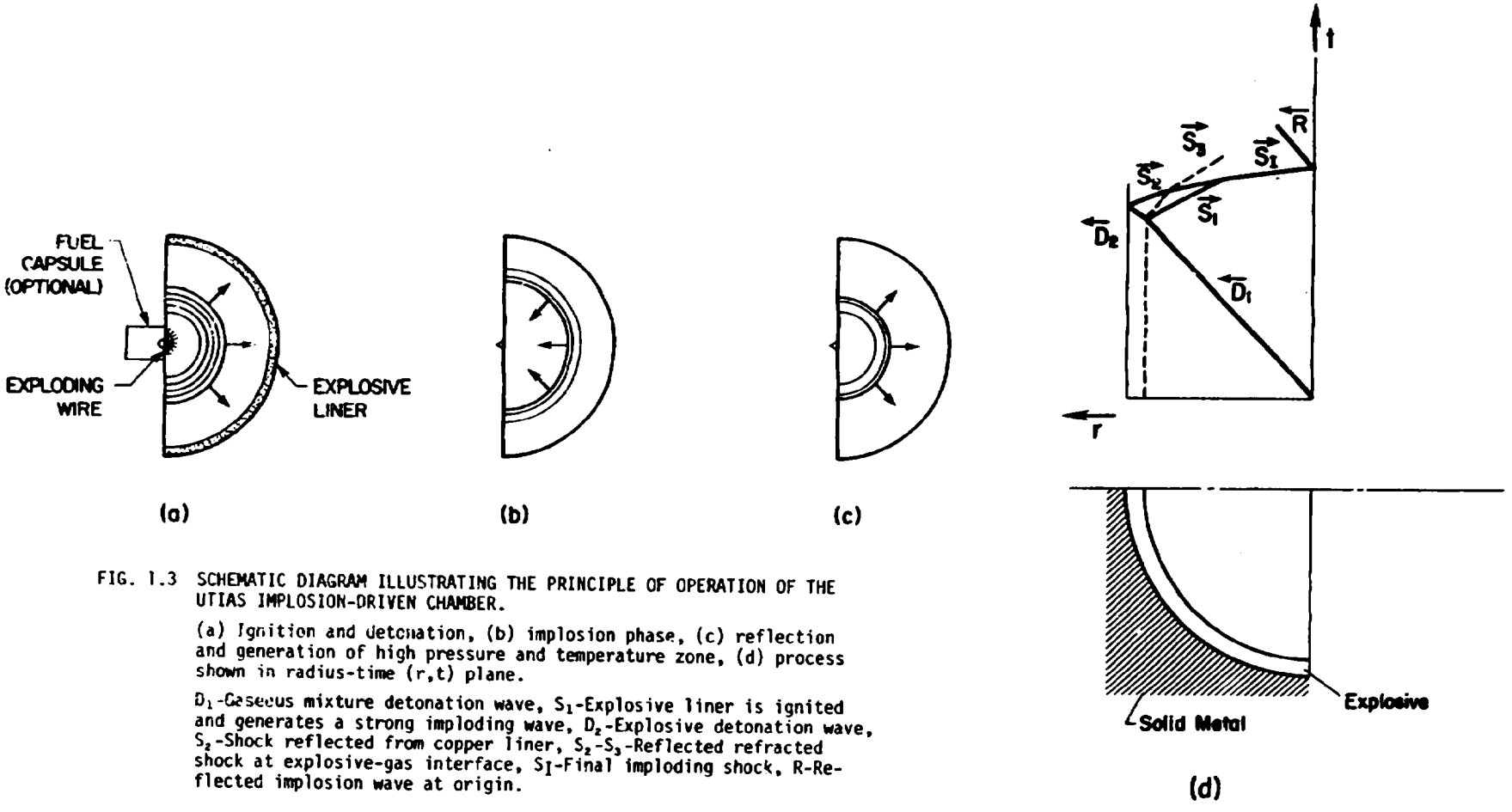

FIG. 1.3 SCHEMATIC DIAGRAM ILLUSTRATING THE PRINCIPLE OF OPERATION OF THE UTIAS IMPLOSION-DRIVEN CHAMBER.

(a) Ignition and detonation, (b) implosion phase, (c) reflection and generation of high pressure and temperature zone, (d) process shown in radius-time (r,t) plane.

D_1-Gaseous mixture detonation wave, S_1-Explosive liner is ignited and generates a strong imploding wave, D_2-Explosive detonation wave, S_2-Shock reflected from copper liner, S_3-S_3-Reflected refracted shock at explosive-gas interface, S_I-Final imploding shock, R-Reflected implosion wave at origin.

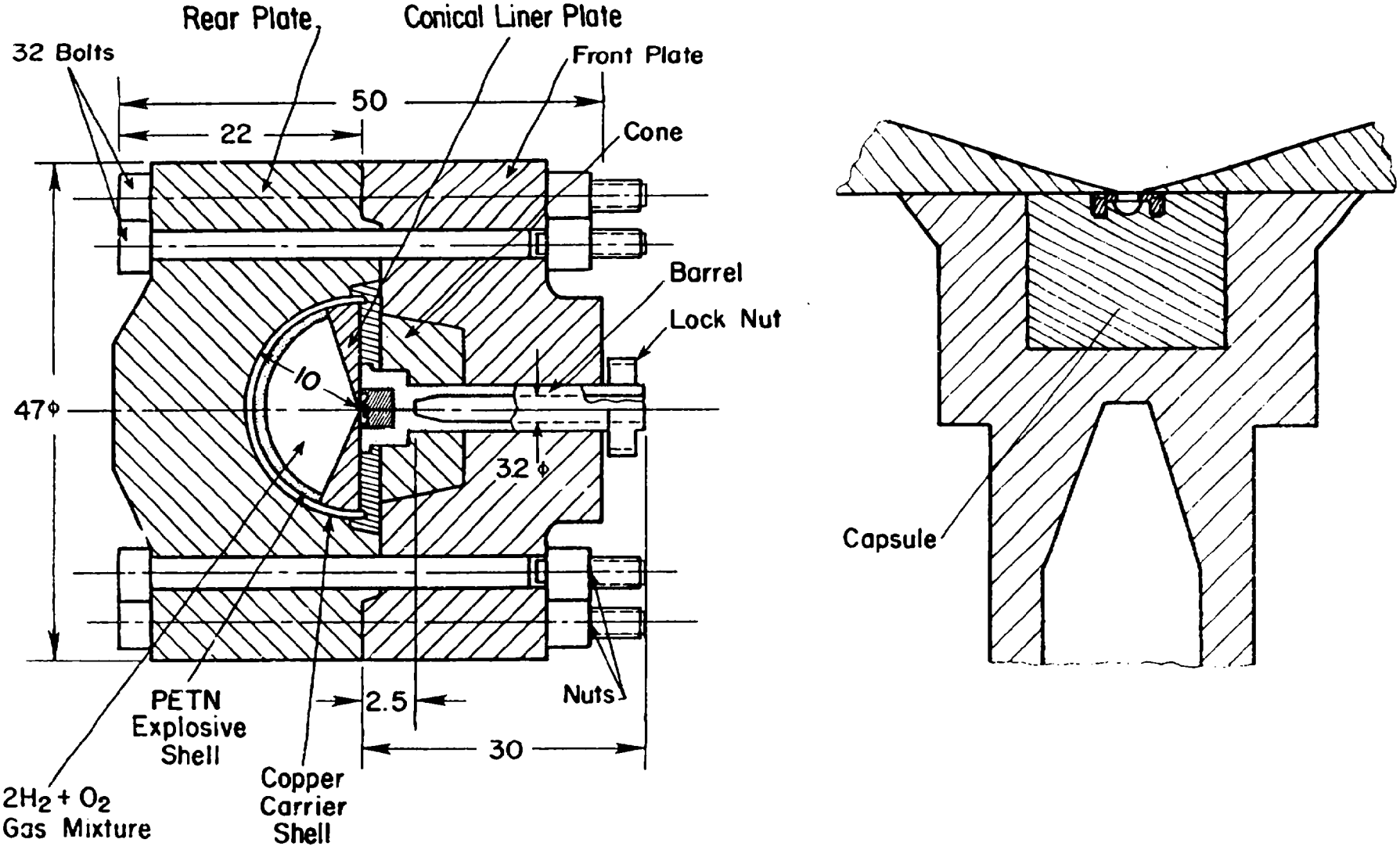

FIG. 1.4 UTIAS IMPLOSION-CHAMBER FACILITY INCLUDING A DEUTERIUM CAPSULE (VOITENKO-COMPRESSOR MODE).

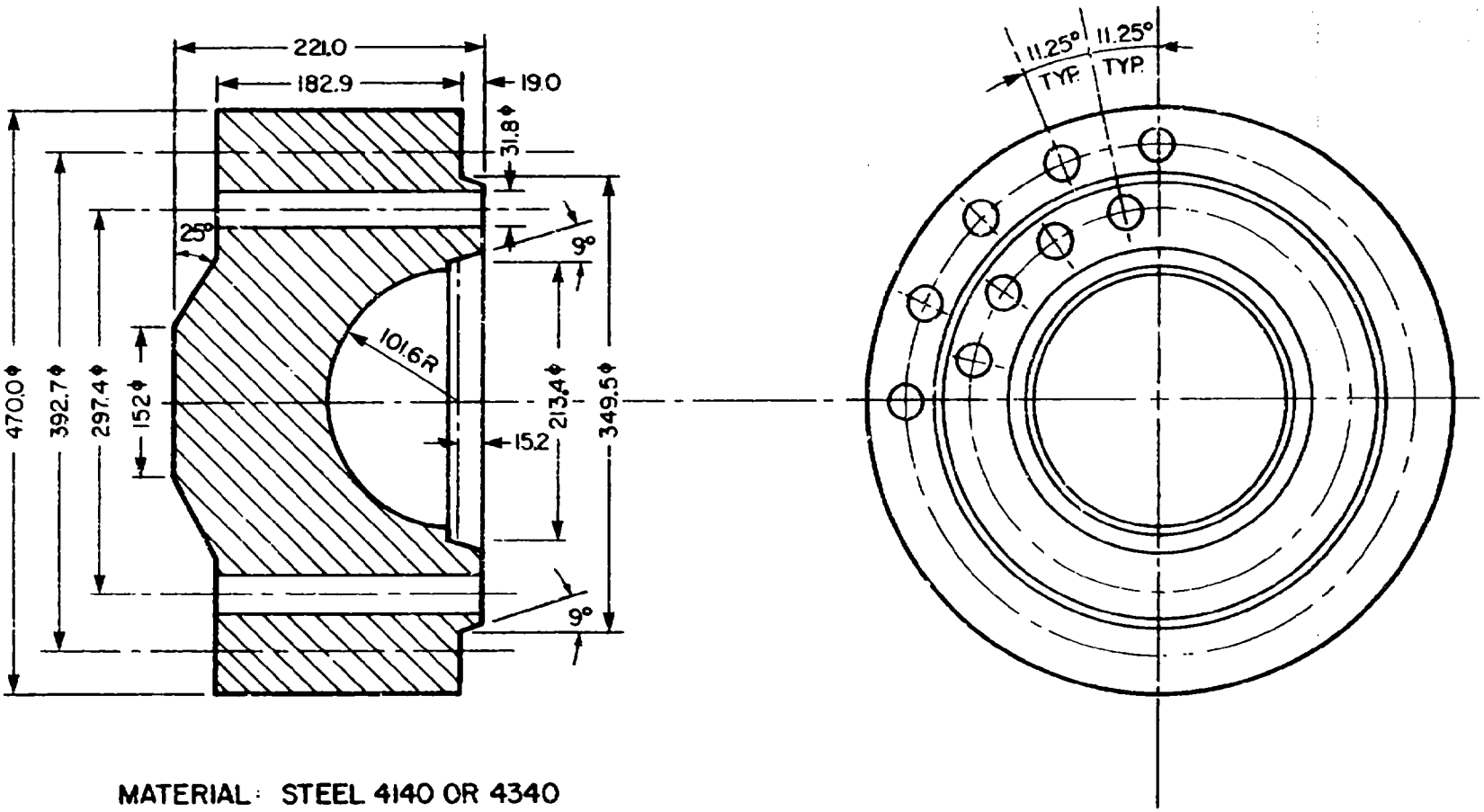

MATERIAL: STEEL 4140 OR 4340

FIG. 2.1(a) IMPLOSION CHAMBER REAR PLATE.

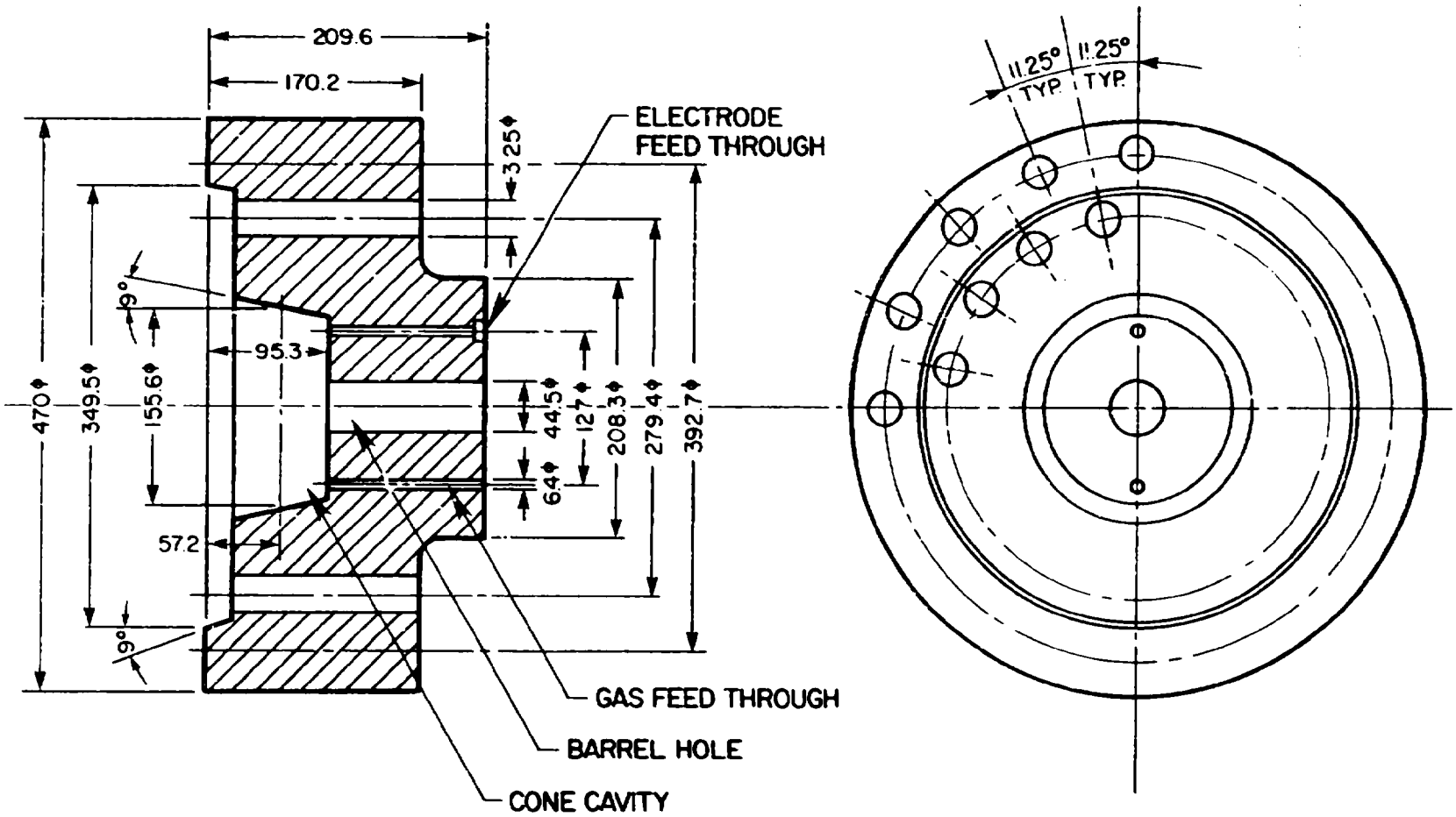

MATERIAL: STEEL 4140 OR 4340

FIG. 2.1(b) IMPLOSION CHAMBER FRONT PLATE.

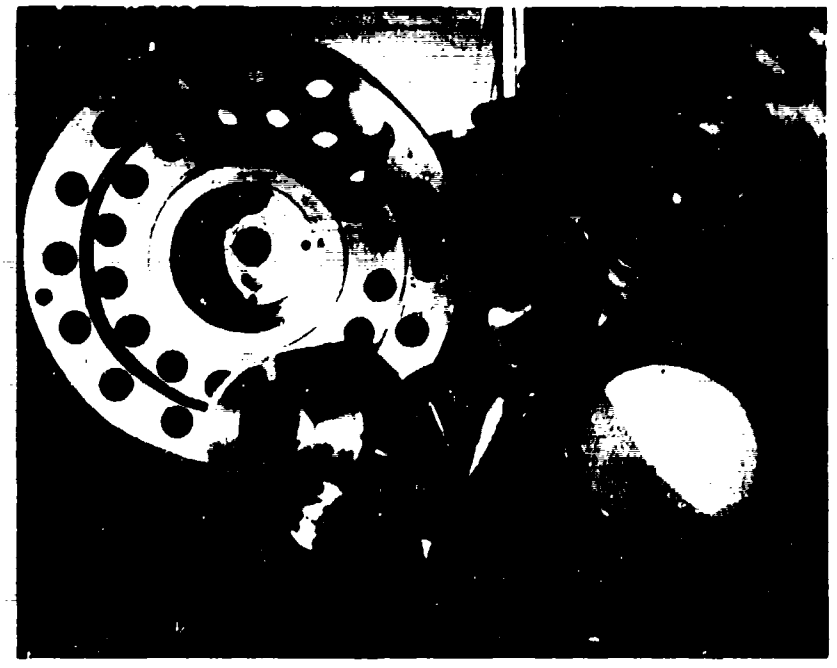

FIG. 2.2 IMPLOSION-DRIVEN CHAMBER – EXPLODED VIEW.

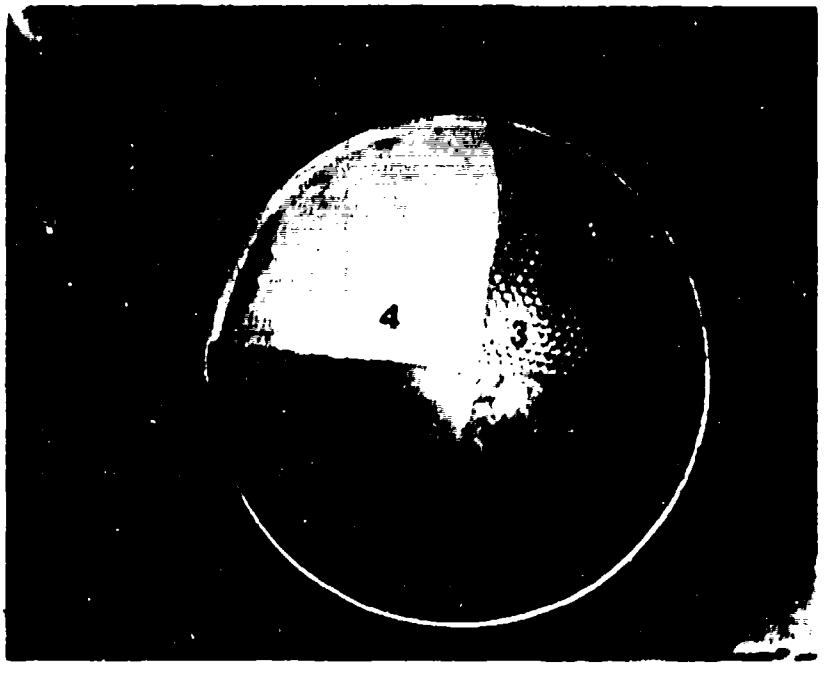

FIG. 2.3 VIEW OF A MODK-UP SHOWING THE STEPS IN THE MANUFACTURE OF EXPLOSIVE PACKAGE.

1. Bare copper liner. 2. Thin coat of cement. 3. Plastic honeycomb matrix. 4. PETN and cotton fiber slurry forced into the matrix.

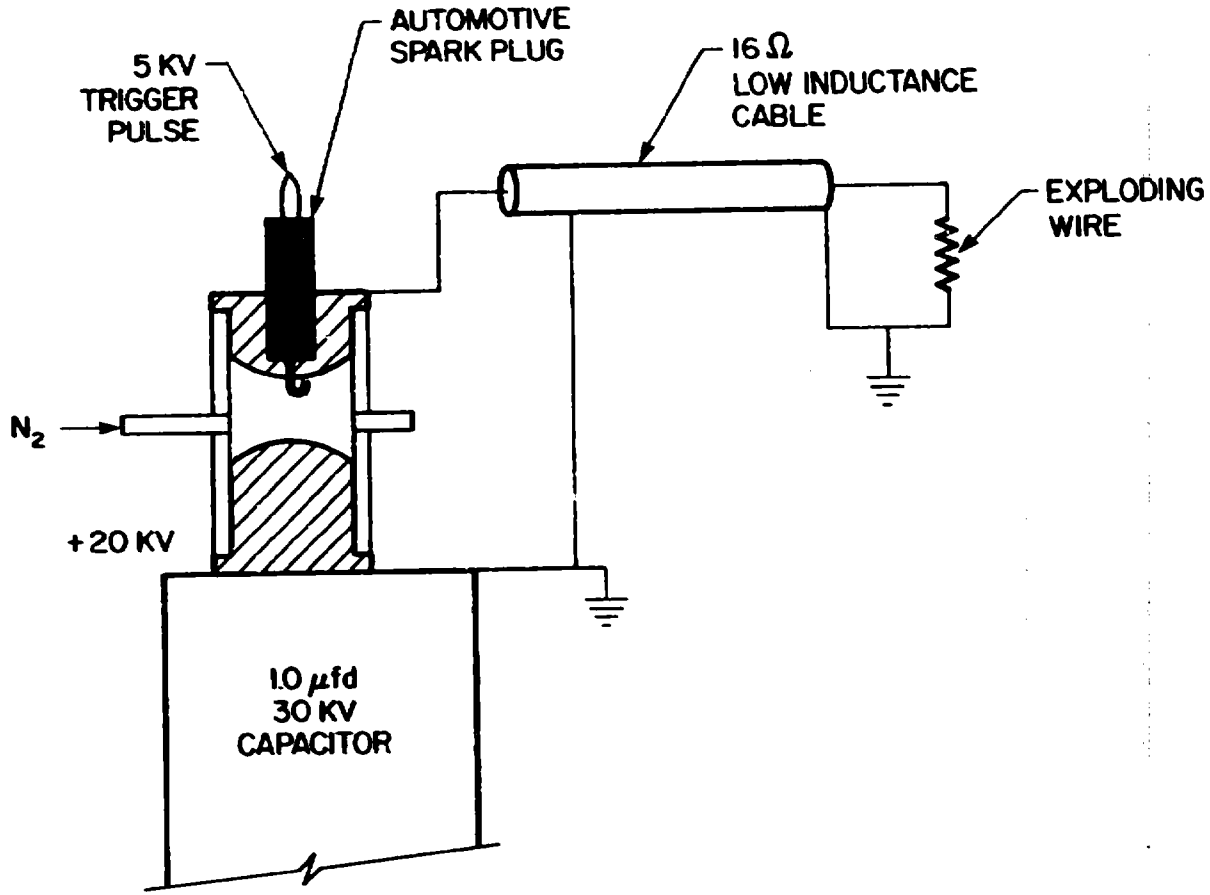

FIG. 2.4 IGNITION ASSEMBLY.

The spark gap, consisting of 2 brass electrodes in a Plexiglas tube with a spark-plug trigger, is dehumidified by flowing compressed nitrogen. The capacitor is then charged to 20 kV and a 5 kV trigger pulse to the spark-plug initiates the discharge (Ref. 24).

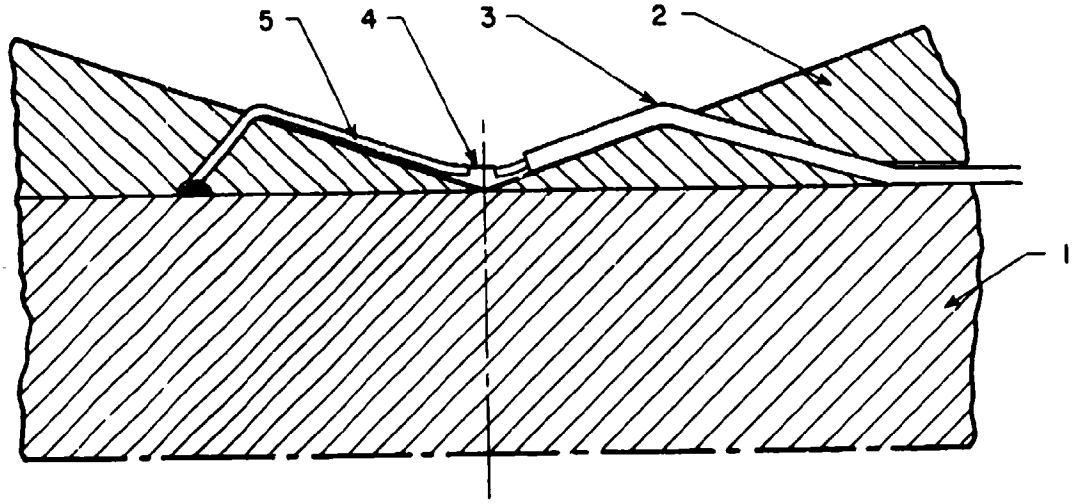

FIG. 2.5(a) EXPLODING-WIRE ASSEMBLY, MODEL I.

1. Capsule body. 2. Conical liner. 3. Teflon tube. 4. Exploding wire. 5. Ground terminal.

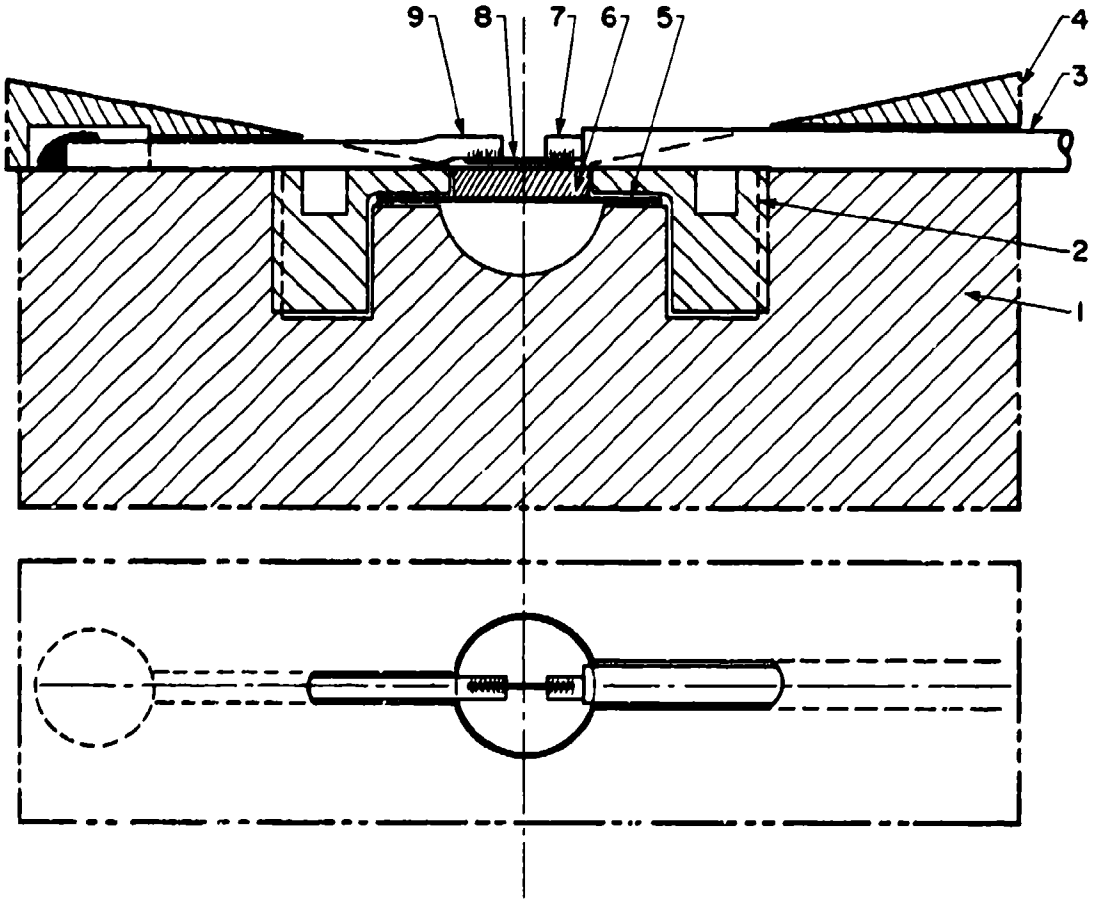

FIG. 2.5(b) EXPLODING-WIRE ASSEMBLY, MODEL II.

1. Capsule body. 2. Fastening nut. 3. Teflon tube. 4. Conical liner. 5. Diaphragm. 6. Piston. 7. High voltage terminal. 8. Nickel exploding wire. 9. Ground terminal.

FIG. 2.6 VIEW OF EXPLODING-WIRE ASSEMBLY OVER DIAPHRAGM OF DEUTERIUM CAPSULE.

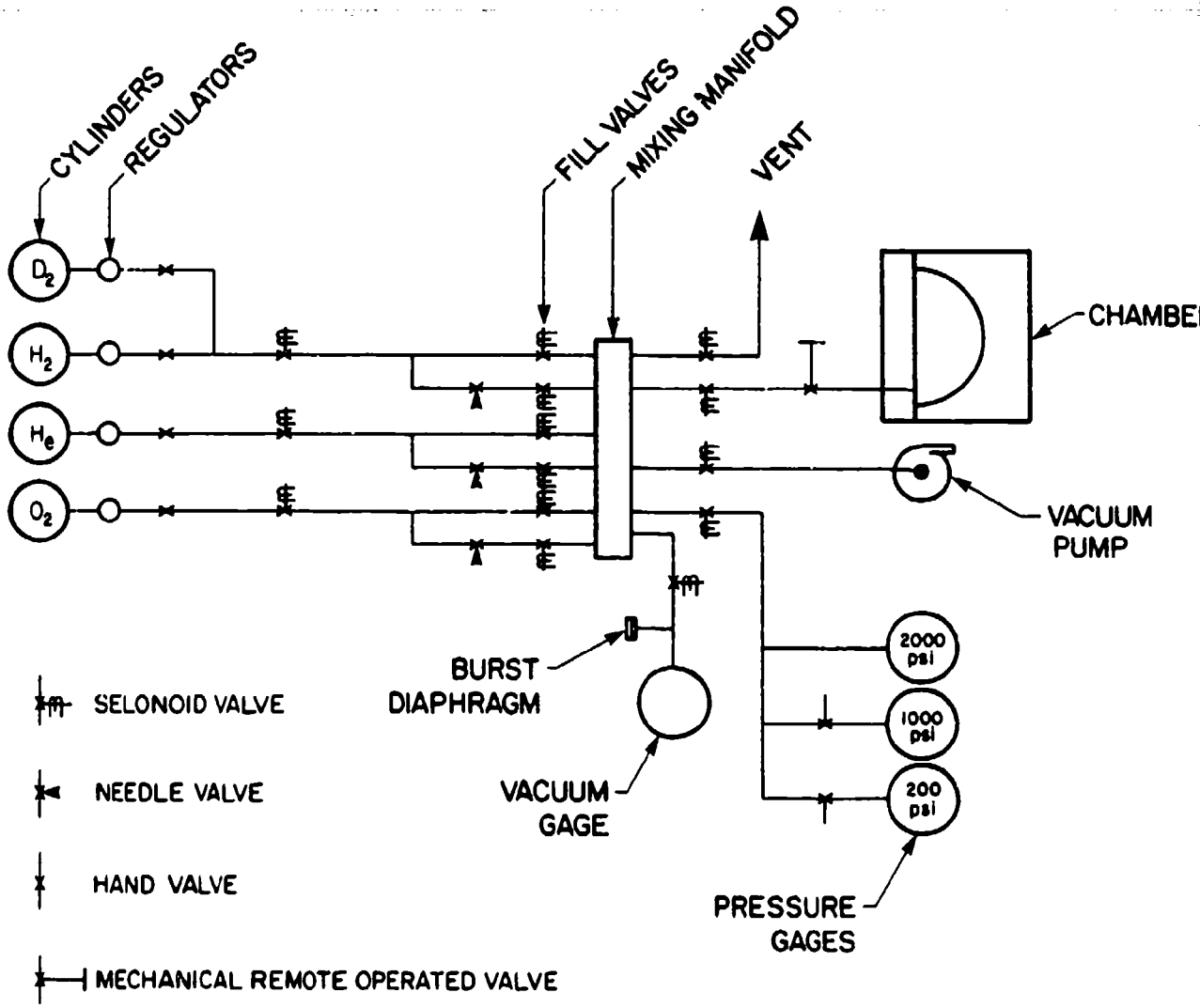

FIG. 2.7 SCHEMATIC DIAGRAM OF PRESSURE AND VACUUM SYSTEM.

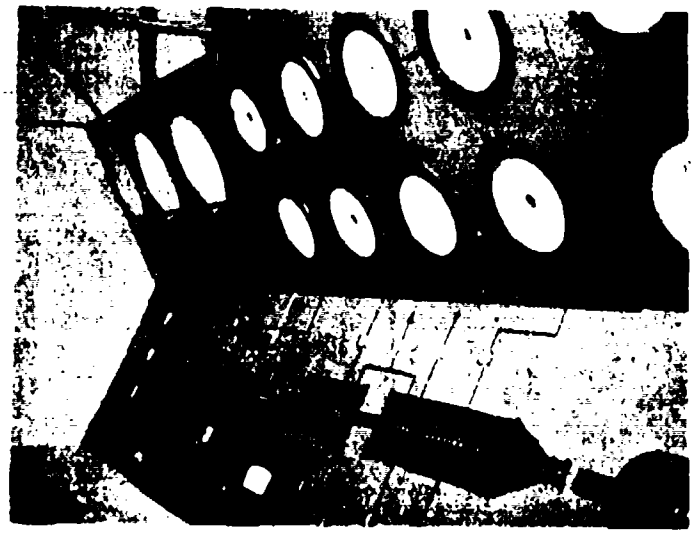

FIG. 2.8 CONTROL PANEL.

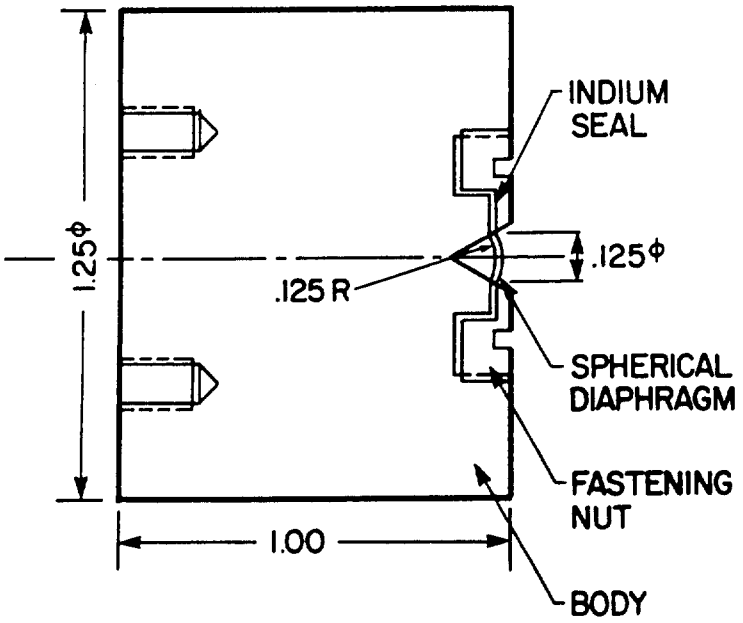

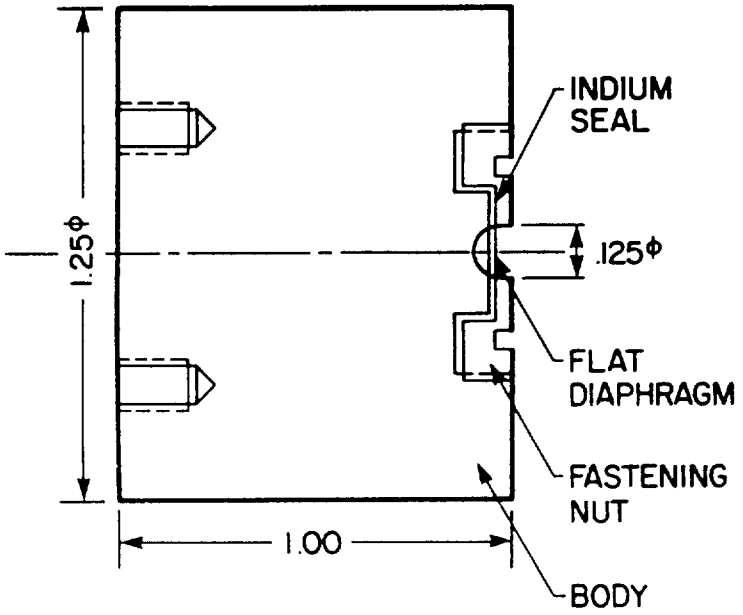

FIG. 2.9 TYPICAL CAPSULES.

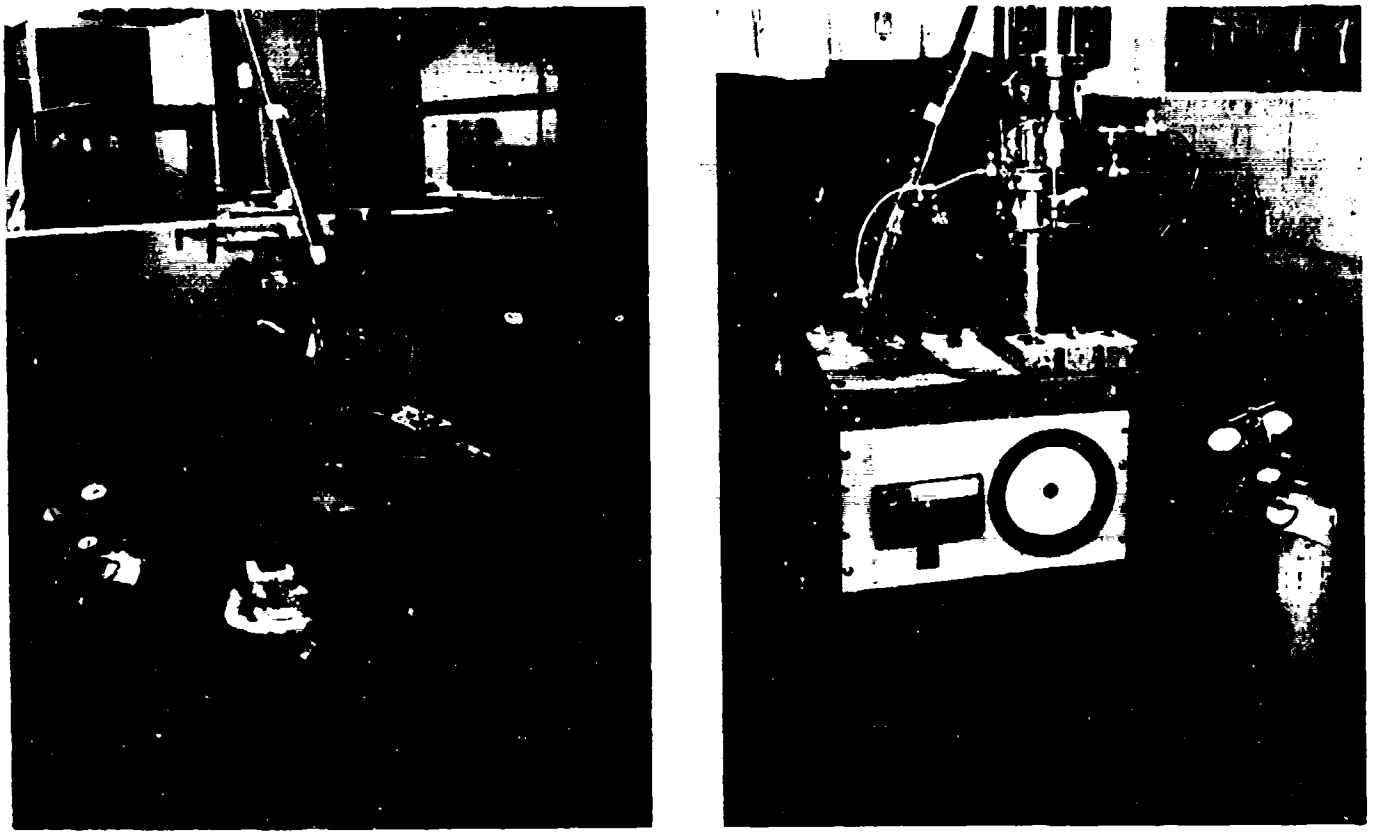

FIG. 2.10 VIEW OF DEUTERIUM FILLING SYSTEM.

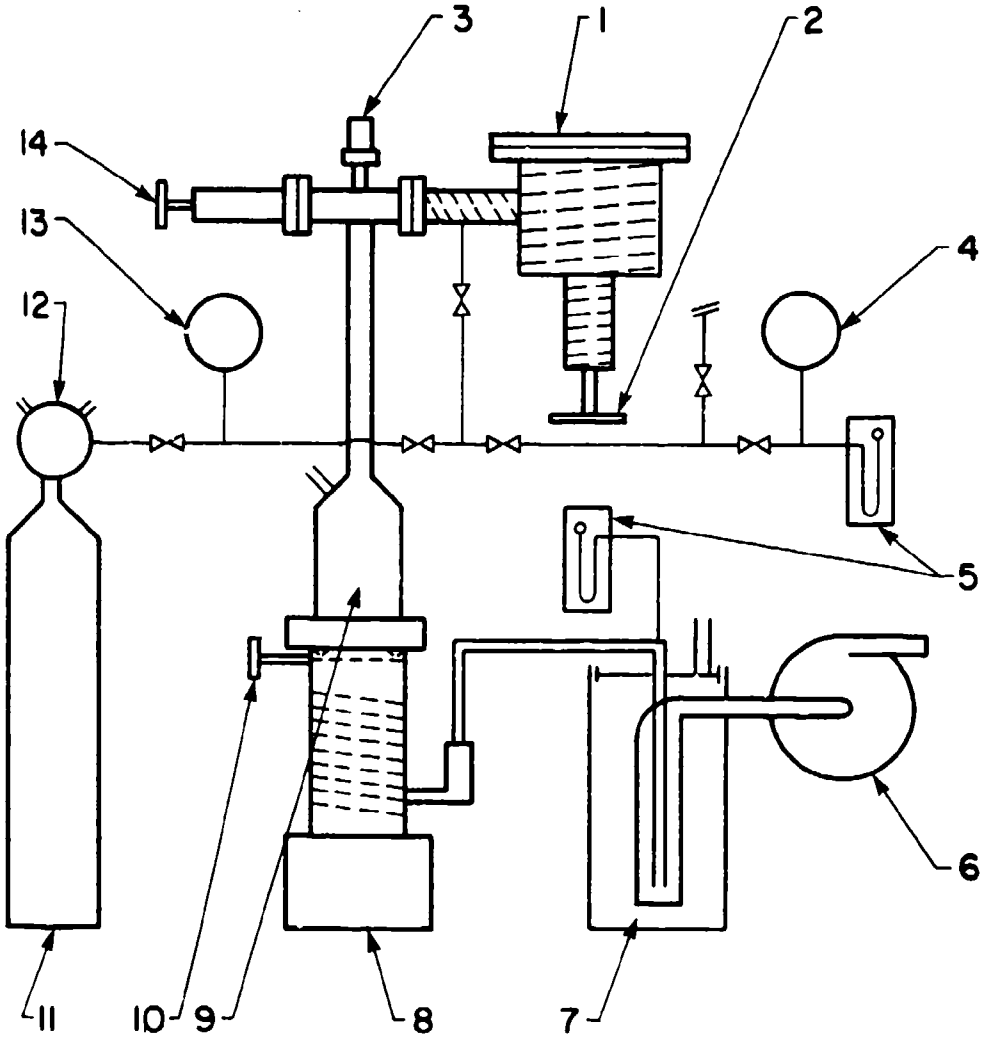

FIG. 2.11 DEUTERIUM FILLING SYSTEM – SCHEMATIC VIEW.

1. Vacuum chamber. 2. Capsule closing external handle. 3. Pirani high-vacuum gage. 4. Pressure gage. 5. McLeod vacuum gages. 6. Rotary pump. 7. Liquid nitrogen cold trap. 8. Diffusion pump. 9. Liquid nitrogen cold trap. 10. Diffusion pump baffle. 11. Deuterium cylinder. 12. Pressure regulator. 13. Pressure gage. 14. Chamber vacuum valve. ⋈ Vacuum valve. ≡≡ Water cooled zone.

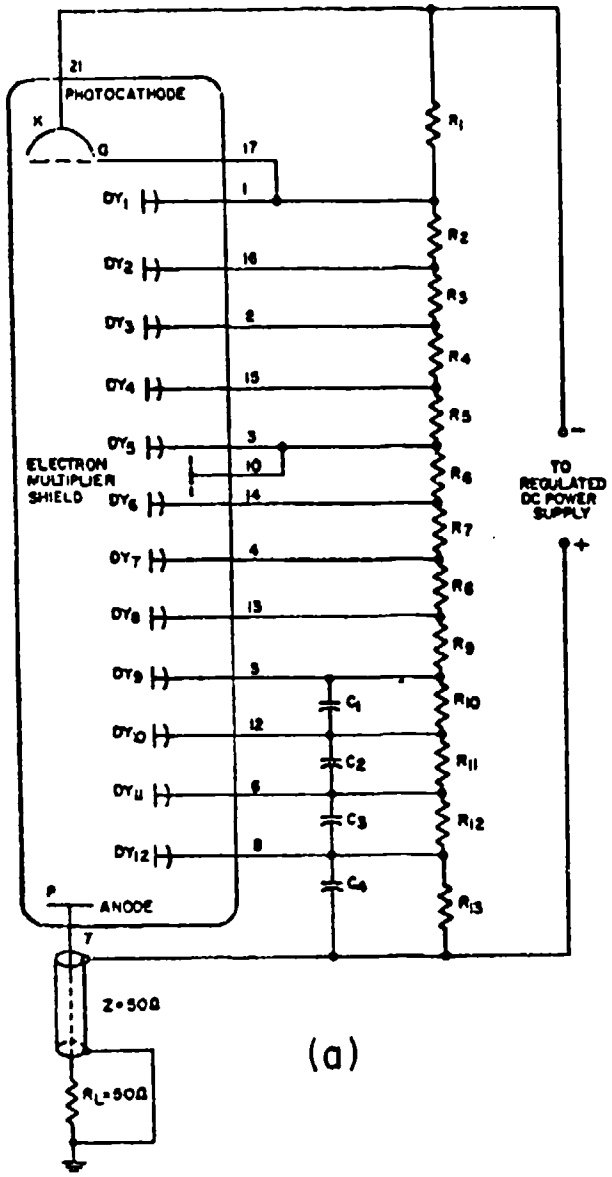

(a)

Fast Pulse Response Applications, to 3000 V
(Typical circuit values)

C_1: 0.005 μF, 20%, Ceramic Disc, 500 V dc
C_2: 0.01 μF, 20%, Ceramic Disc, 500 V dc
C_3: 0.02 μF, 20%, Ceramic Disc, 500 V dc
C_4: 0.05 μF, 20%, Ceramic Disc, 500 V dc

R_1: 400 kΩ (4-100 kΩ, 5%, 1/2 W in series)
R_2: 100 kΩ, 5%, 1/2 W
R_3: 130 kΩ, 5%, 1 W
R_4 through R_{13}: 100 kΩ, 5%, 1/2 W

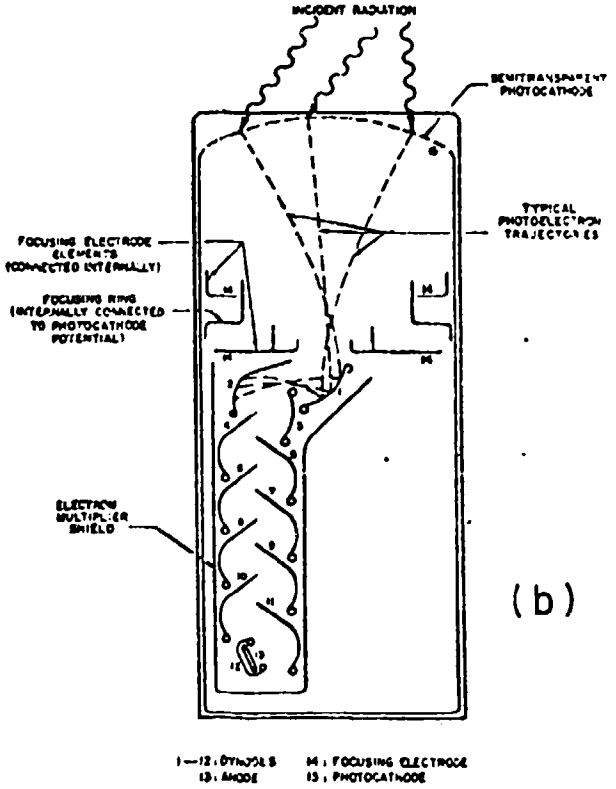

(b)

FIG. 2.12 SCHEMATIC DIAGRAMS OF RCA MODEL 8575 PMT.
(a) Electrical, (b) mechanical,
current spectrum.

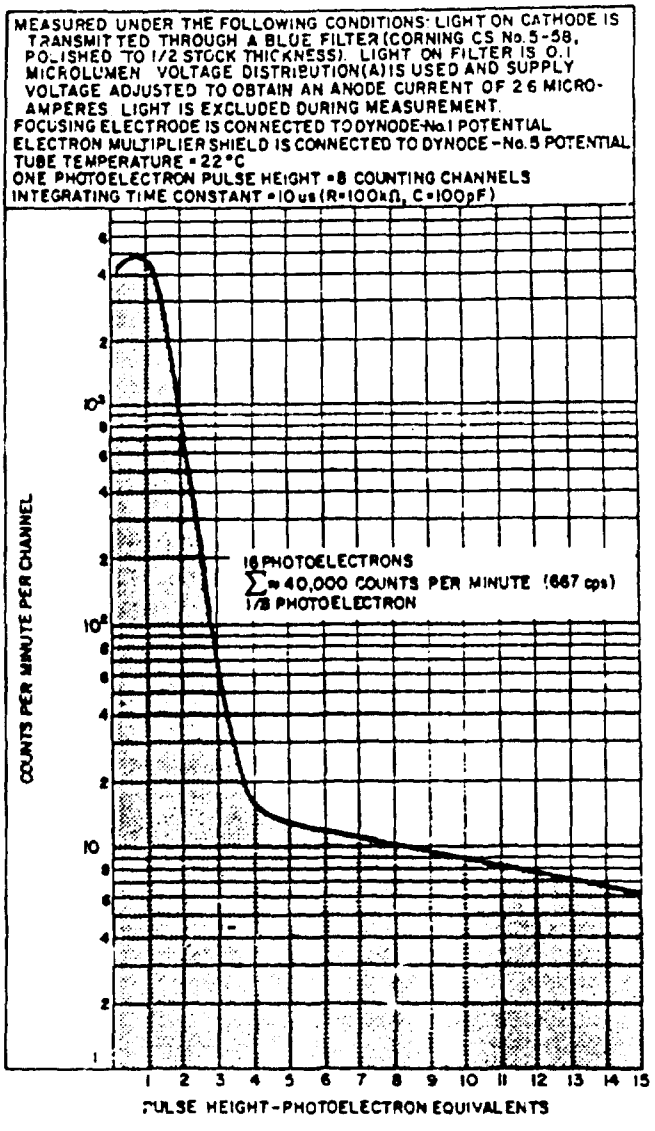

(c) typical dark

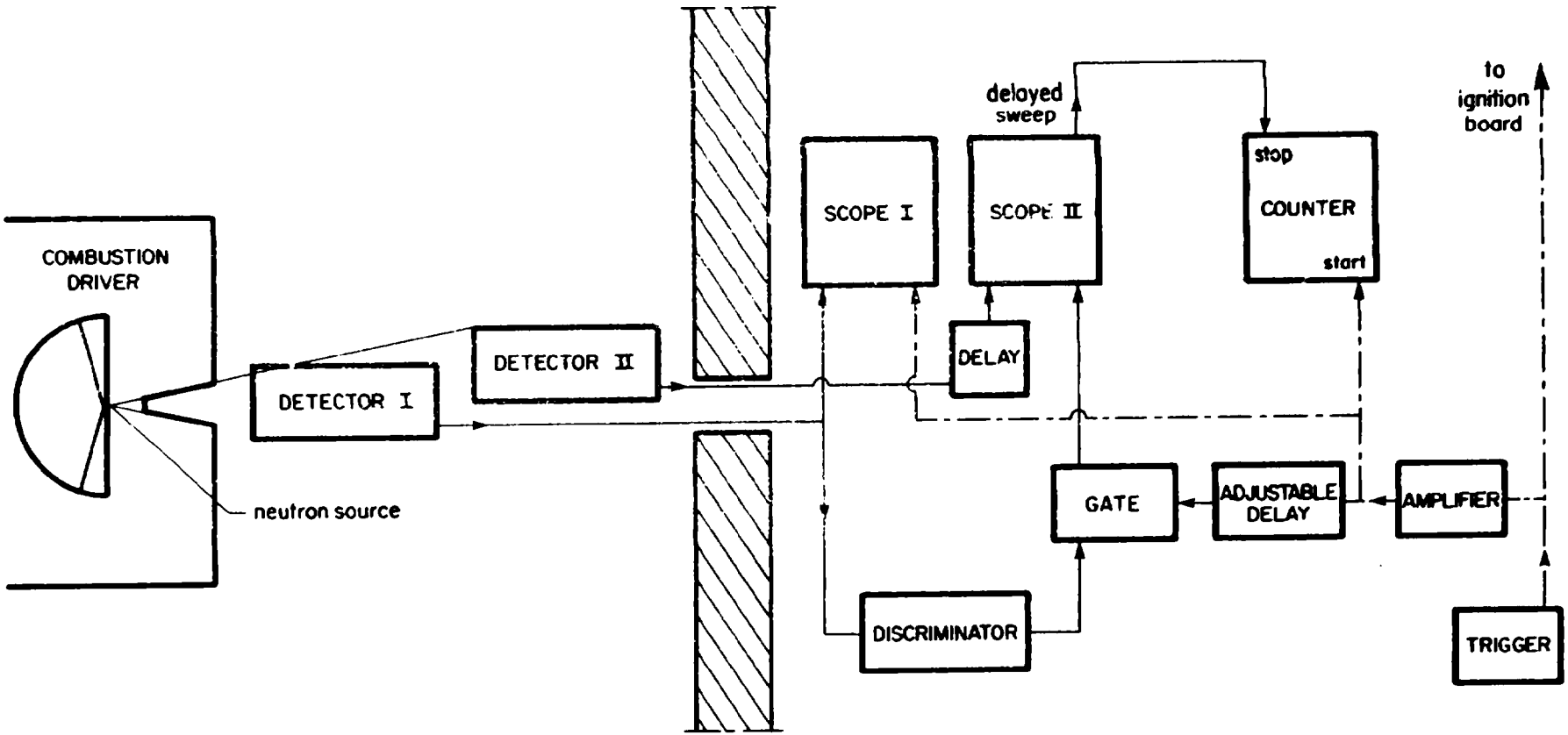

FIG. 2.13 SCHEMATIC VIEW OF NEUTRON-DETECTION SYSTEM.

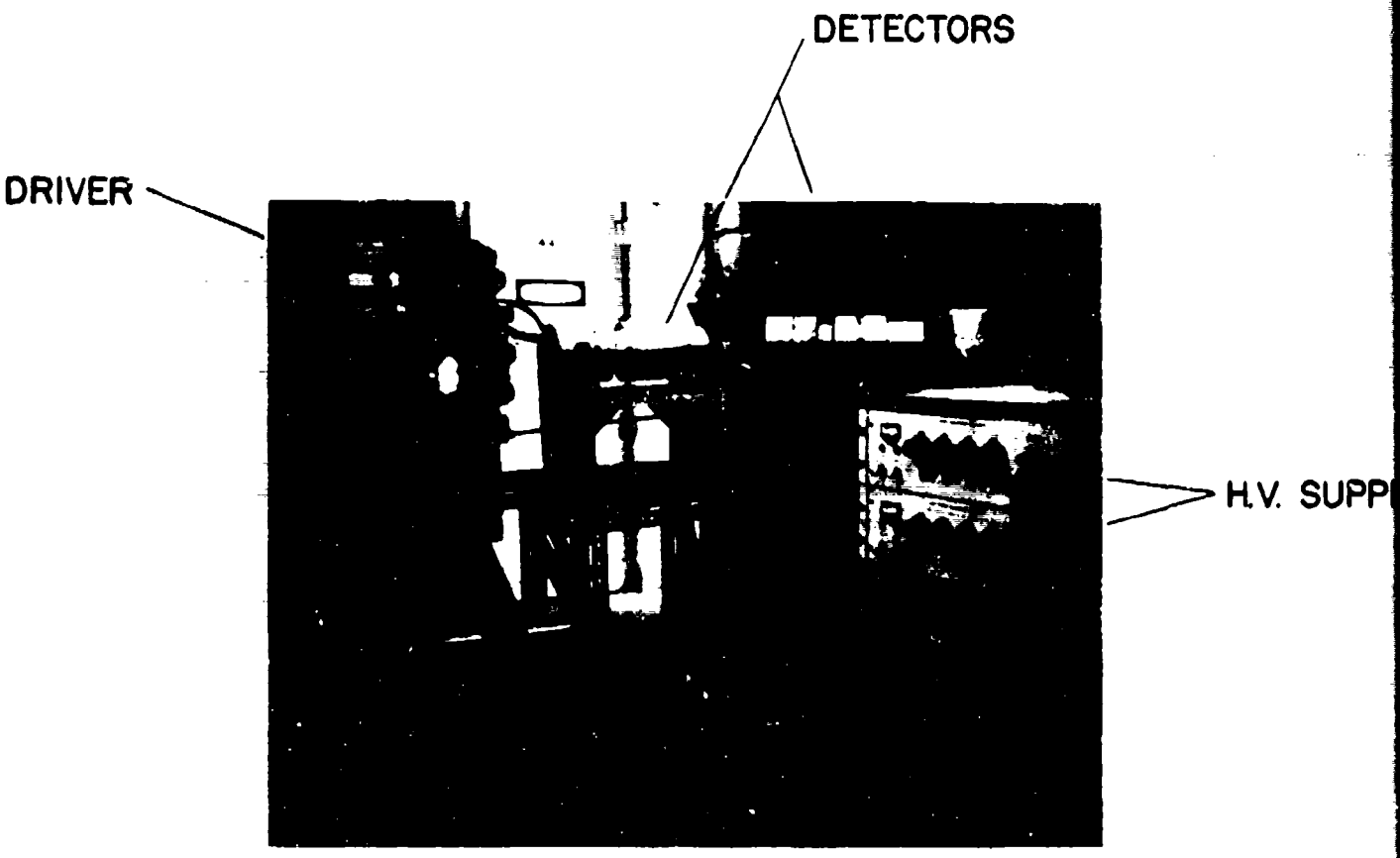

FIG. 2.14 VIEW OF EQUIPMENT INSIDE EXPLOSION ROOM.

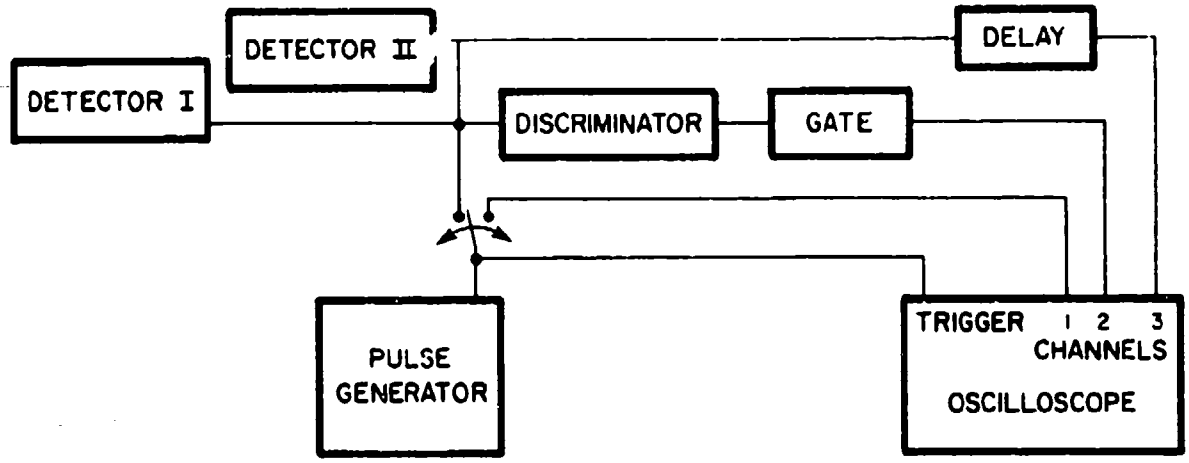

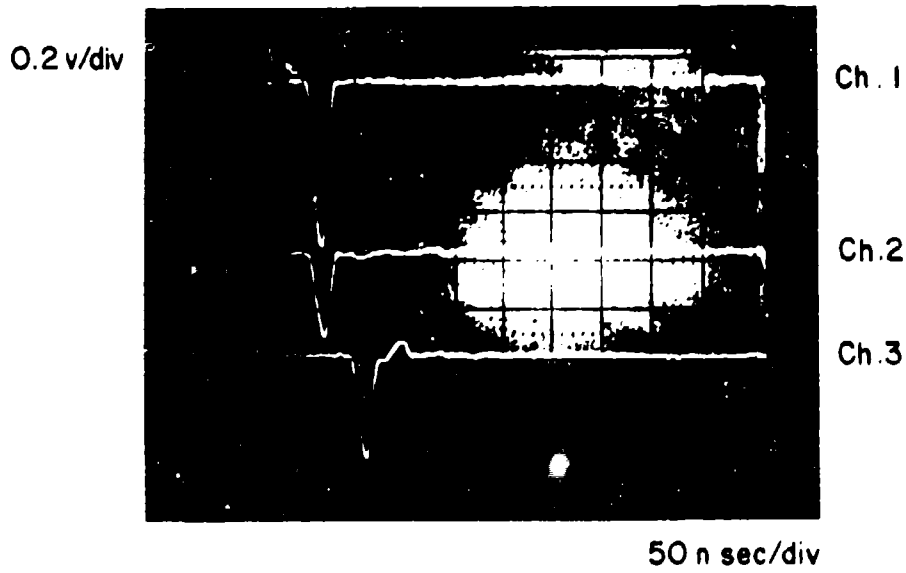

FIG. 2.15 CALIBRATION OF THE "BACK VIEW" SYSTEM. ORIGINAL COMPONENTS AND CABLES ARE USED.

Channel 1: Directly from the pulse generator
Channel 2: Signal from the wiring of detector I
Channel 3: Signal from the wiring of detector II

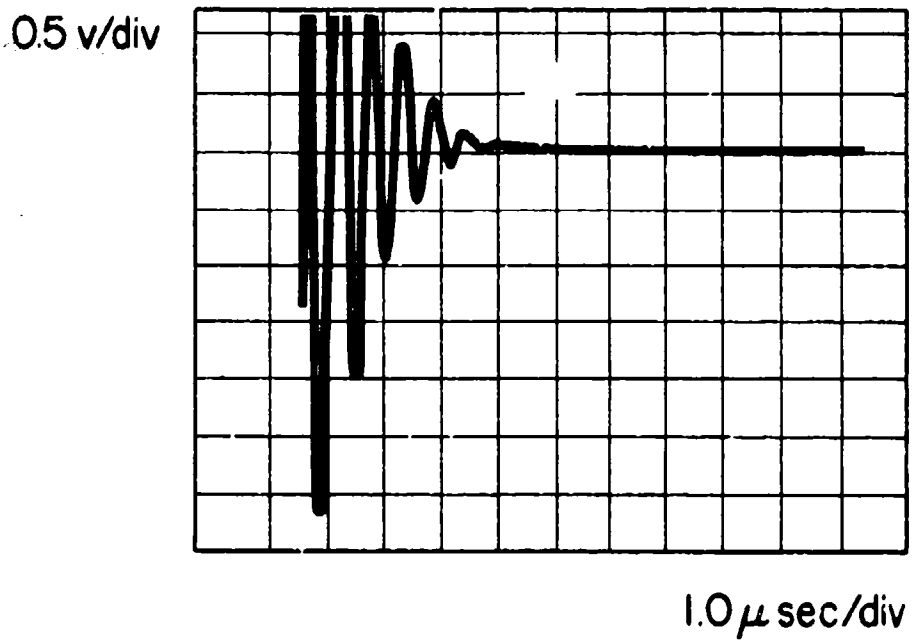

FIG. 2.16 TRACE WITHOUT FUSION SCOPE I. THE OSCILLATIONS ARE DUE TO THE CAPACITOR DISCHARGE AND VANISH WITHIN 35 μSEC.

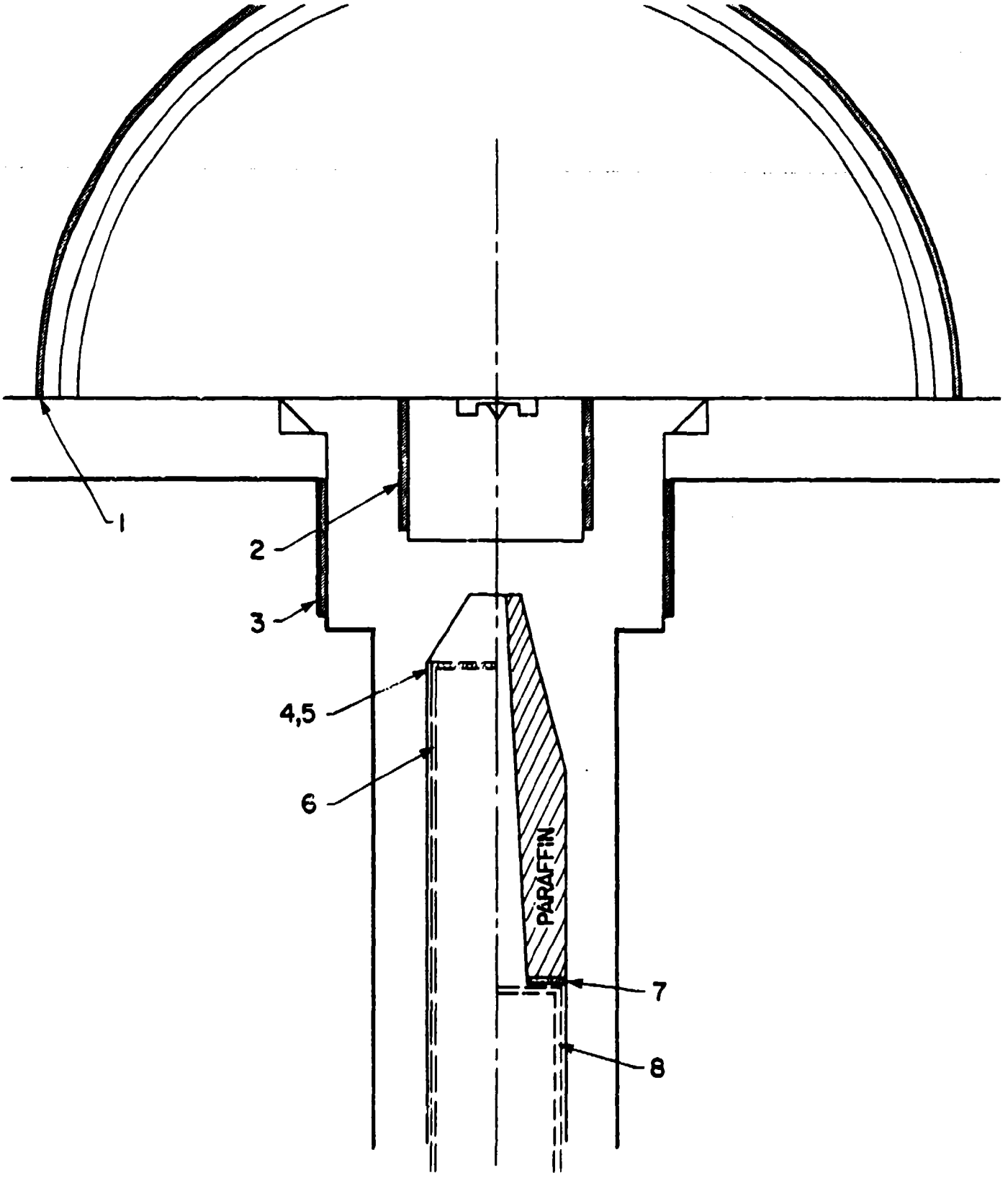

FIG. 2.17 SOME NEUTRON ACTIVATION TECHNIQUES.

1. Hemispherical envelope. 2. Capsule envelope. 3. Barrel envelope. 4. Foil in barrel; fast n. 5. U^{238} + film, recoil track. 6. Gold-plated Geiger. 7. Foil in barrel; slow n. 8. Boron-plated Geiger, slow n.

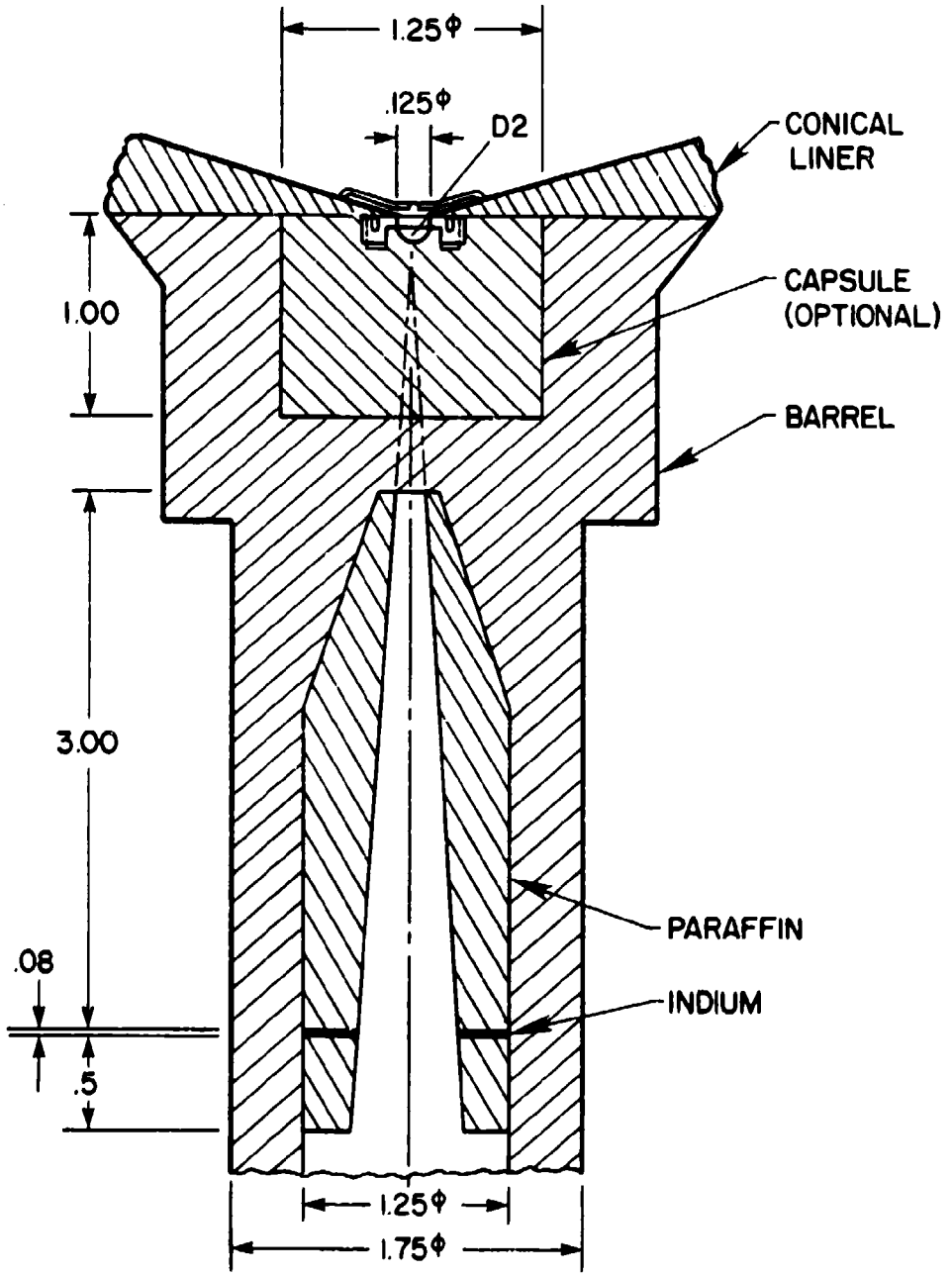

FIG. 2.18 ACTUAL DESIGN FOR INDIUM ACTIVATION.

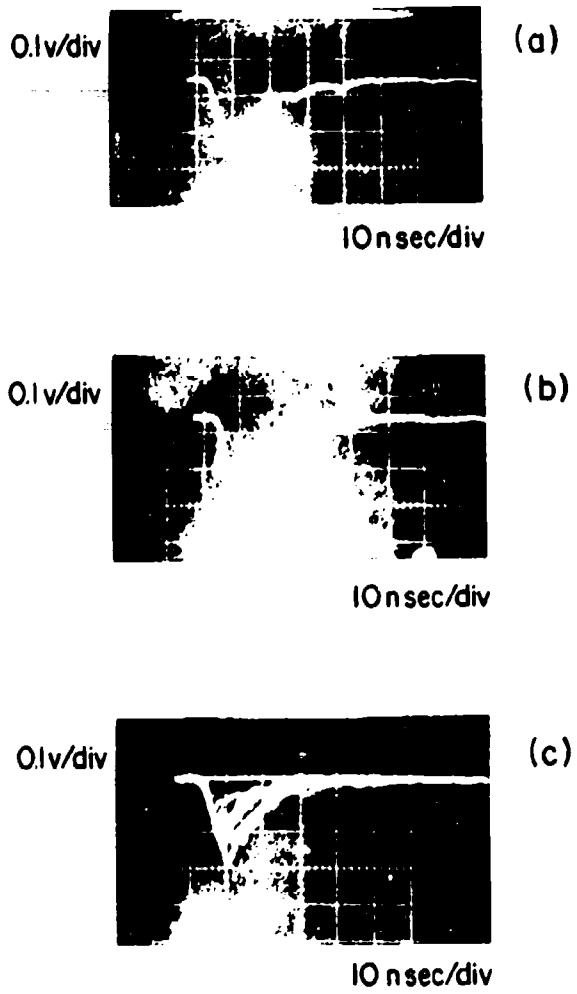

FIG. 3.1 TYPICAL PHOTOMULTIPLIER-SCINTILLATOR ASSEMBLY SIGNALS (PMT II). (a) Electron emission signal, (b) Co^{60} signal, (c) spectra of Co^{60} signals.

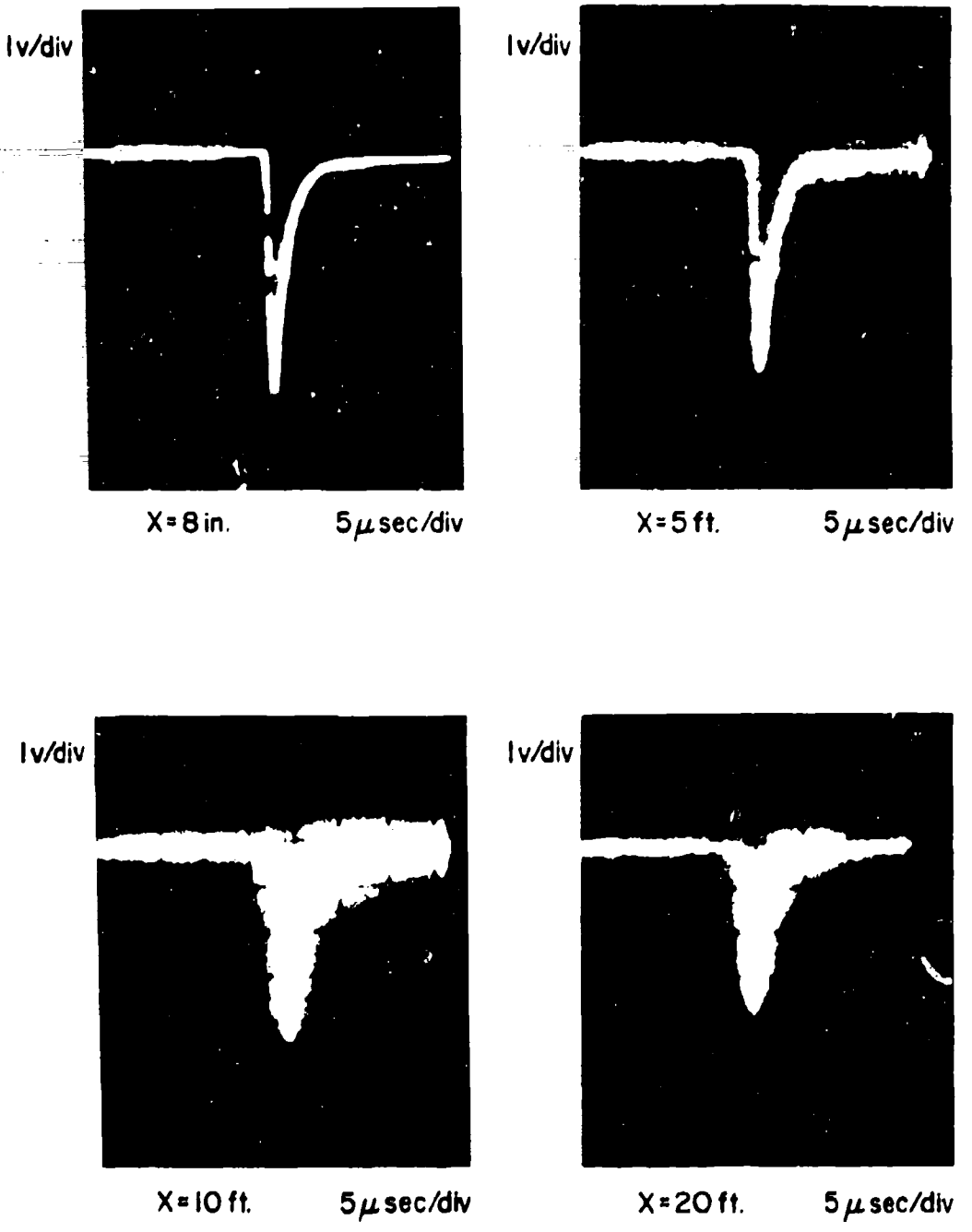

FIG. 3.2 DETECTOR I SIGNALS AS A FUNCTION OF DISTANCE FROM D-D SOURCE OF 3×10^5 NEUTRONS.

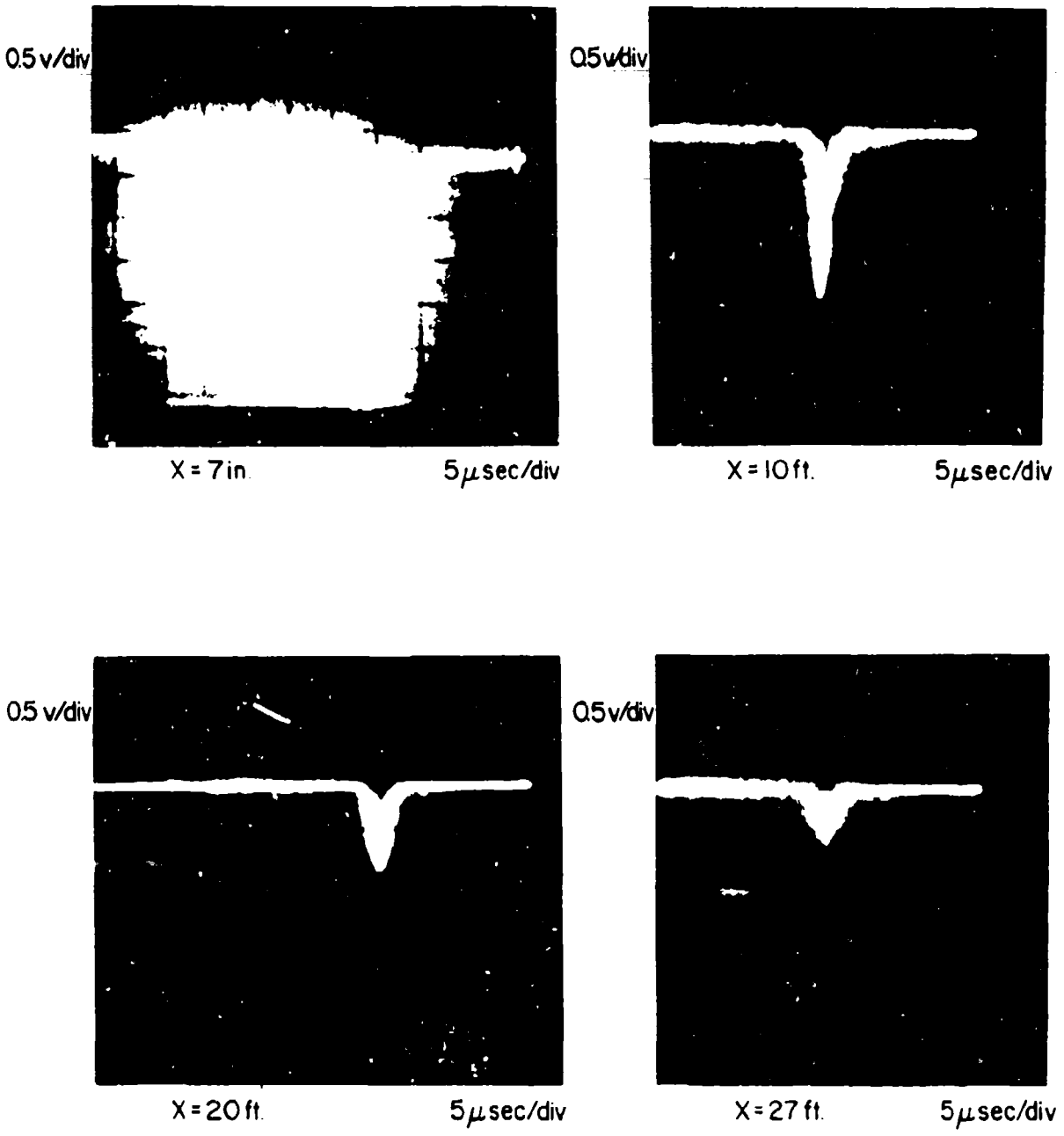

FIG. 3.3 DETECTOR II SIGNALS AS A FUNCTION OF DISTANCE FROM D-D SOURCE OF 3×10^5 NEUTRONS.

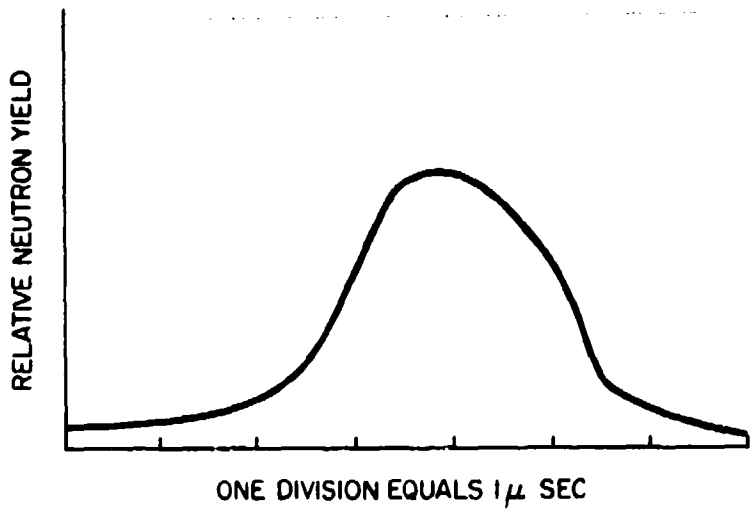

FIG. 3.4 KAMAN NEUTRON GENERATOR MODEL A-800. TOTAL YIELD: 3×10^5 NEUTRONS FROM D-D REACTION (REF. 33).

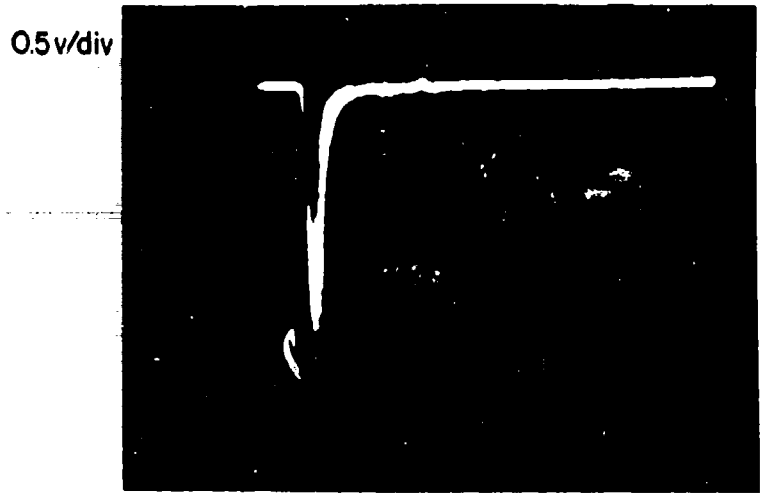

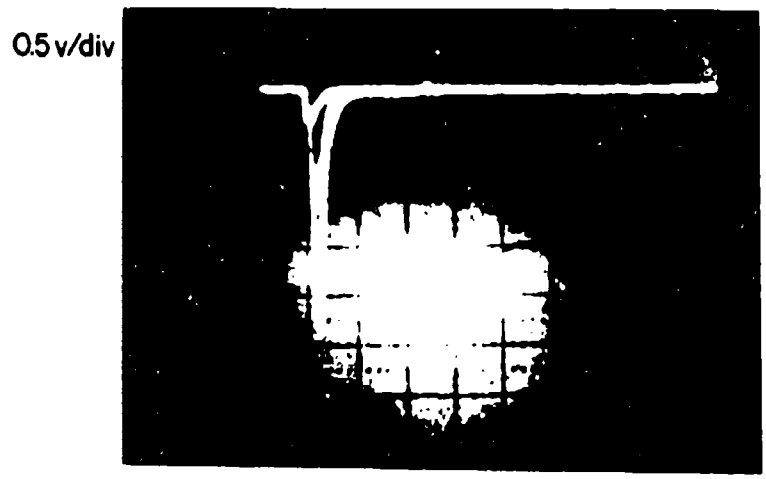

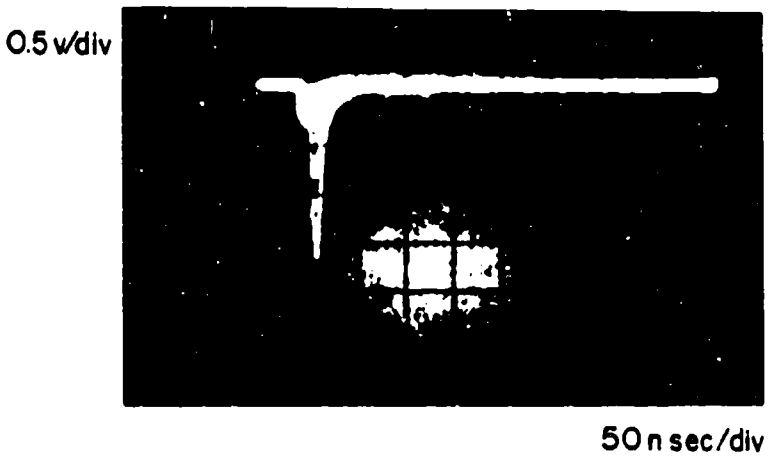

FIG. 3.5 "COSMIC RAYS" AS DETECTED BY DETECTOR II.

(a) Highest amplitude recorded in 10 min, (b) "cosmic rays" of several strengths, (c) "cosmic rays" and Co^{60} photons imposed.

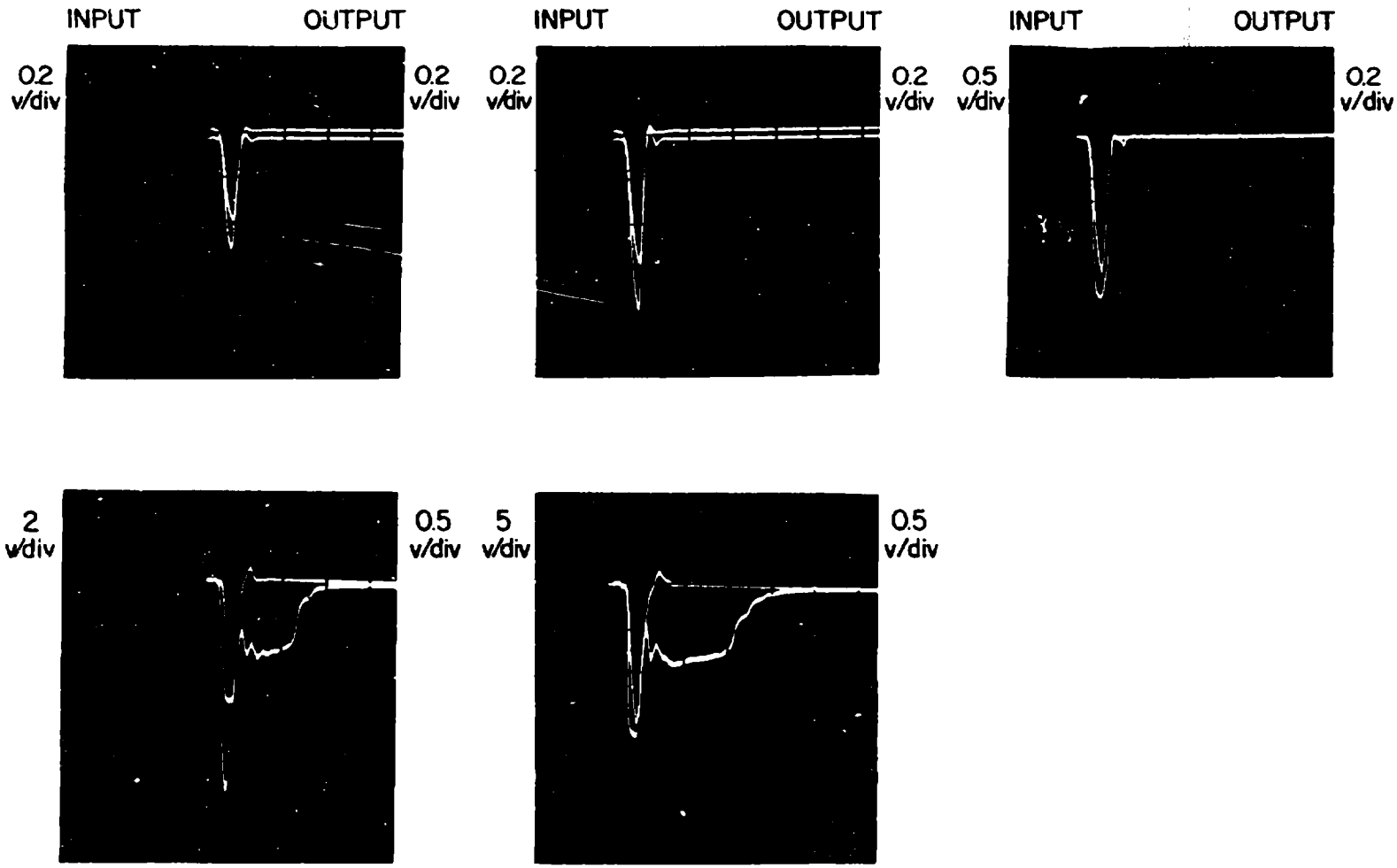

FIG. 3.6 INPUT VS OUTPUT SIGNALS OF DISCRIMINATOR. SWEEP RATE: 50 NSEC/DIV.

Note: Output is always smaller than input.

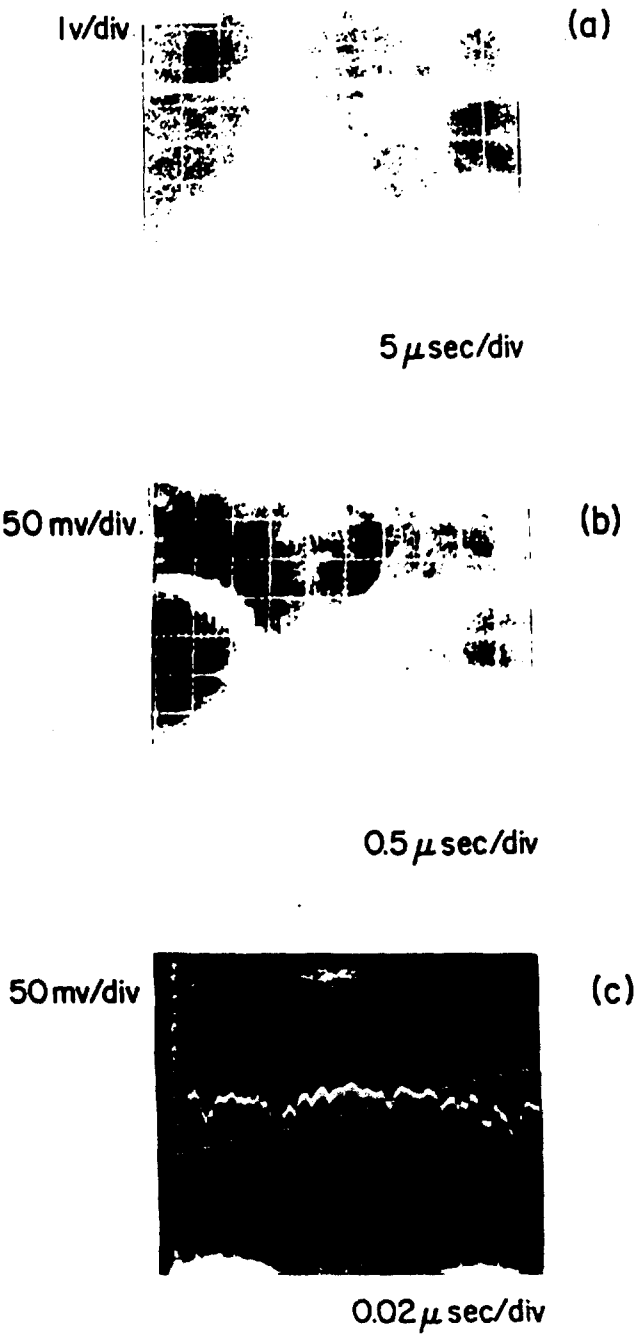

FIG. 3.7 DETECTOR II SIGNALS AT 30 FT-8 IN FROM NEUTRON SOURCE.
(b) is equal to (a) but with higher sensitivity and faster sweep rate, while (c) is a further enlargement of signal tail of (b).

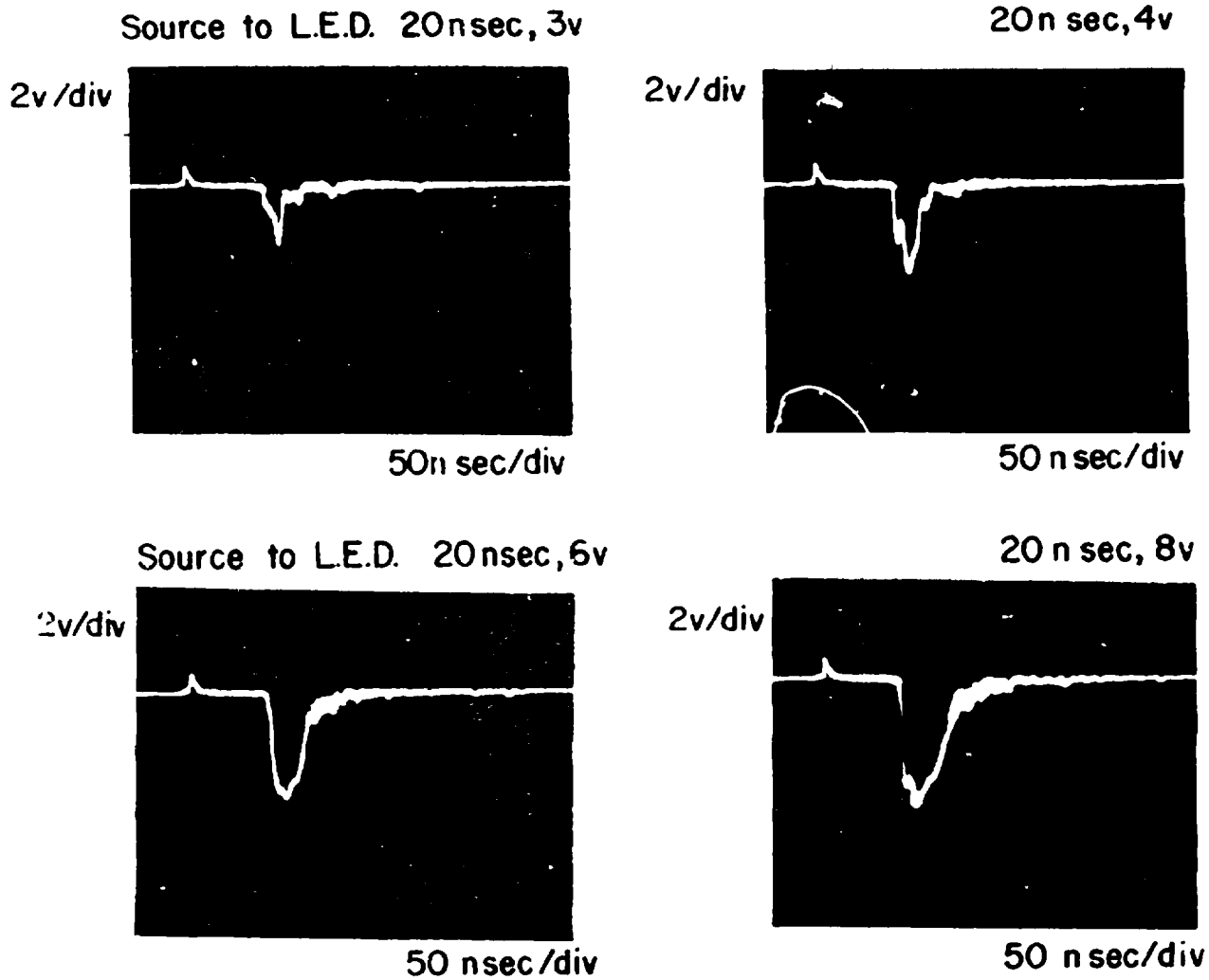

FIG. 3.8 OUTPUT OF PMT I FOR SEVERAL VOLTAGE INPUTS, WITH CONSTANT DURATION TO LED.

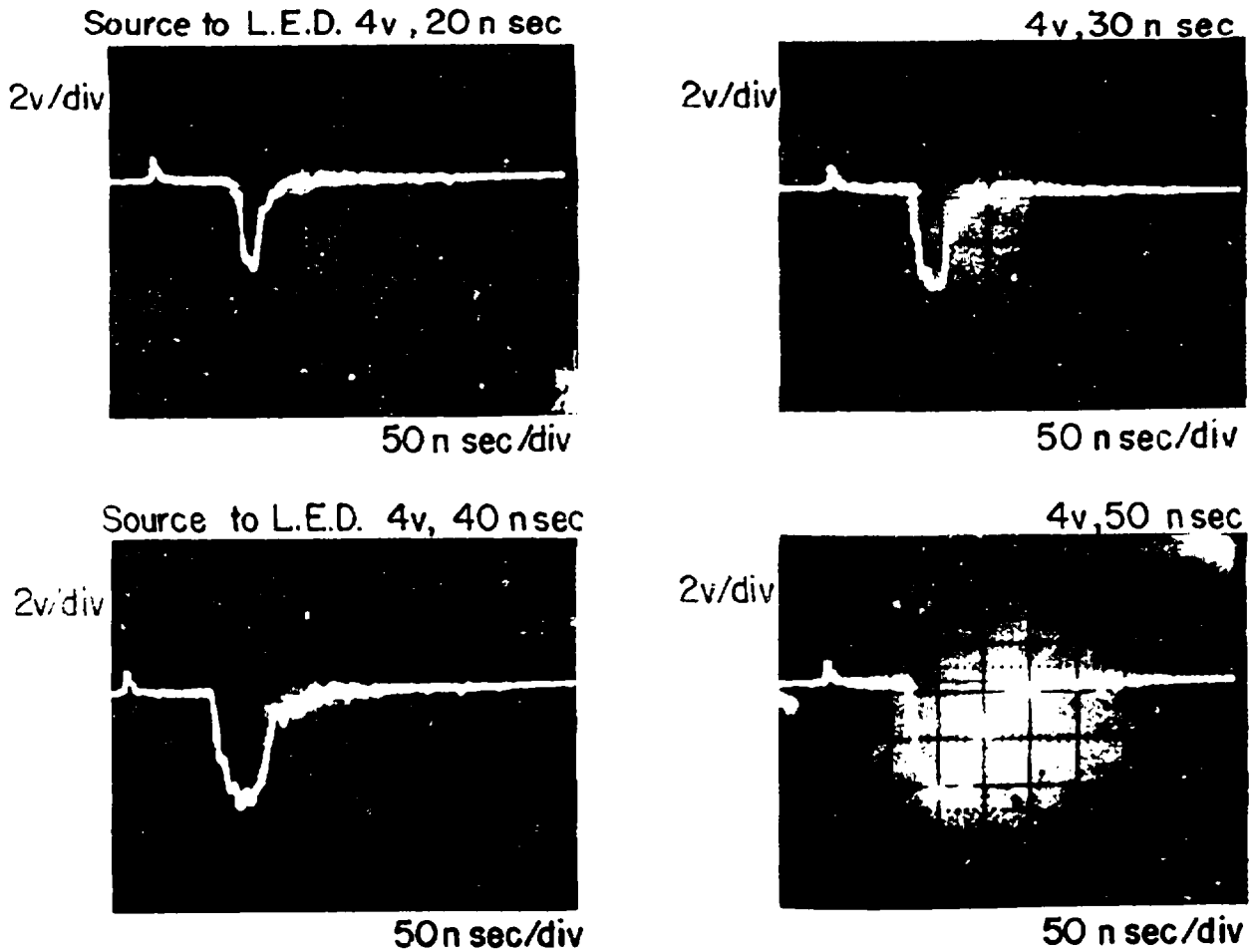

FIG. 3.9(a) OUTPUT OF PMT I FOR SEVERAL DURATIONS, AT CONSTANT VOLTAGE INPUTS TO LED.

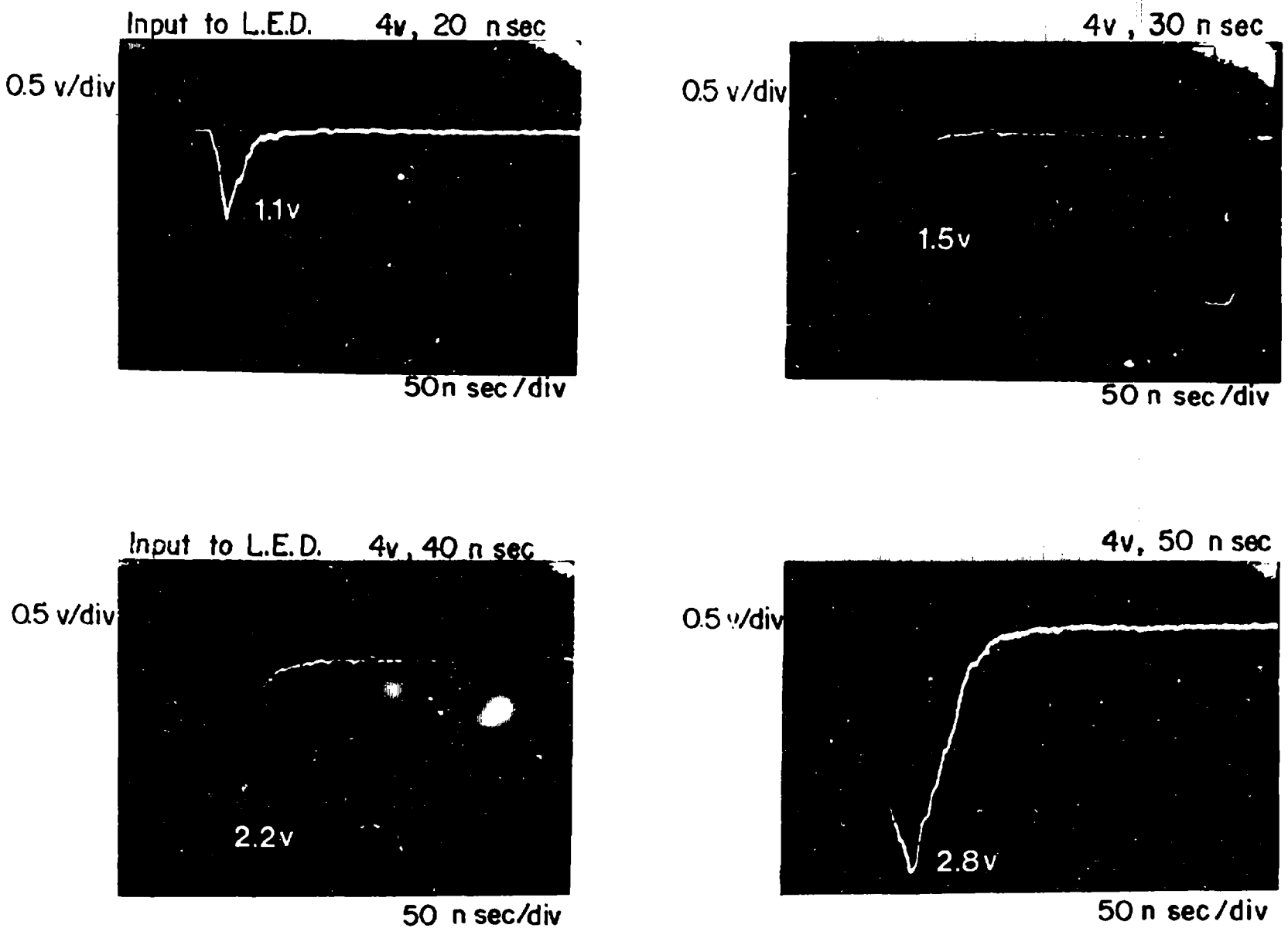

FIG. 3.9(b) OUTPUT OF PMT II FOR SEVERAL DURATIONS AT CONSTANT VOLTAGE INPUTS TO LED.

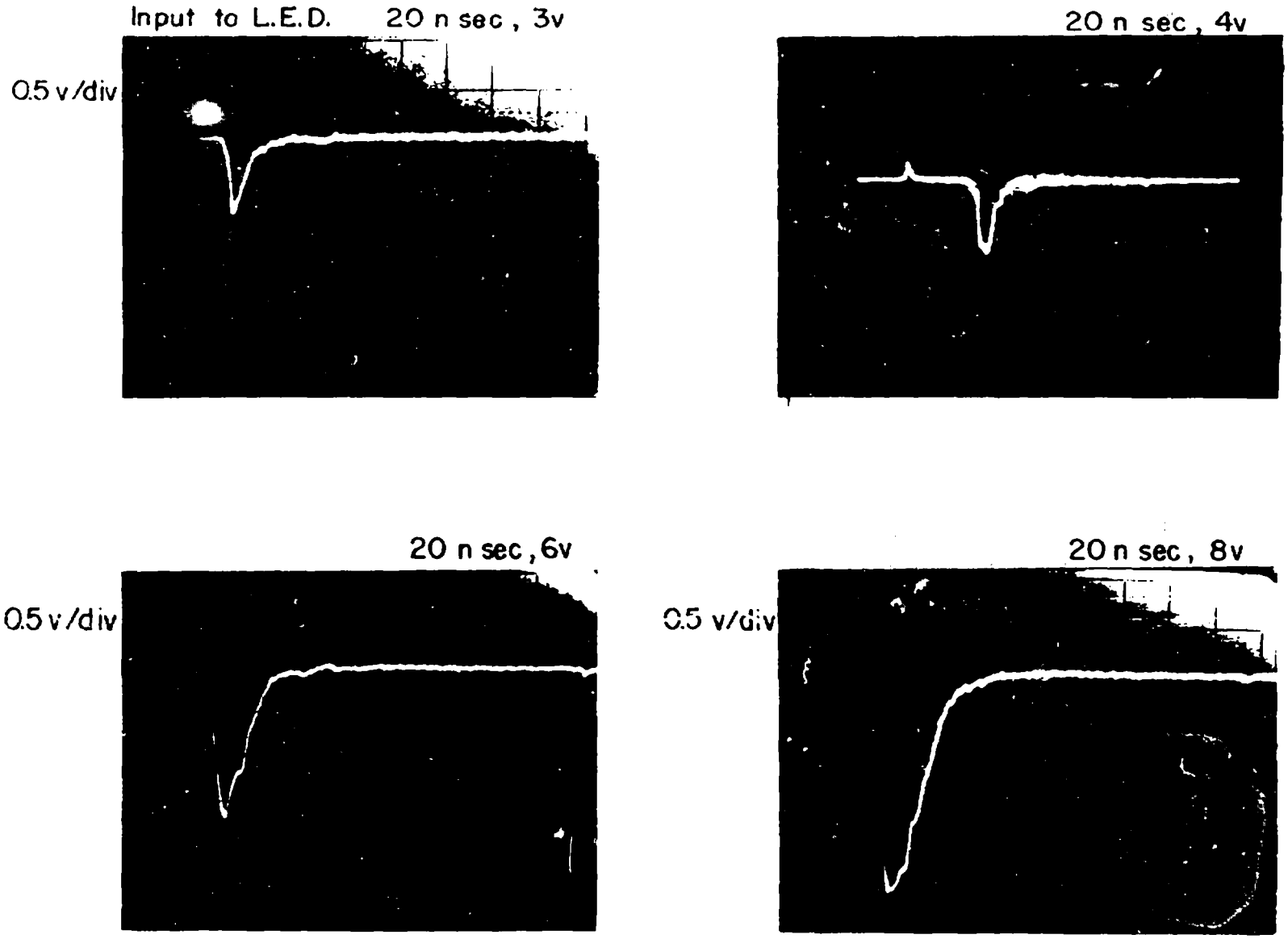

FIG. 9 - CONTINUED.

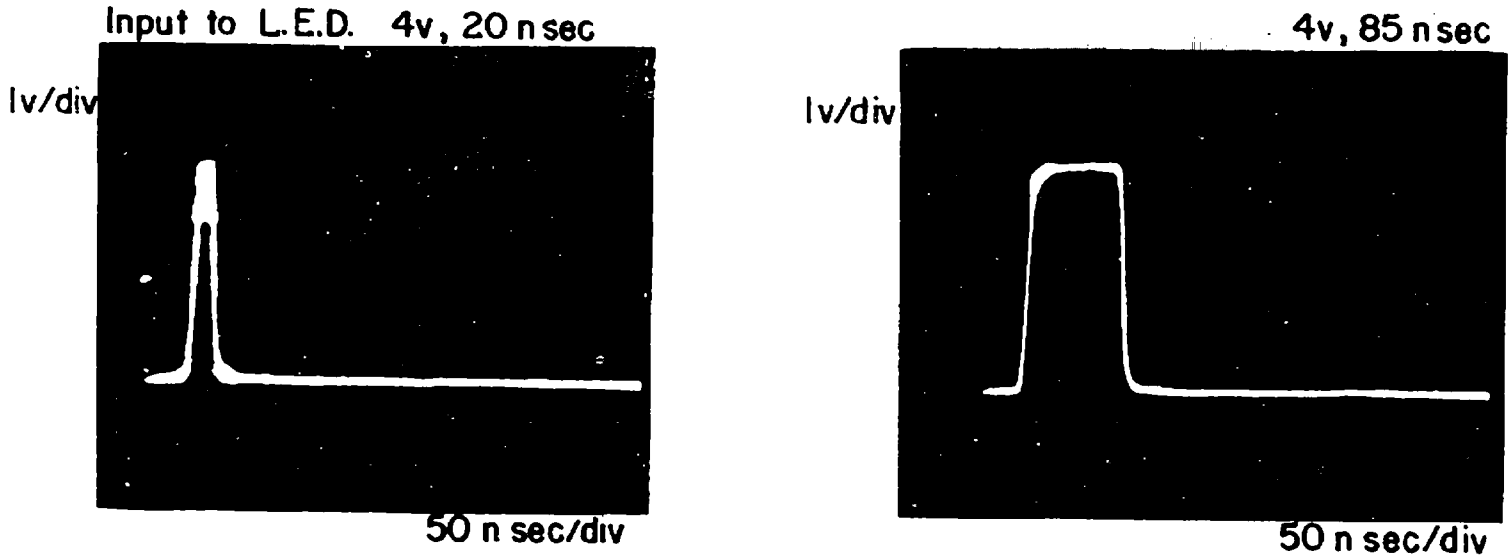

FIG. 3.9(c) TYPICAL INPUTS TO LED.

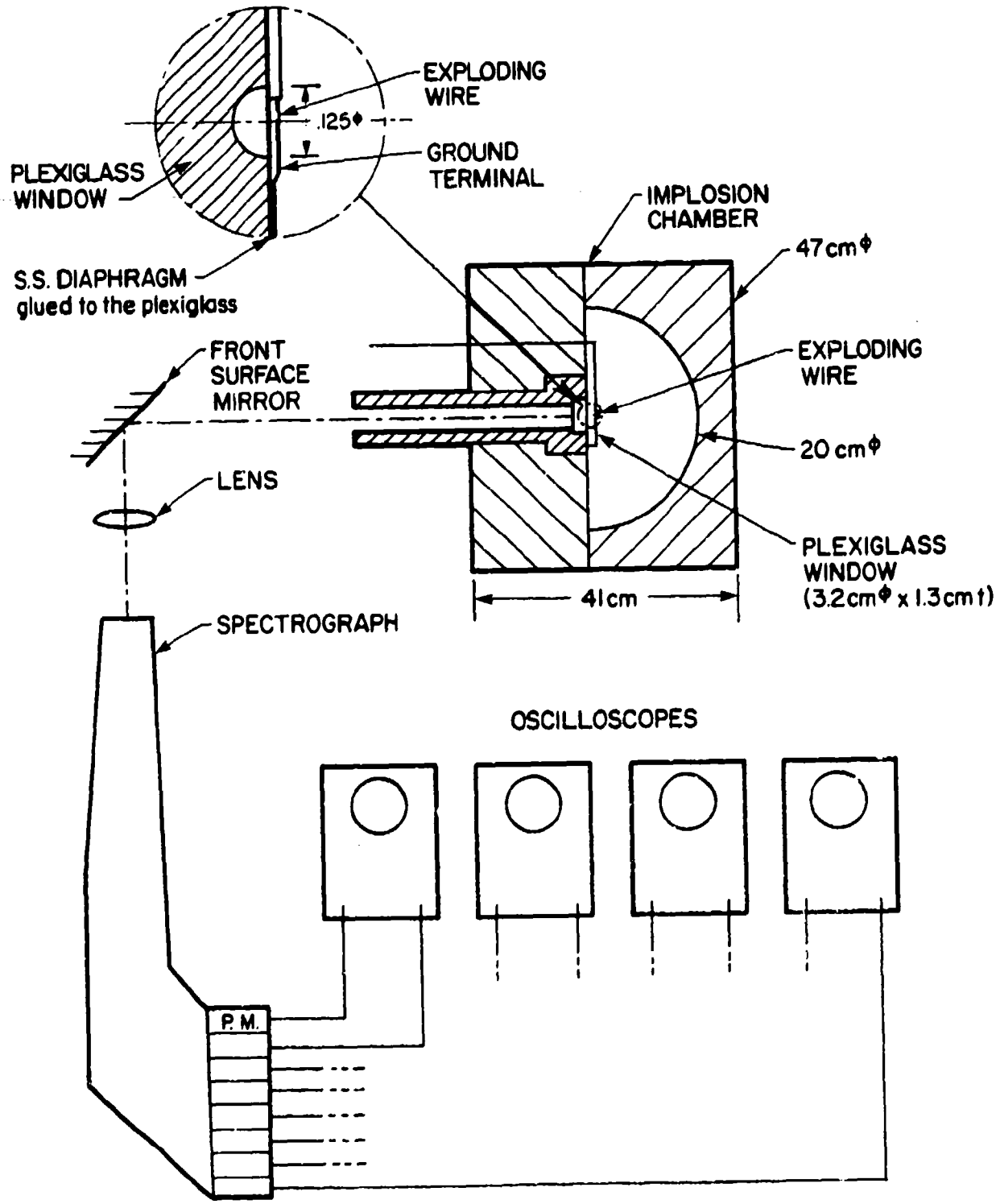

FIG. 3.10(a) SCHEMATIC DIAGRAM OF EXPERIMENTAL FACILITY USED TO STUDY DIAPHRAGM SURVIVAL DURING DETONATION-IMPLOSION PROCESS.

Note: The system was originally used to study temperatures near spherical implosion foci (Ref. 21).

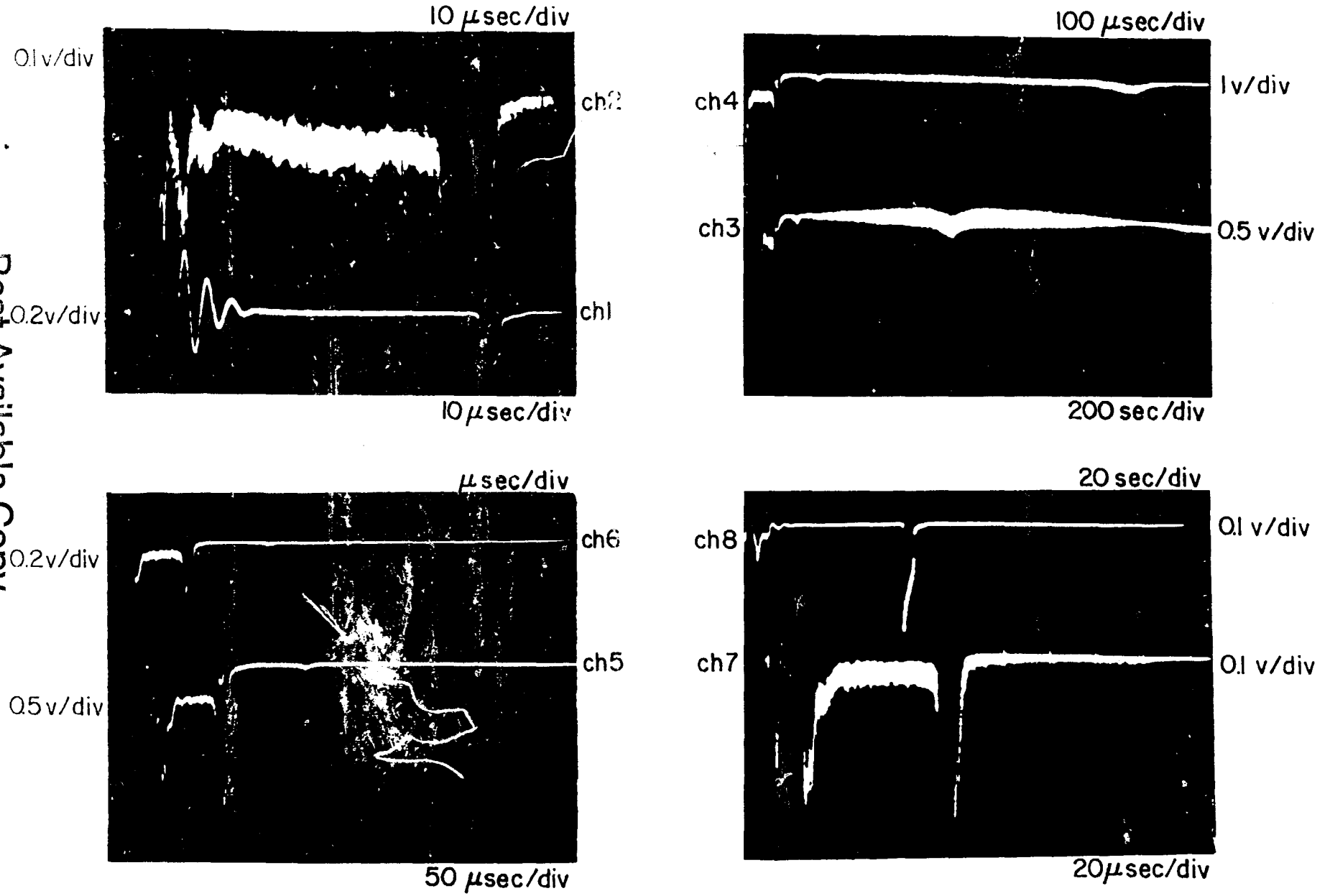

FIG. 3.10(b) SPECTROSCOPE-PMT DISPLAYS SHOWING COLLAPSE OF A .002" STAINLESS STEEL DIAPHRAGM. INITIAL PRESSURE IN THE CHAMBER: 400 PSI

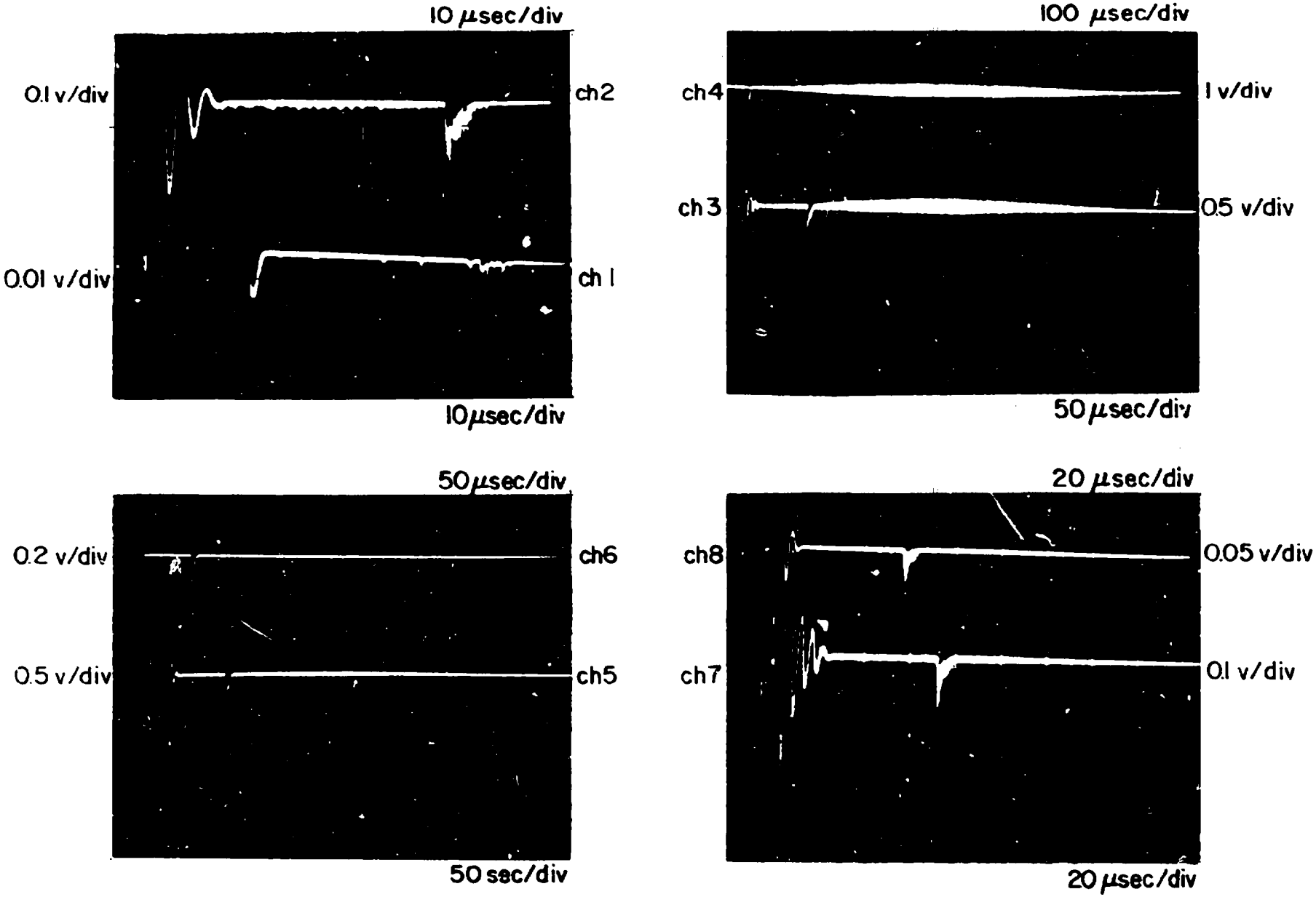

FIG. 3.10(c) SPECTROSCOPE-PMT DISPLAYS SHOWING COLLAPSE OF A .C05" STAINLESS STEEL DIAPHRAGM. INITIAL PRESSURE IN THE CHAMBER: 400 PSI.

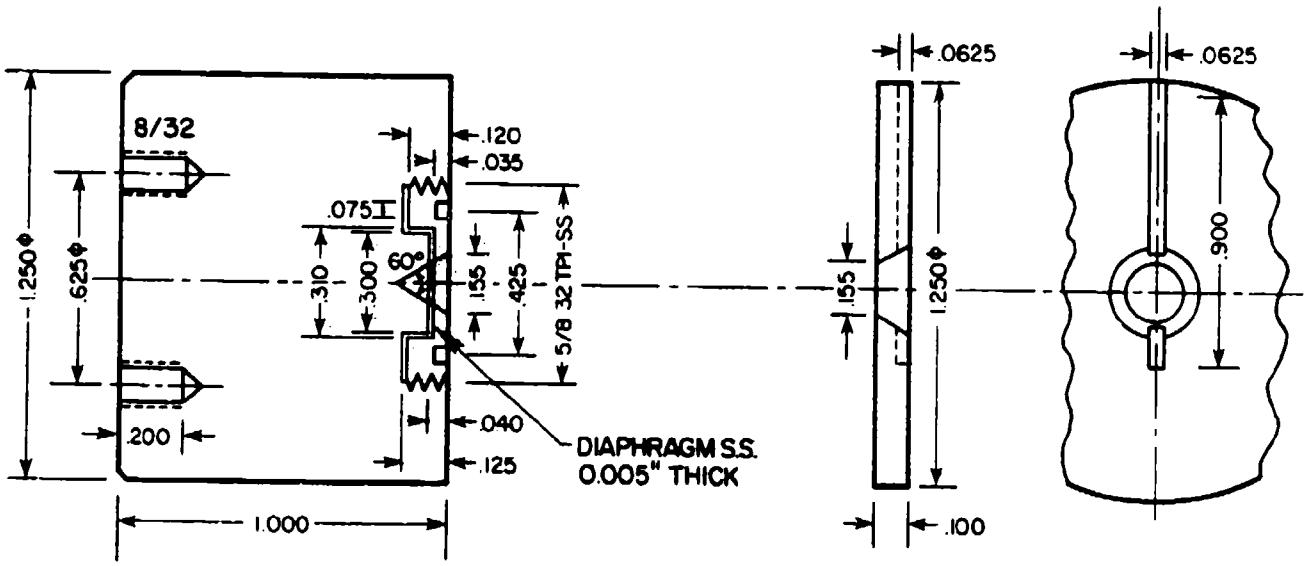

FIG. 3.11 FLAT DIAPHRAGM CAPSULE. MATERIAL: 440C STAINLESS STEEL – HARDENED.

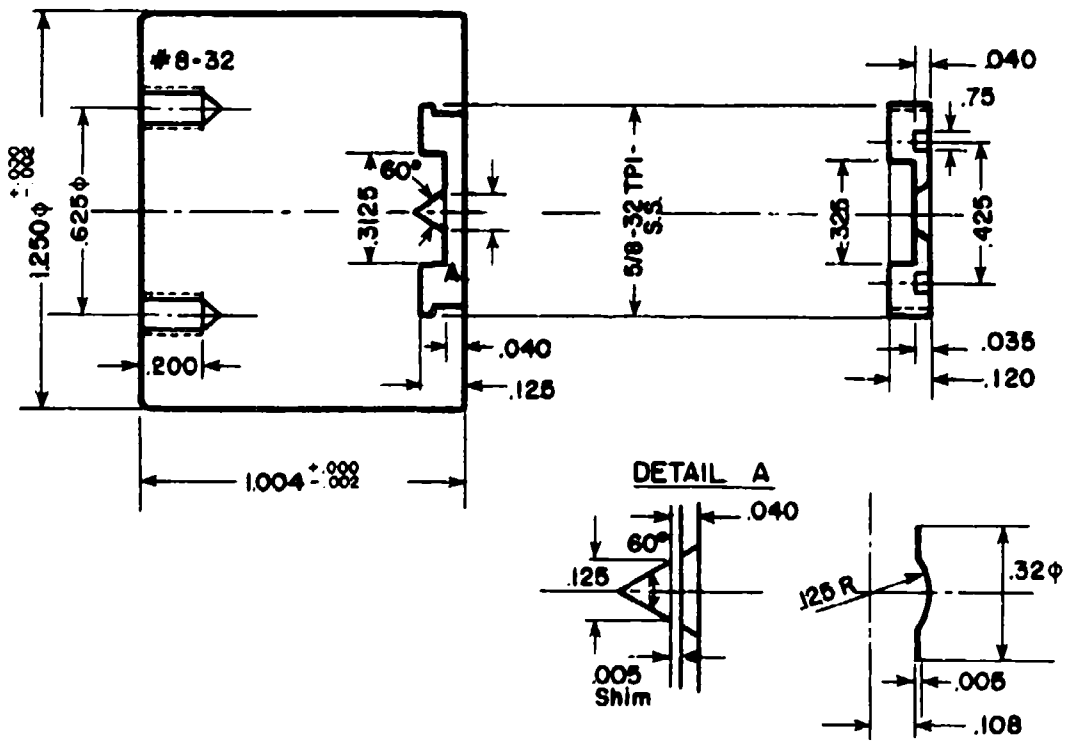

FIG. 3.12(a) SPHERICAL SECTOR CAPSULE. MATERIAL: 440C STAINLESS STEEL – HARDENED.

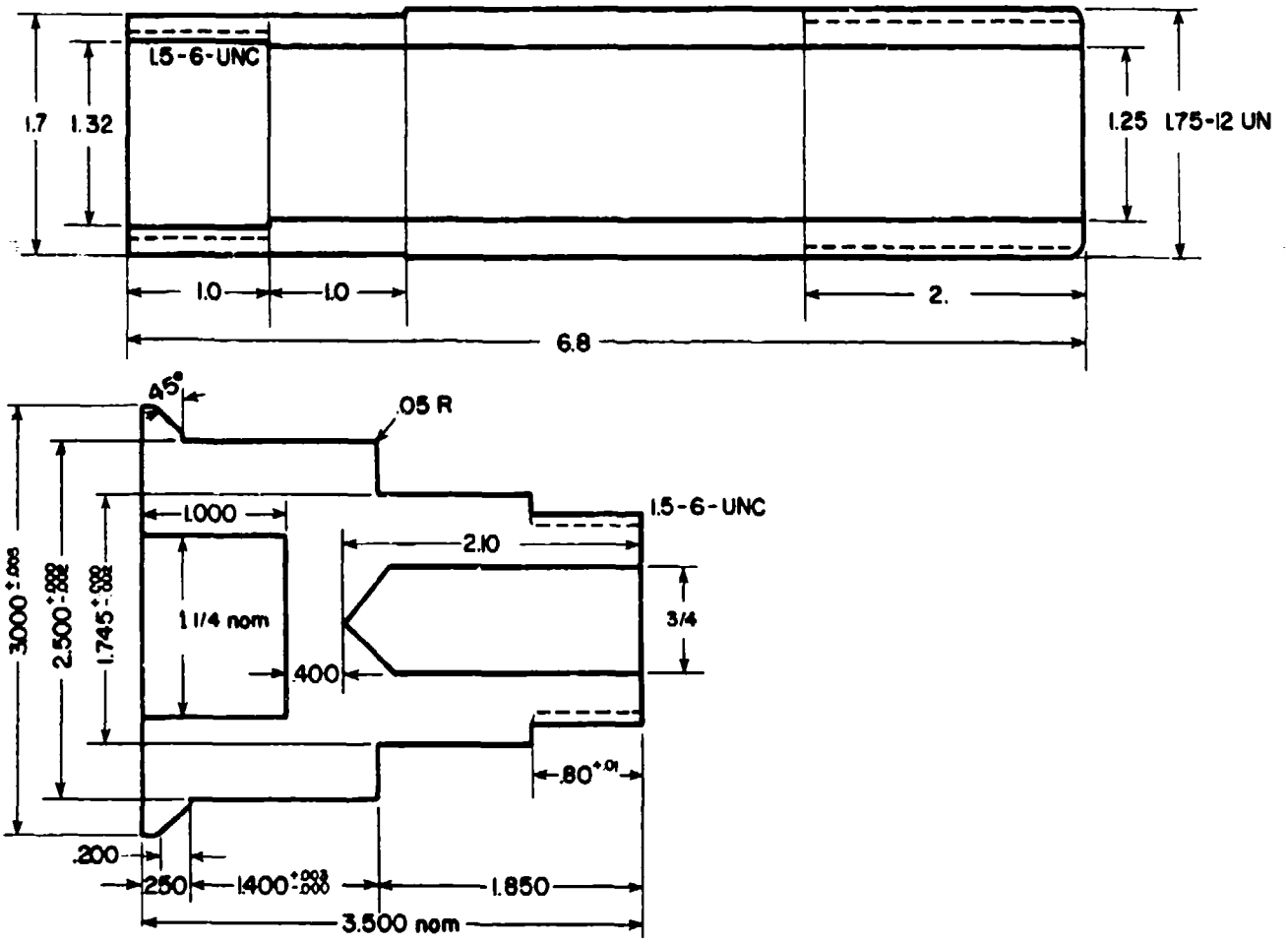

FIG. 3.12(b) STANDARD BARREL AND EXTENSION TUBE.

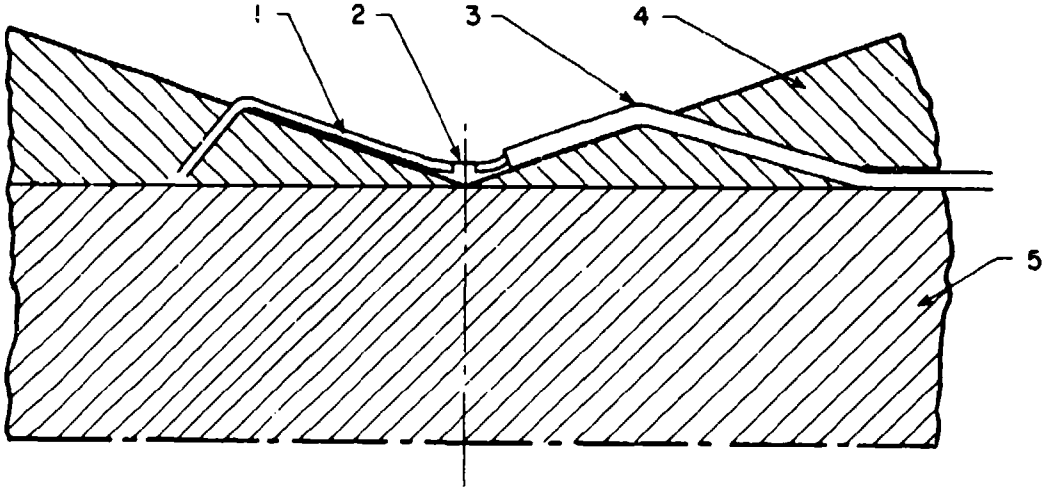

FIG. 3.13 EXPLODING WIRE FOR DIRECT IMPLOSION OF $2D_2+O_2$ MIXTURE.

1. Copper terminal. 2. Nickel exploding wire. 3. Teflon insulated terminal. 4. Conical liner. 5. Barrel.

Note: For general view see Fig. 1.4.

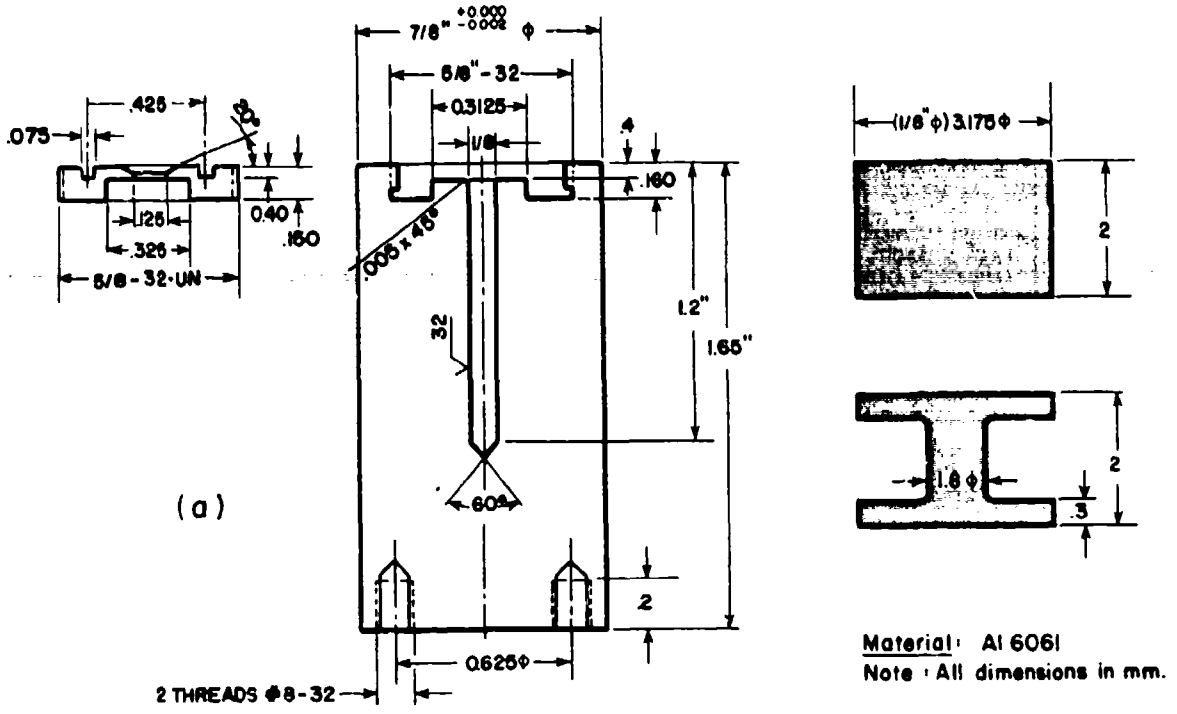

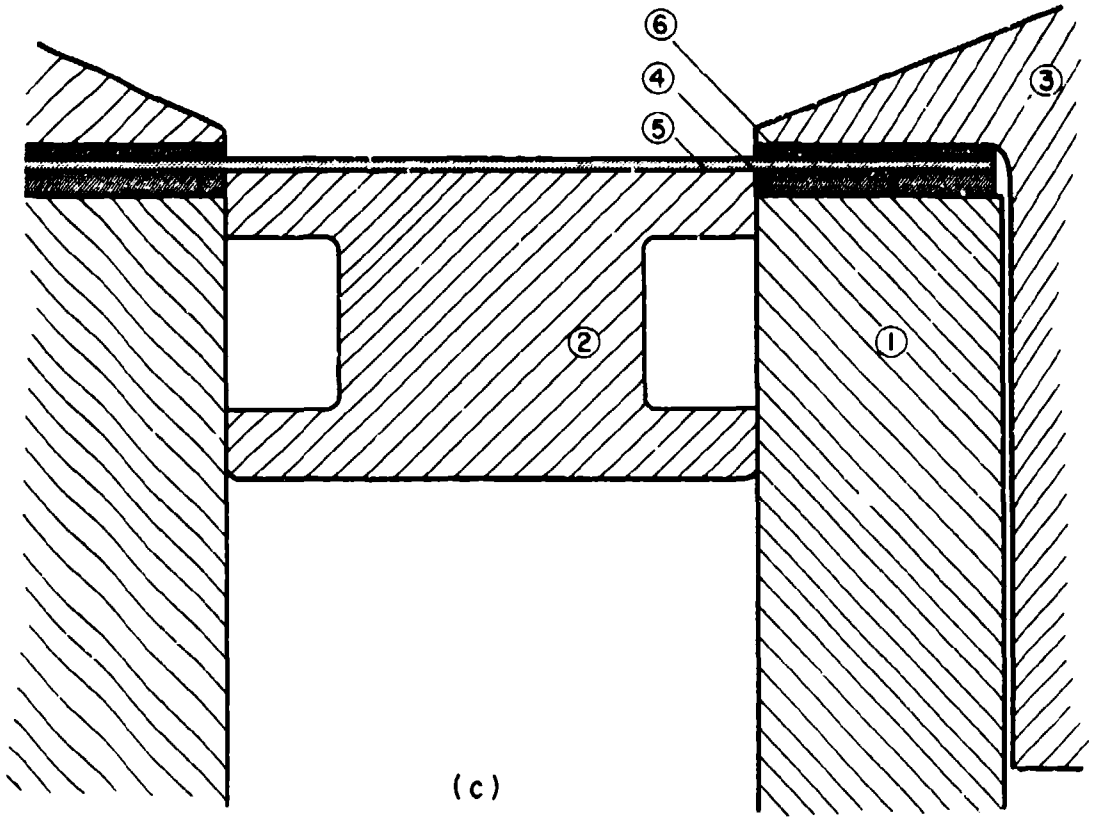

FIG. 3.14 CAPSULE AND PROJECTILE.

(a) Projectile capsule. (b) Projectile. (c) Projectile capsule assembly details.

1. Capsule body, hardened stainless steel. 2. Projectile, Al 6061. 3. Squeezing nut, steel. 4. Polyethylene seal, 0.008". 5. Diaphragm, 0.005" stainless steel. 6. Washer, 0.002" Mylar.

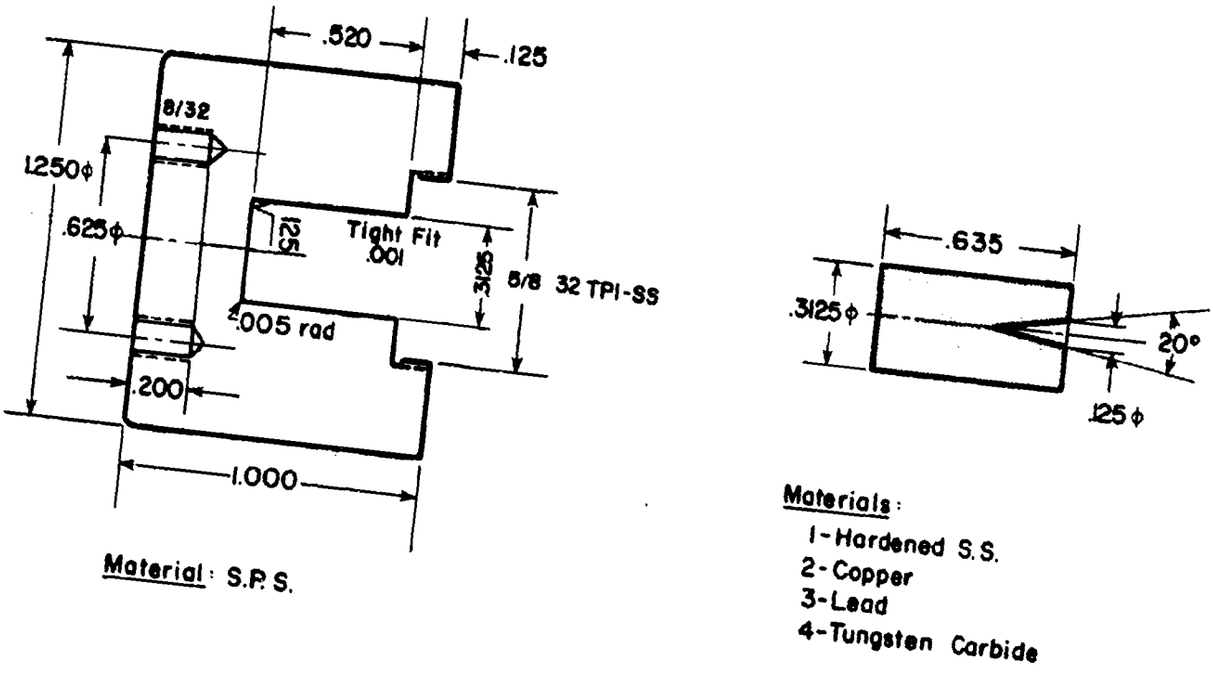

FIG. 3.15 SHALLOW CONE CAPSULE.

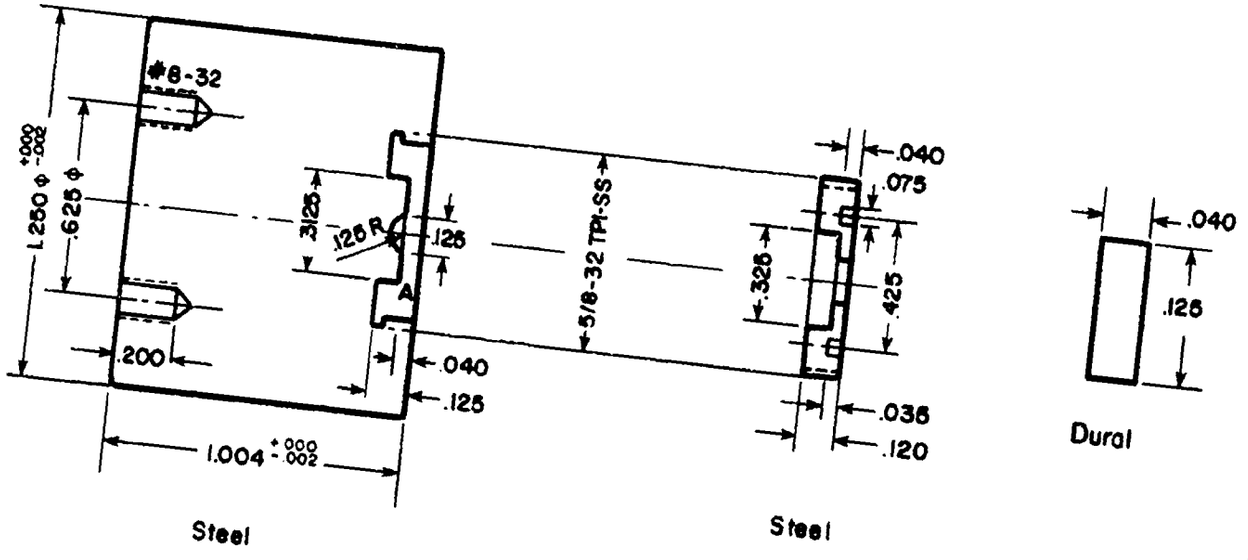

FIG. 3.16(a) VOITENKO CAPSULE.

FIG. 3.16(b) VOITENKO CAPSULE – ASSEMBLY DETAILS.

1. Capsule body, hardened stainless steel. 2. Polyethylene seal, 0.008". 3. Stainless steel diaphragm, 0.005". 4. Mylar washer, 0.002". 5. Squeezing nut, steel. 6. Stem, aluminum, 0.04". 7. Conical liner.

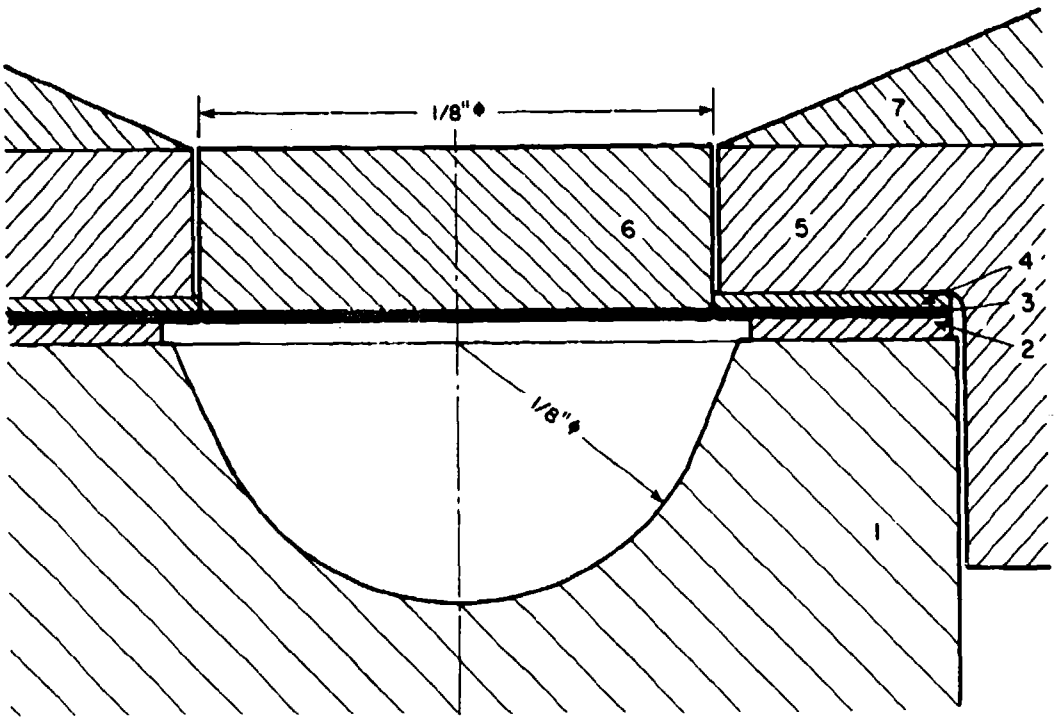

FIG. 3.16(c) VOITENKO CAPSULE WITH FLYER PLATE ASSEMBLY DETAILS. SCALE 30:1.

1. Capsule body, hardened stainless steel. 2. Polyethylene seal, 0.008". 3. Mylar diaphragm, 0.028" (not to scale). 4. Mylar washer, 0.002". 5. Squeezing nut, steel. 6. Stem, aluminum, 0.04". 7. Conical liner. 8. Aluminum flyer, 0.04" (not to scale).

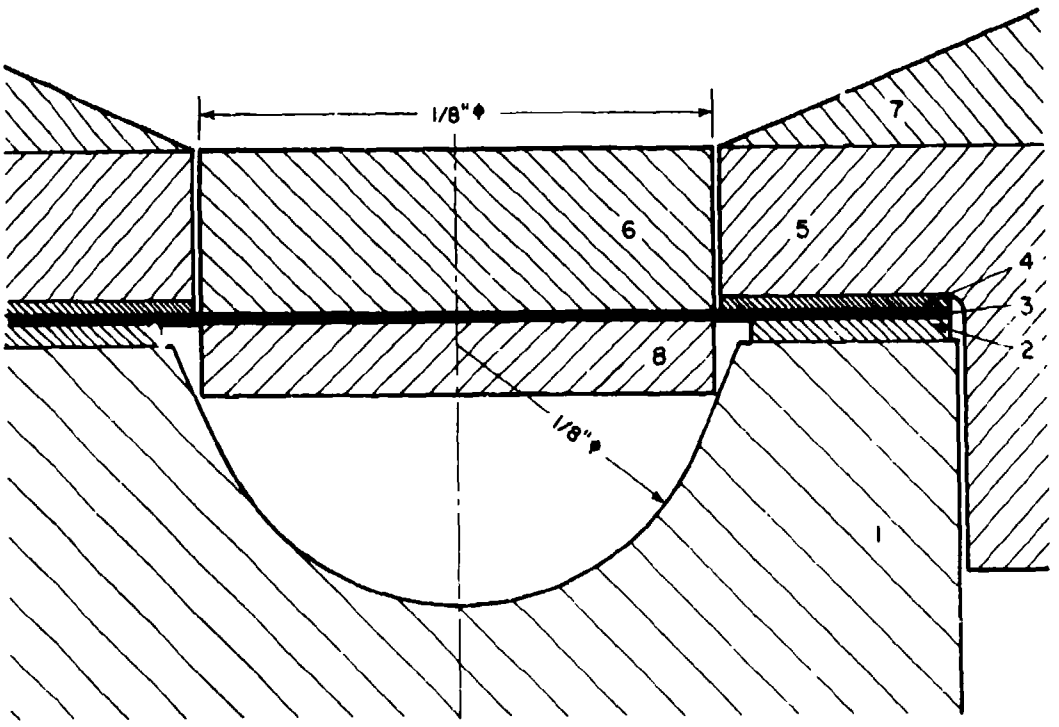

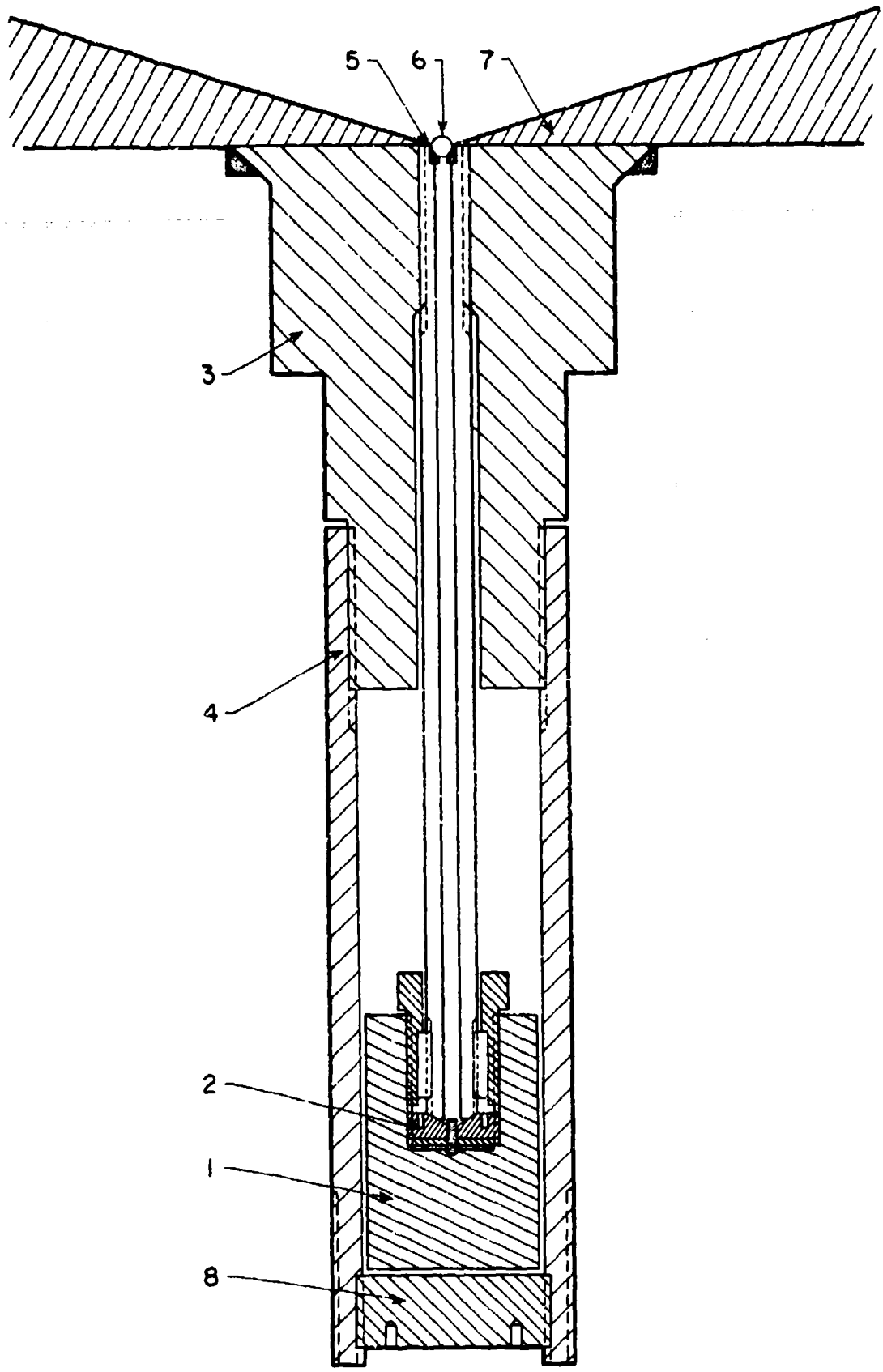

FIG. 3.17(a) 9" ACCELERATION TUBE. SCALE 1:1.

1. Capsule body. 2. Capsule nut. 3. Barrel. 4. Barrel extension. 5. Inlet sealing seat. 6. Projectile. 7. Conical liner. 8. Safety shield.

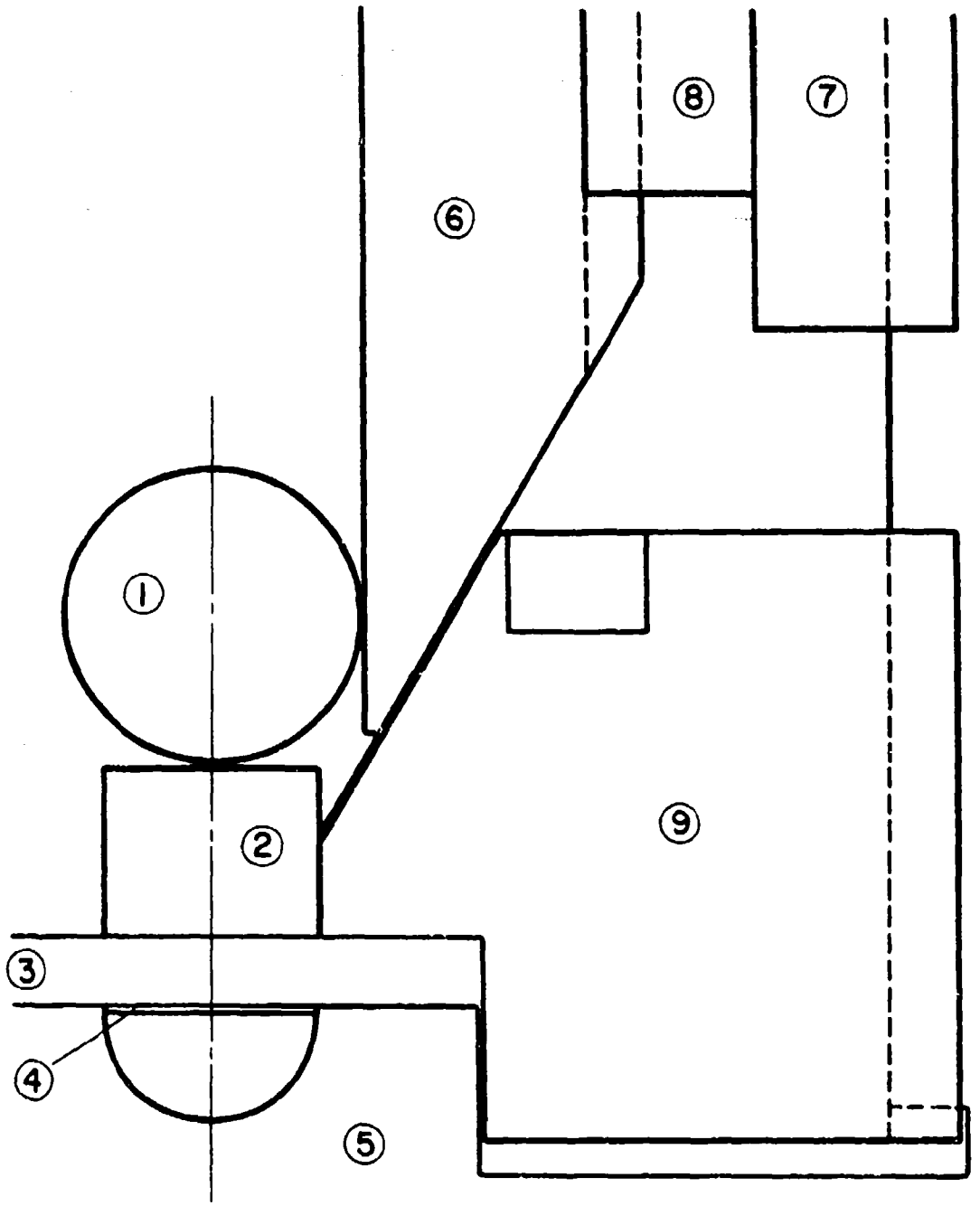

FIG. 3.17(b) COMMERCIAL DESIGN — DETAILS OF CAPSULE ASSEMBLY.

1. Projectile (steel). 2. Aluminum buffer. 3. Polyethylene diaphragm. 4. Stainless steel flyer. 5. Capsule (steel. 6. Accelerating tube (steel). 7. Gland nut (standard). 8. Sleeve (standard). 9. Squeezing nut.

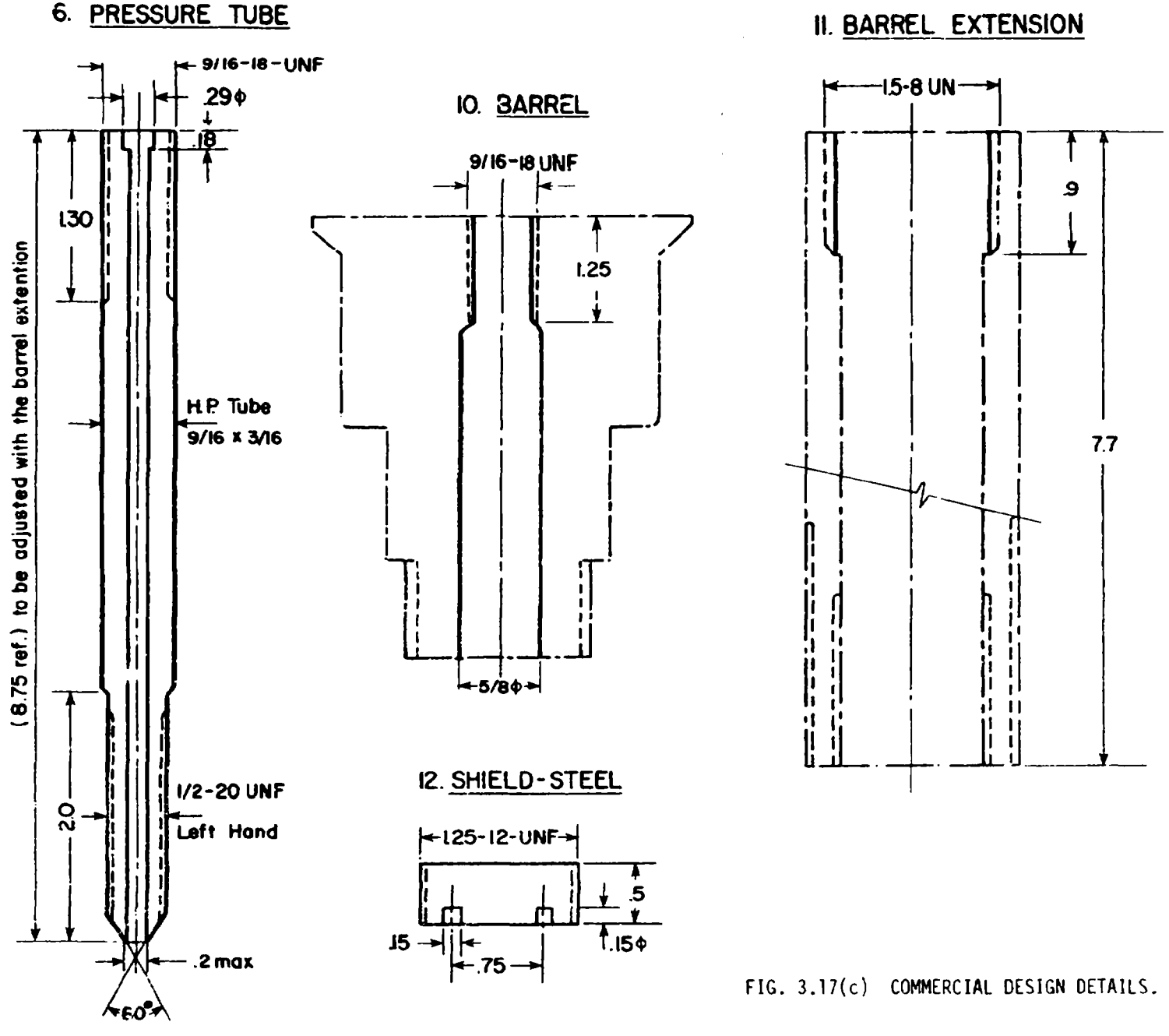

FIG. 3.17(c) COMMERCIAL DESIGN DETAILS.

9. SEALING NUT
S.P.S. Steel

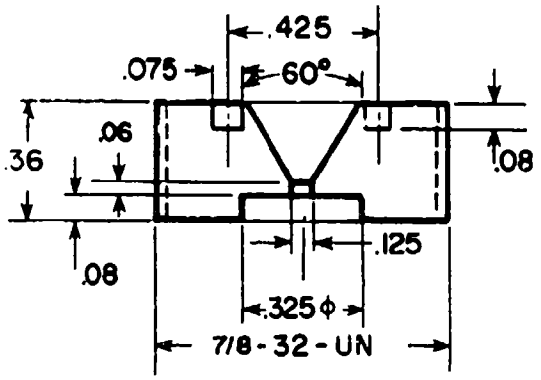

7. NUT
Mat. S.P.S. Steel

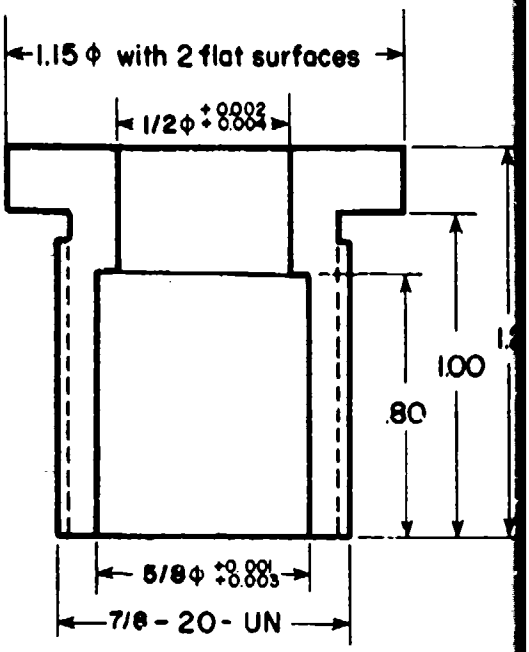

5. CAPSULE
Mat. S.P.S. Steel

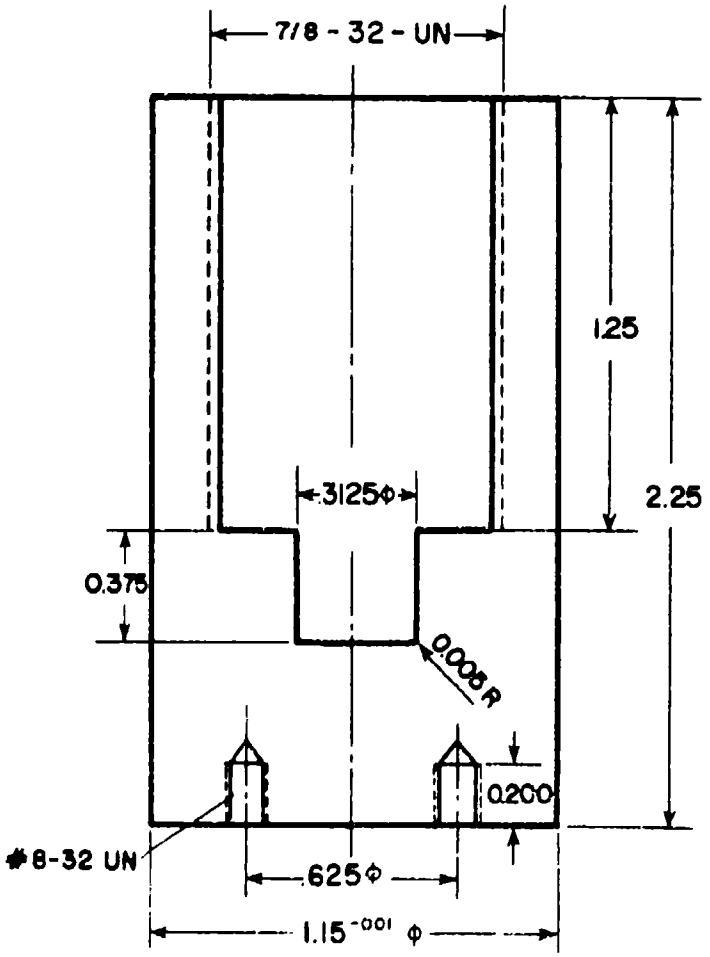

8. SLEEVE
S.P.S. Steel

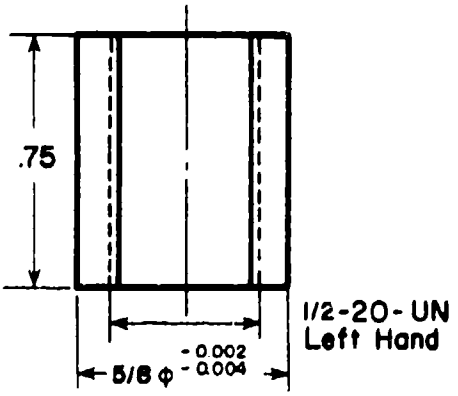

FIG. 3.17(d) COMMERCIAL DESIGN DETAILS.

FIG. 3.17e BARREL OF COMMERCIAL DESIGN AFTER RUN. THE DAMAGE AT THE ACCELERATING TUBE ENTRANCE IS RELATIVELY SMALL, AND THE HOLE THROUGH IS ALMOST CLEAR.

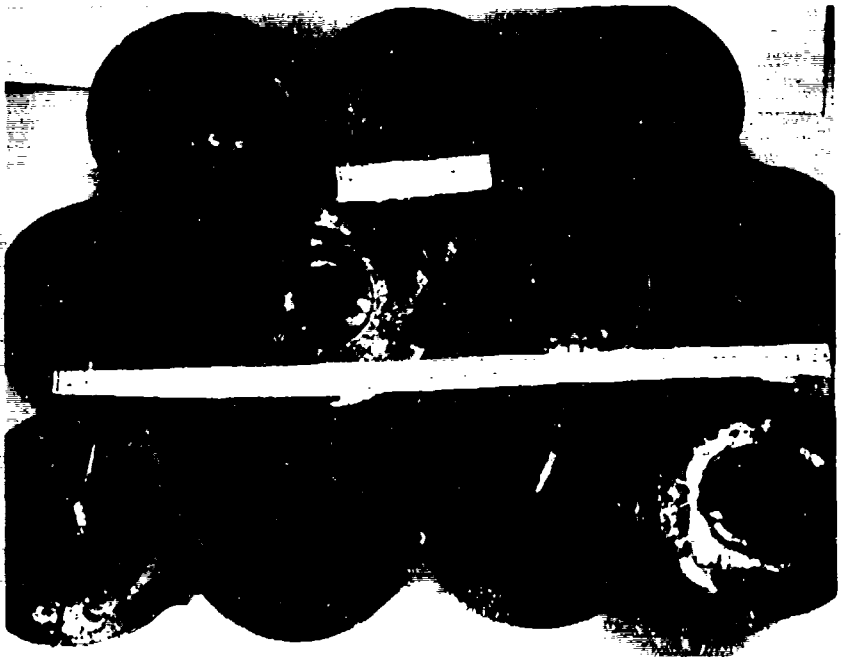

FIG. 3.18a TYPICAL CRATERS: UPPER ROW – DEFOCUSED RUNS, CENTRE ROW – TYPICAL 100 + 120g RUNS, LOWER ROW -- TYPICAL 160g RUNS.

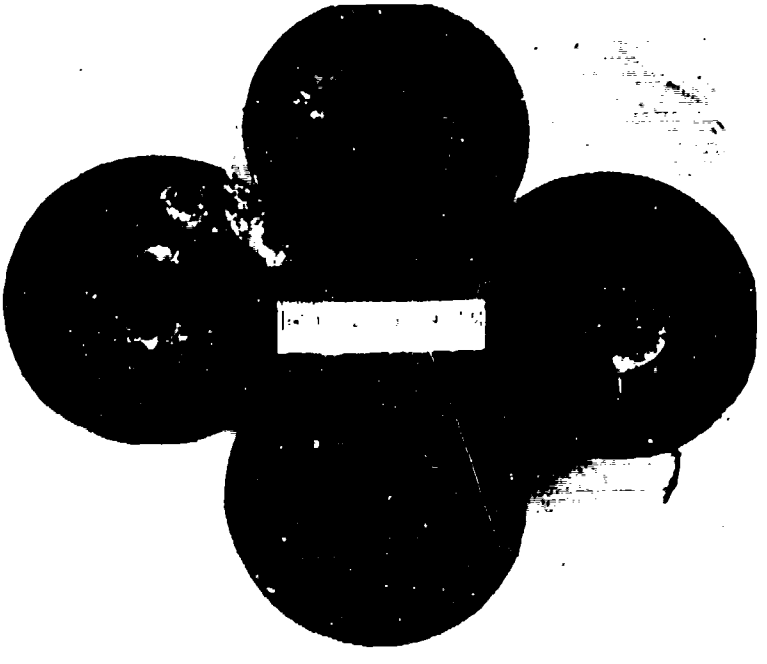

FIG. 3.18b TYPICAL DEFOCUSED RUNS.

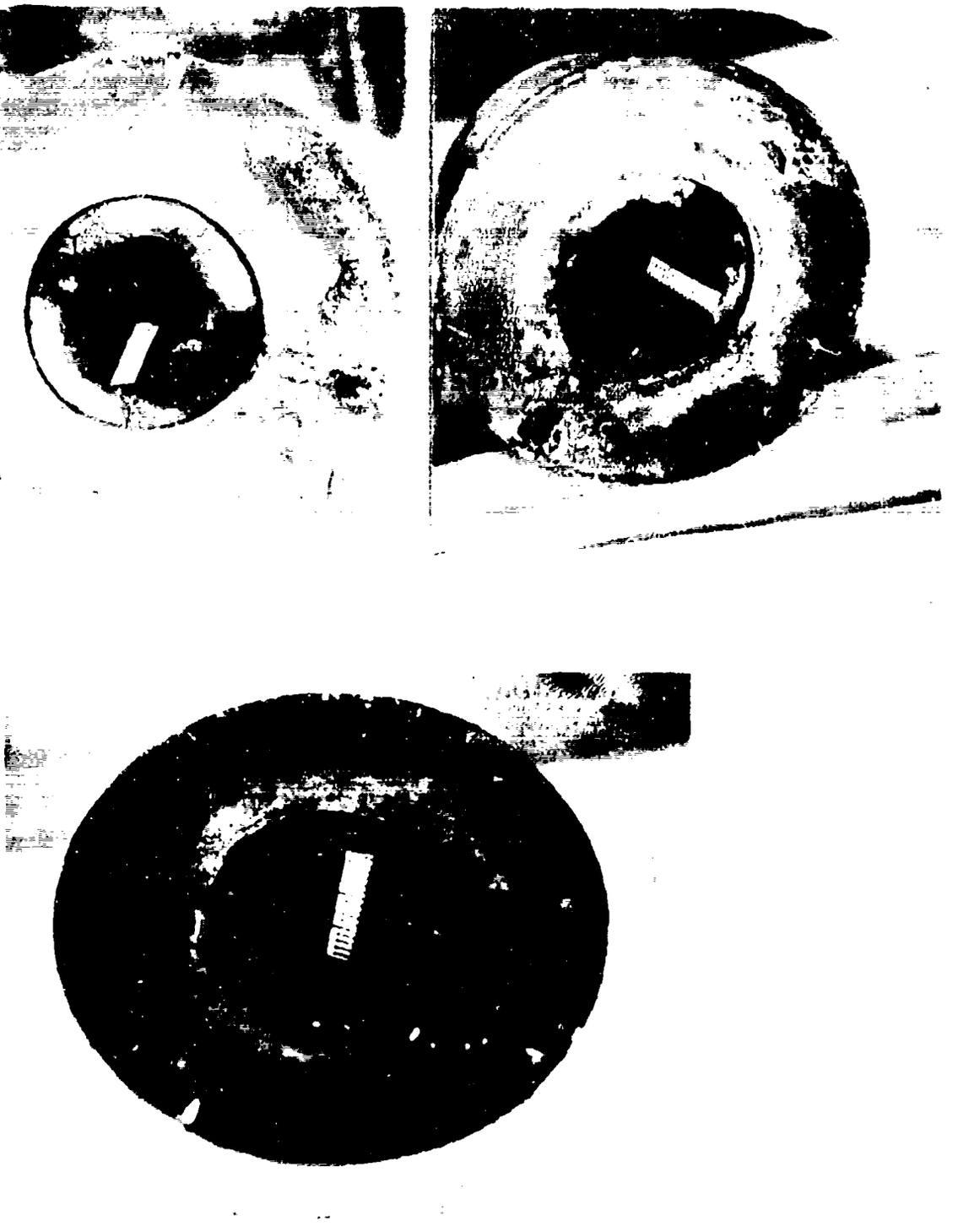

FIG. 3.19 TYPICAL WELL FOCUSED AND CENTERED CRATER.

EXPERIMENT: E1
CAPSULE DESIGN: VOITENKO (FIG. 3.16)
EXPLOSIVE WEIGHT: 113g
CRATER DIMENSIONS: 19mm DIA x 15mm DEEP

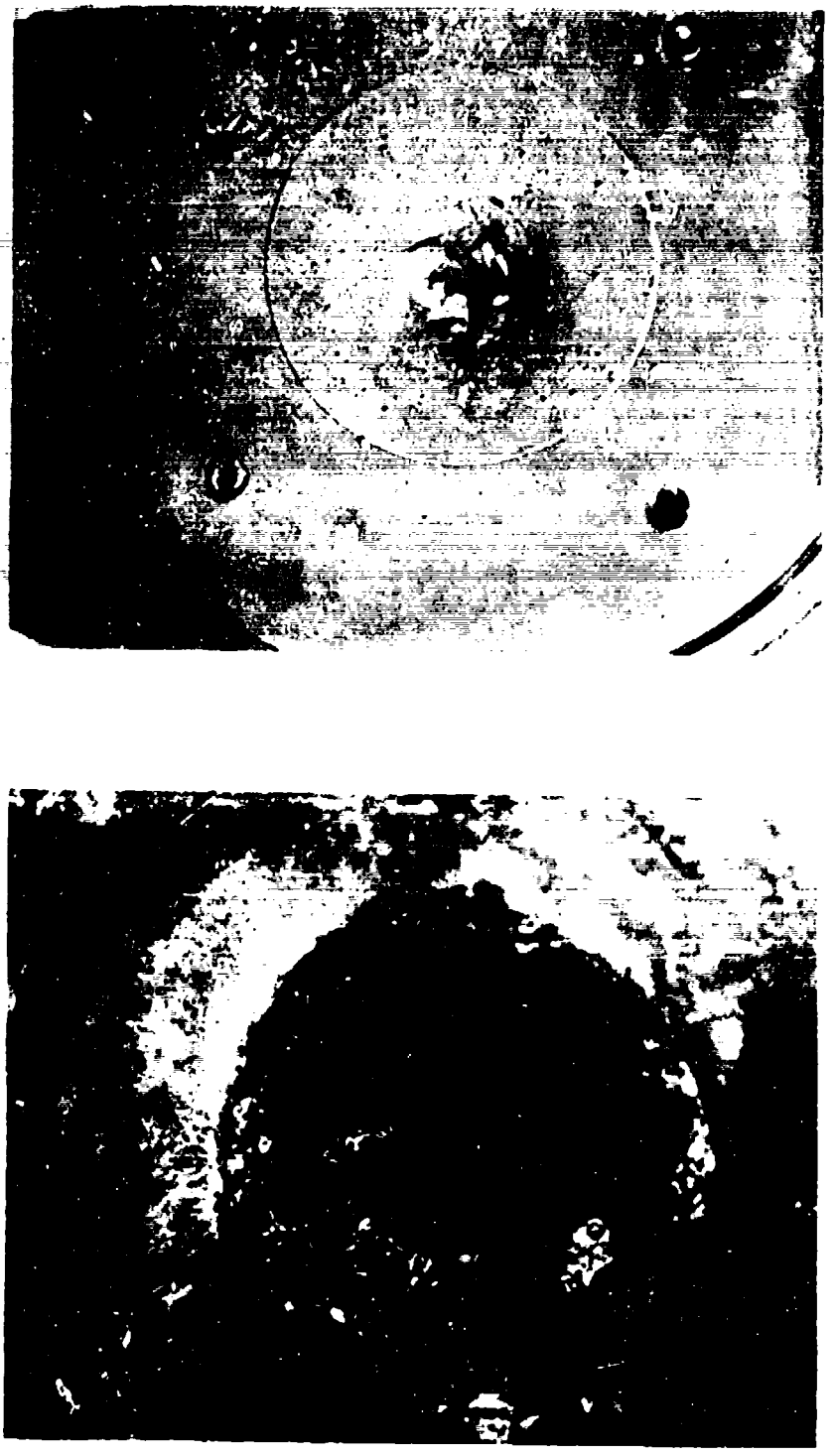

FIG. 3.20 CRATER BEFORE (a), AND AFTER (b) REMOVAL OF THE CONICAL LINER.

EXPERIMENT: A1
CAPSULE DESIGN: CONE (FIG. 3.11)
EXPLOSIVE WEIGHT: 162g
CRATER DIMENSIONS: 25mm DIA x 20mm DEEP

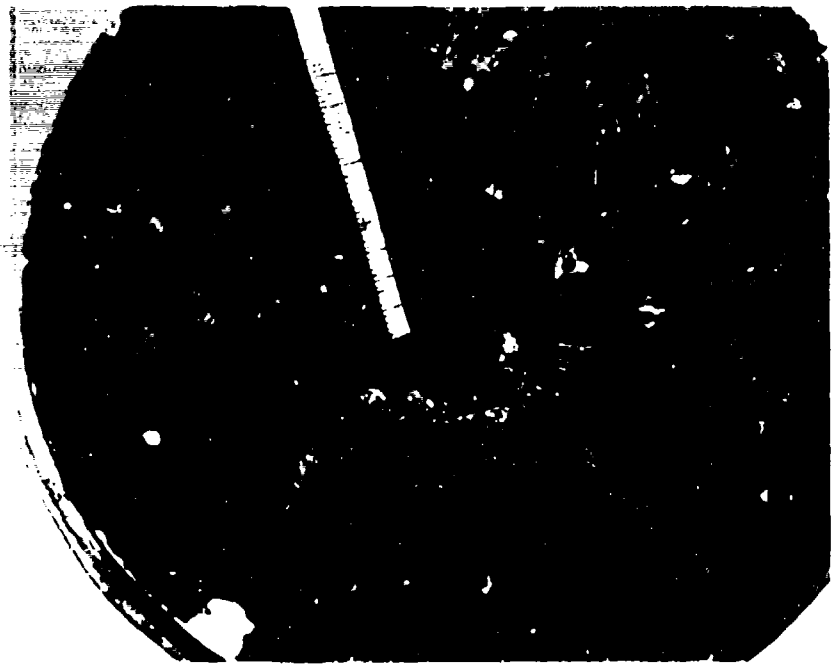

(a)

(b)

FIG. 3.21 CRATER BEFORE (a), AND AFTER (b) REMOVAL OF THE CONICAL LINER.

EXPERIMENT:	A2
CAPSULE DESIGN:	STANDARD CONE (FIG. 3.12)
EXPLOSIVE WEIGHT:	162g
CRATER DIMENSIONS:	20mm DIA x 15mm DEEP, OFF CENTRE BY 8mm

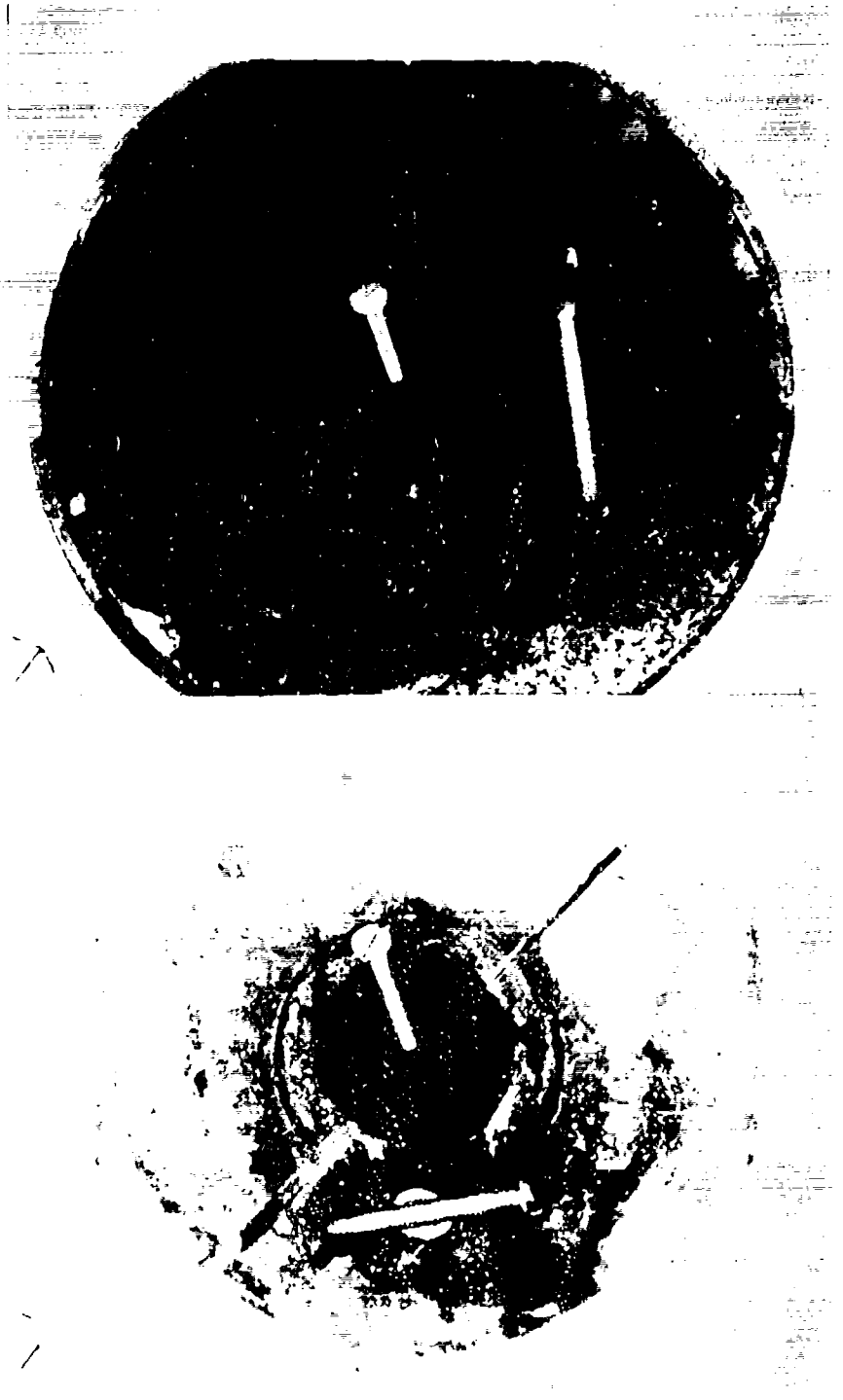

FIG. 3.22 CRATER BEFORE (a), AND AFTER (b) REMOVAL OF THE CONICAL LINER.

EXPERIMENT:	A3
CAPSULE DESIGN:	STANDARD CONE (FIG. 3.12)
EXPLOSIVE WEIGHT:	171g
CRATER DIMENSIONS:	21mm DIA x 18mm DEEP

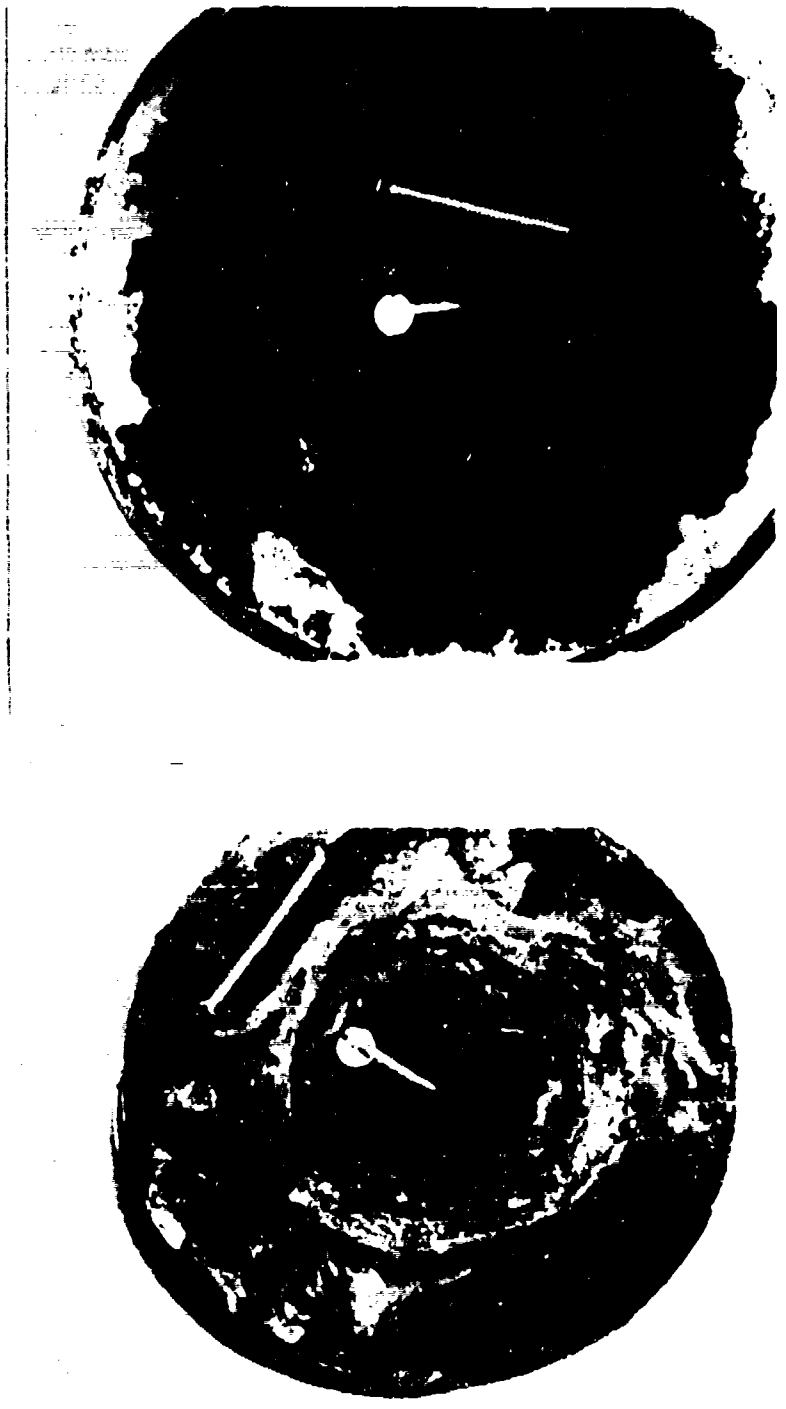

FIG. 3.23 WELL-FOCUSED CRATER, (a) AS TAKEN FROM THE CHAMBER, (b) AFTER REMOVAL OF THE CONICAL LINER.

EXPERIMENT: C2
CAPSULE DESIGN: SHALLOW CONE (FIG. 3.15)
EXPLOSIVE WEIGHT: 111g
CRATER DIMENSIONS: 15mm DIA x 20mm DEEP

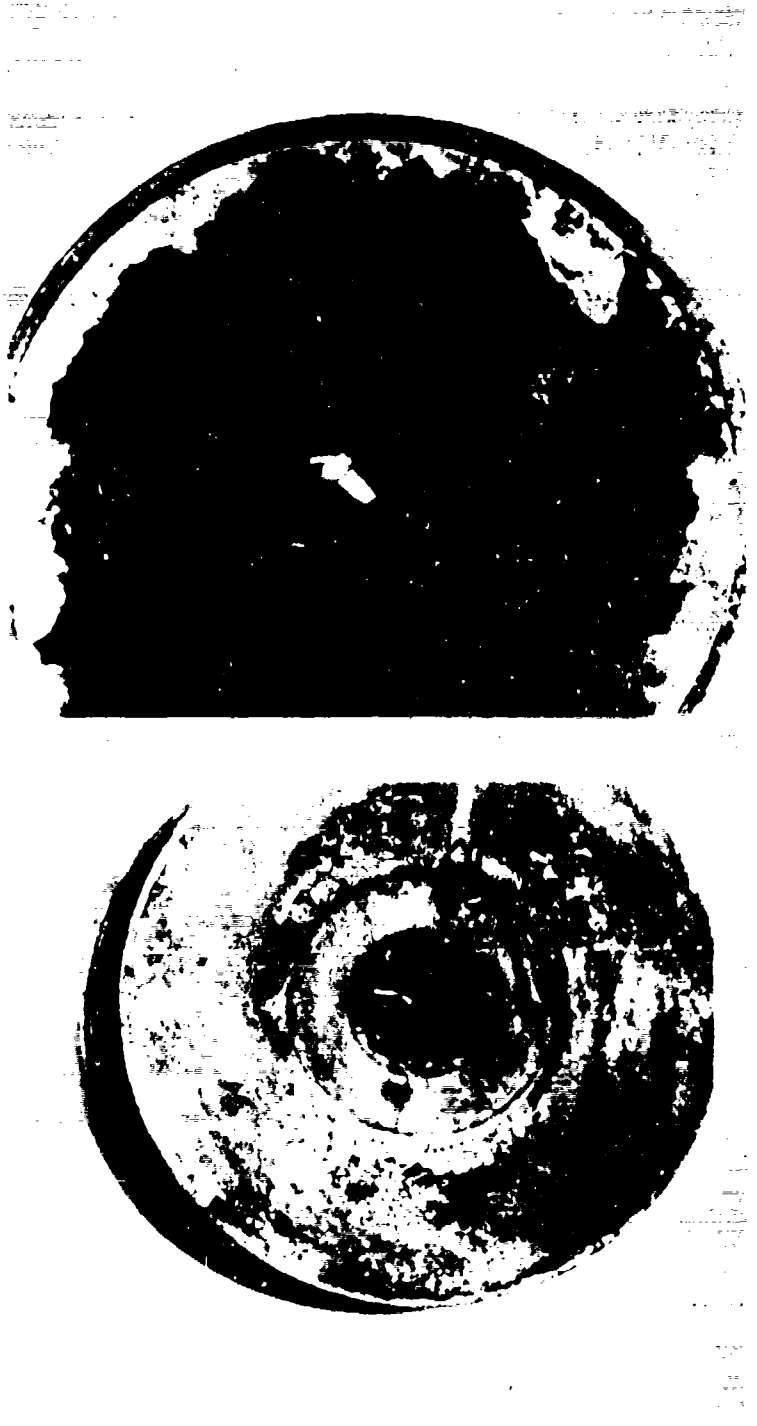

FIG. 3.24 WELL-FOCUSED CRATER, (a) AS TAKEN FROM THE CHAMBER, (b) AFTER REMOVAL OF THE CONICAL LINER.

EXPERIMENT: C3
CAPSULE DESIGN: STANDARD CONE (FIG. 3.12)
EXPLOSIVE WEIGHT: 132g
CRATER DIMENSIONS: 13mm DIA x 13mm DEEP

FIG. 3.25 CRATER BEFORE (a), AND AFTER (b) REMOVAL OF THE CONICAL LINER.

EXPERIMENT:	D2
CAPSULE DESIGN:	SHALLOW CONE (FIG. 3.15)
EXPLOSIVE WEIGHT:	108g
CRATER DIMENSIONS:	13mm DIA x 14mm DEEP

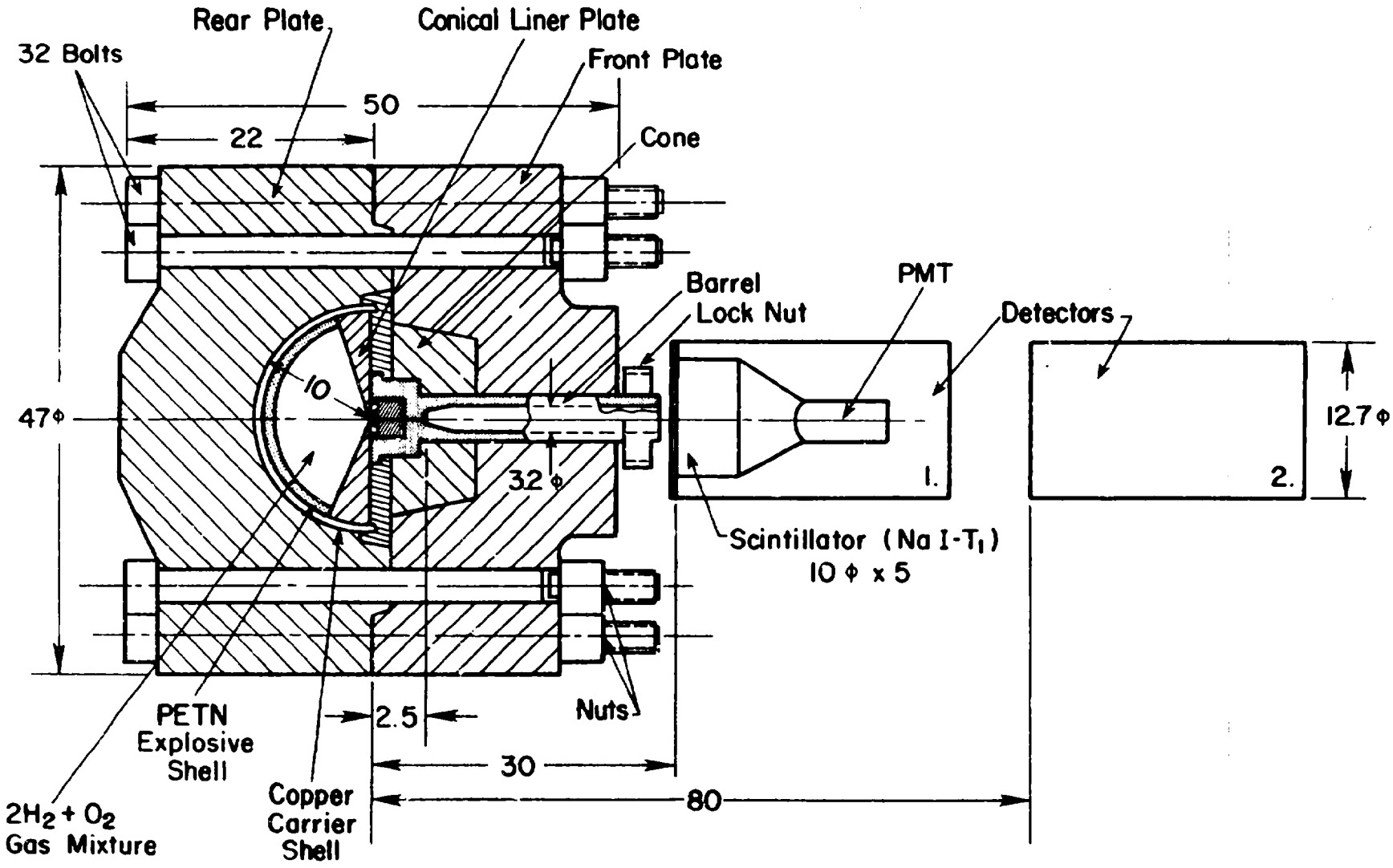

FIG. 3.26 UTIAS IMPLOSION CHAMBER FACILITY AND SCINTILLATOR DETECTORS.

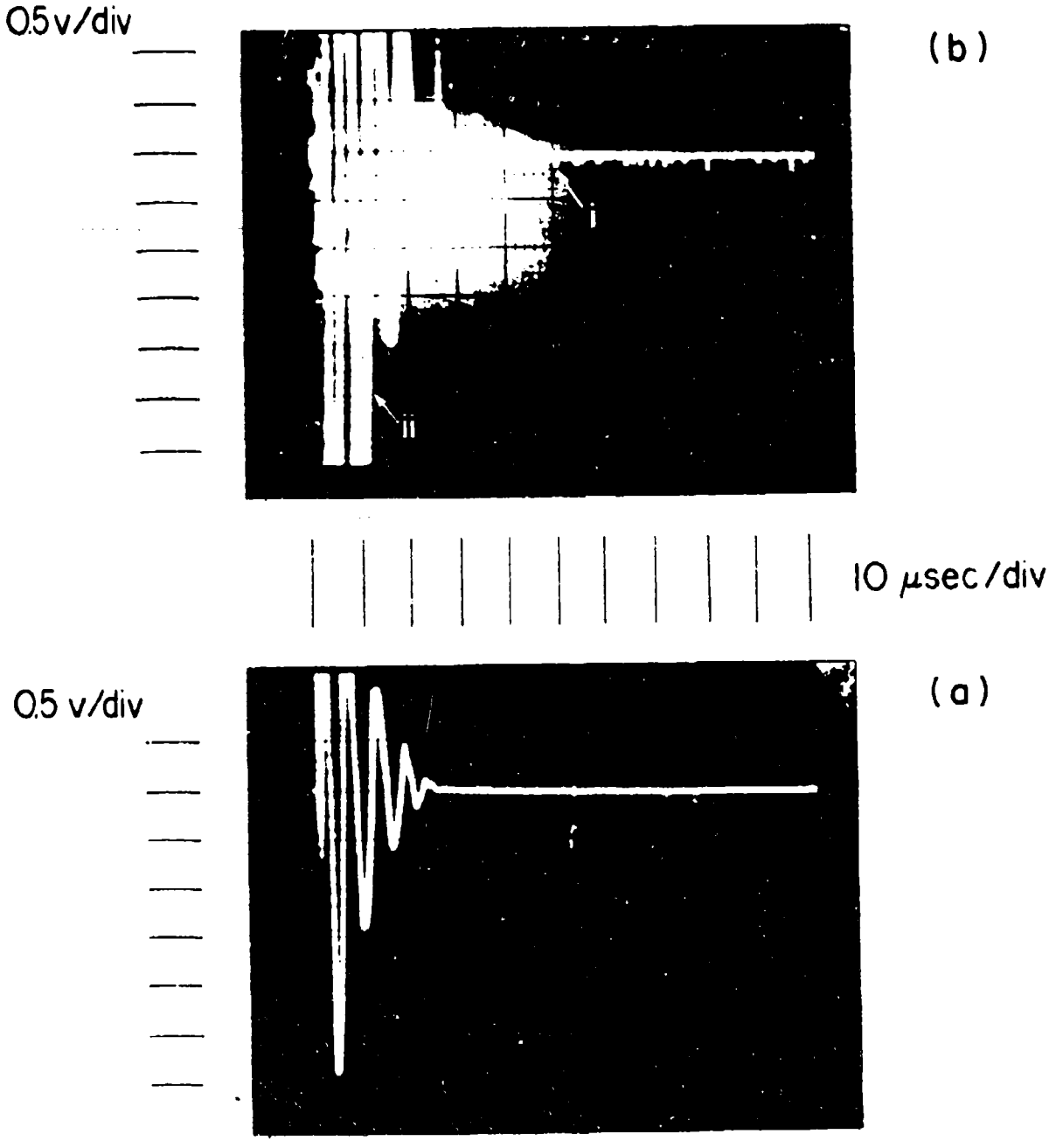

FIG. 3.27 OSCILLOSCOPE RECORD FROM DETECTOR I.

(a) Without fusion, $2H_2+O_2$ mixture at 400 psi + 127g PETN explosive.
(b) With fusion, $2D_2+O_2$ mixture at 800 psi + 97g PETN explosive.
(i) Arrival of implosion and beginning of events at 47 μsec.
(ii) Ignition noise.

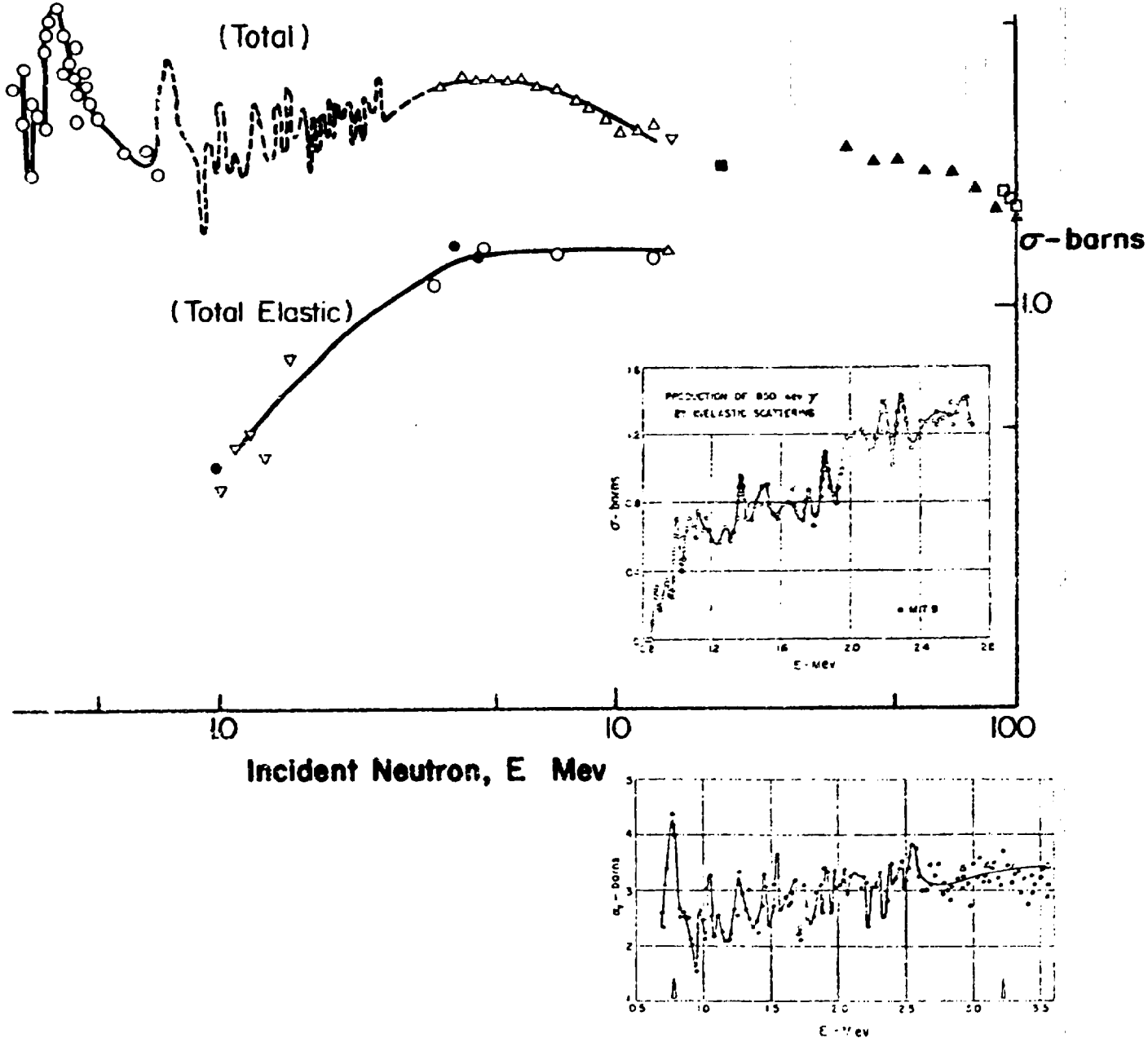

FIG. 3.28 CROSS-SECTIONS FOR NEUTRONS AND $_{26}$Fe INTERACTIONS (REF. 39).

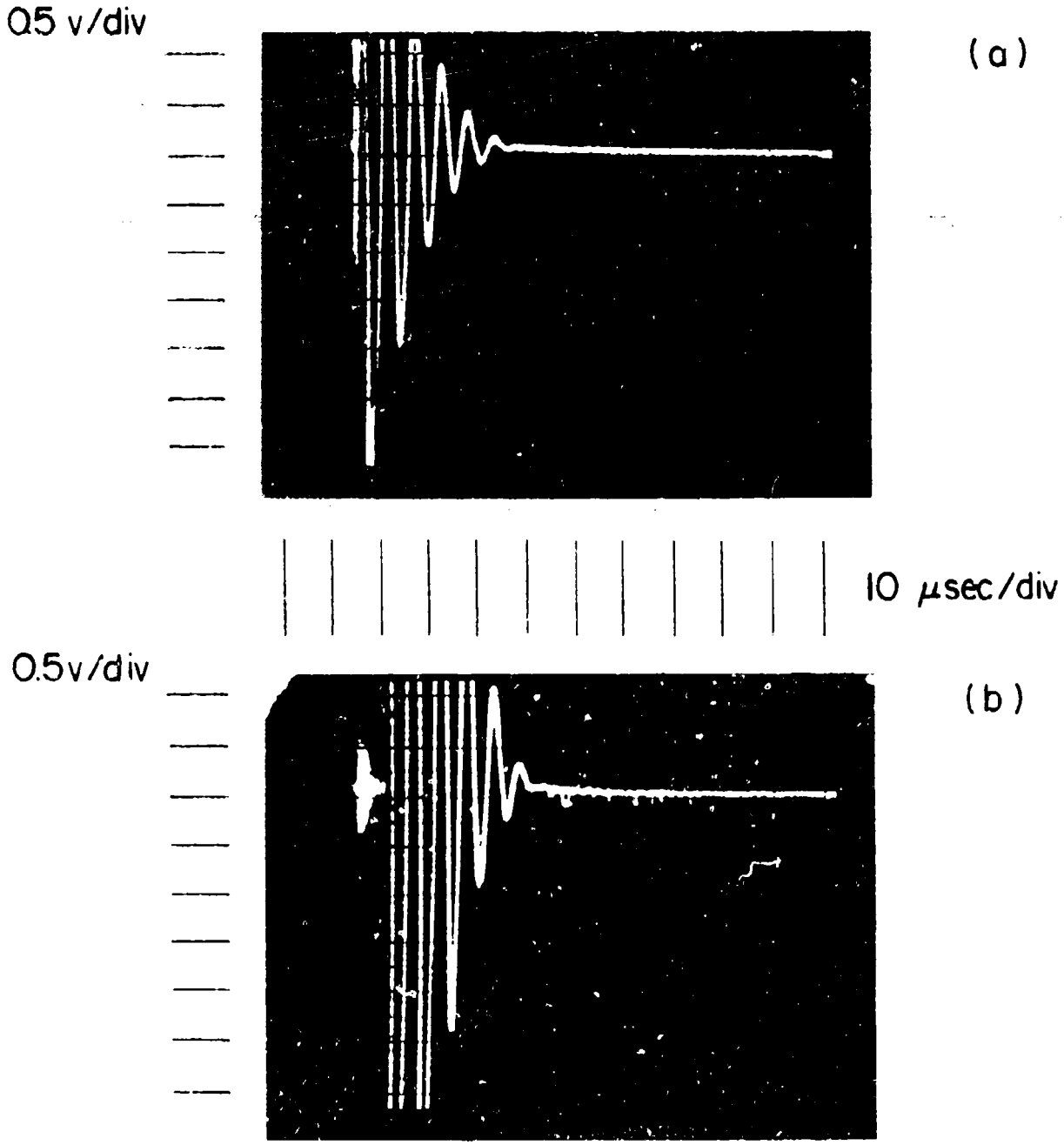

FIG. 3.29 DISPLAY OF DETECTOR I WITHOUT FUSION (a) AND WITH FUSION (b). EXPERIMENT E1 (VOITENKO COMPRESSOR), 113g PETN, $2H_2+O_2$ AT 400 PSI, D_2 IN CAPSULE AT 17.65 PSI. DISTRIBUTED NEGATIVE SIGNALS DUE TO NEUTRONS OR γ-RAYS START AT 43 μSEC.

APPENDIX A1

DIRECT AND INDIRECT APPROACHES TO FUSION

1.1 Direct Approach

The simplest means of obtaining fusion in the UTIAS Implosion Facility is to substitute deuterium for the hydrogen in the stoichiometric mixture ($2D_2 + O_2$). [Further improvements could be obtained by using a mixture of deuterium and tritium.] Using some of the data from Saito (Ref. 21) estimates of temperatures can be obtained of about 440,000 K (38 eV) at a 10μ radius and 2,000,000 K (170 eV) at 1μ for this mixture having a low value of $\gamma = 1.14$. The temperature after reflection is only about half the value behind the initial imploding shock wave. However, for gases at very high pressures (megabar) and high temperatures (100 eV), $\gamma \to 1.67$. In th is case the density ratio drops from about 10 for $\gamma = 1.14$ to 2.7 for $\gamma = 1.67$. Consequently, the temperatures are much greater. At a radius of 10μ, the pressure is 10-fold greater and the temperature is about 18×10^6K or 1580 eV. The reflected shock now supplies additional heating by a factor of 1.6 and yields a temperature of about 29×10^6K or 2528 eV. The actual ideal attained temperature will lie between the two limits provided by $\gamma = 1.14$ (where it starts) and 1.67 (where it ends).

Liquid densities can be reached as a result of shock and isentropic compression behind the implosion. Consequently, the simple gas law no longer applies and covolume and pressure effects must be considered. All in all temperatures in the range of a few hundred eV can be expected at a 10-μ radius and in the KeV range at smaller radii.

Some limitations to the calculations should be mentioned:

(a) The self-similar solutions computed by Saito (Ref. 21) are valid as long as the gasdynamic equations do not break down when the implosion wave radius becomes small $\sim 1\mu$. (At a particle number density of $n = 10^{22}/cm^3$ and $T = 10^6$K the mean-free-path $\lambda \sim 0.03\mu$; at $n = 10^{22}/cm^3$ and 10^7K, $\lambda \sim 2.3\mu$.)

(b) Any departure from spherical symmetry (caused by the boundary layer on the wall of the major diameter or by irregularities near the origin) could have a serious effect on accurate focussing.

(c) In the present hemispherical geometry, energy dissipation by viscous and radiative effects is enhanced.

(d) The compression process (compared to lasers) is relatively slow and the power density is low. Consequently, energy losses are high thereby limiting the final attainable temperatures.

(e) The use of oxygen introduces a large dissociation and ionization heat sink providing the means of radiating energy away from the fusion plasma.

1.2 Indirect Approach

A number of solid fuels could be placed at the focus of the implosion in order to initiate fusion Some of these materials are listed in Table A1.1. Small hemispherical targets might be used or flat targets for the implosion to focus on (Fig. A1.a). Some initial calculations were done for such schemes but none was tried experimentally.

Other possibilities exist in using small hemispherical shells filled with deuterium and tritium placed at the implosion focus, either with the hemispherical surface above the major diameter of the facility (Figs. A1.b, c) or below it (like a Voitenko compressor, Fig. A1.d). In Fig. A1.c the fuel itself forms the hemispherical shell. Another variant is a small cone filled with the fusion fuel with its base parallel with the major diameter (Fig. A1.e) or with a spherical sector (Fig. A1.f). A projectile capsule was also tried (Fig. A1.g). However, only the Voitenko compressor type (Fig. A1.3) yielded fusion neutrons, as noted in the main text.

Table A1.1. Characteristics of Fusion Target Materials

Target	Molecular Weight	Deuterium Density (cm^{-3})	$\bar{z}$	$\bar{z}^2/\bar{z}$	Deuteron Density / Total Particle Density	Solid Density (g/cm^3)	Melting Point
Solid deuterium (D_2)	4	4.2×10^{22}	1	1	0.5	0.14	18°K
Lithium deuteride (LiD)	8.95	6.2×10^{22}	2	2.5	0.166	0.92	680°C
Deuterium oxide (D_2O)	20	6.64×10^{22}	3.33	6.6	0.154	1.10	0°C
Lithium borodeuteride ($LiBD_2$)	25.8	7.3×10^{22}	2.0	3.17	0.22	0.79	275°C
Paraffin ($C_{36}D_{7h}$)	580	7.2×10^{22}	2.64	4.71	0.18	0.94	72°C
Polyethylene $(CO_2\text{-}CD_2)_n$	$2000 \div 10^5$	7.2×10^{22}	2.66	4.75	0.18	0.94÷0.96	120÷130°C

$\bar{z}$ - mean atomic number.

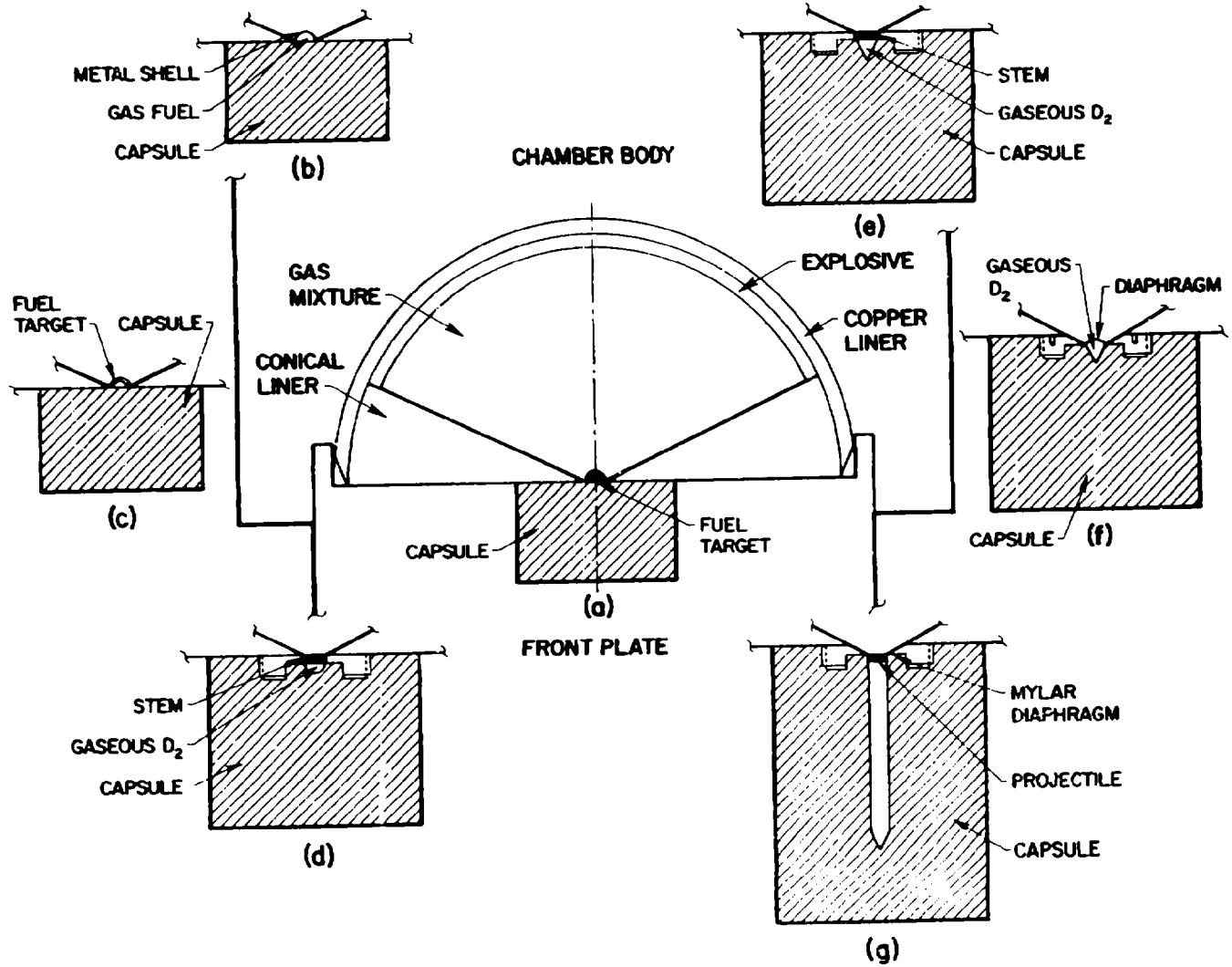

FIG. A.1.1 POSSIBLE INDIRECT CONFIGURATIONS FOR FUSION USING THE UTIAS IMPLOSION CHAMBER. THE BASIC CONFIGURATION IS SHOWN IN (a), AND (b) TO (f) INDICATED SECTION VIEWS OF THE CENTRAL AREA. CONFIGURATIONS (d), (e), (f) AND (g) HAD SOME INITIAL TRIALS AND ONLY (d) (VOITENKO-TYPE COMPRESSOR) WAS SUCCESSFUL.

APPENDIX A2

NEUTRON DETECTION SYSTEM

A2.1 Neutron Detectors

The detector, as designed by Dr. A. K. Kudian, is shown in Fig. A2.1. The main components are as follows:

(a) NaI(Tl) (thallium activated, sodium iodide) scintillator made by Nuclear Enterprises, Model NE102, 4 in diam, 2 in thick. Additional technical data are given in Table A2.1.

(b) Leading cone of highly polished aluminum to collimate the light leading to the PMT cathode.

(c) RCA photomultiplier (PMT) model 8575 with main specifications as follows:

Quantum efficiency typical 31% at 3850Å, 27% at 4250Å
Current amplification, 1.4×10^7 typical at 2000 V
Low dark noise
Rise time, 2.8 nsec; transit time 37 nsec.

The electronic circuit of the scintillator for the first detector is shown in Fig. A2.2. The circuit is designed to operate with a positive power supply which eliminates the use of a capacitor. This prevents serious problems of high-frequency filtering. The circuit is also characterized by a very high output voltage so that it can be distributed to several components. The electronic circuit of the scintillator of the second detector is shown in Fig. A2.3. It also operates with a positive high-voltage power supply. It is more flexible for adjustment, but gives a lower output.

A2.2 Ancillary Equipment

Light-Emitting Diode (LED)

Electrosonic Industrial Electronic Components Catalogue No. 771. Gallium arsenide phosphide (green light), Cat. No. GL4484, Producer: Litromix.

Peak spectral emission	5650Å
Typical forward volt	2.5V
Forward current	20mA
Luminance or output	1.0mcd
Max. power dissipation	80mW (at 25°C)
Max. rise time	1 nsec

For typical characteristics see Monsanto LED model MV5222.

Oscilloscopes

Hewlett-Packard model 1744A single beam storage scope.

Counter

Hewlett-Packard model 5325A universal counter. Accuracy up to 0.1 μsec.

Cameras

Hewlett-Packard model 197A camera.

Discriminator

The circuit is shown in Fig. A2.4.

Table A2.1. Technical Data for NE 102

General description	Scintillation chemicals in polyvinyl-toluene
Light output	65% that of an anthracene crystal of the same geometry*
Light output vs temperature	Light output independent of temperature between -60°C and +20°C; light output at +60°C is 95% that at +20°C (Ref. 31)
Decay constant	2.2×10^{-9} seconds
Maximum emission	4250 AU
Specific gravity	1.032
Softening temperature	75°C
Refractive index	1.581
Effects of liquids	Soluble in aromatic solvents, acetone, etc. Unaffected by water, dilute acids, dilute alkalis or lower alcohols
No. of atoms per cm barn	H: 0.0525, C: 0.0475, N: 1.8×10^{-4}, O: 1.8×10^{-4}
No. of electrons per cc	3.4×10^{23}
α to β ratio	0.072†

*Conditions of measurement: Source Cs 137 gamma. Basis of comparison: midpoint of falling Compton edge on differential curve, or 1% of maximum counting rate on integral curve. Standard: anthracene crystal of same weight and geometry mounted in M_2O reflector.
†Determined by J. B. Czirr.

APPENDIX A3

SOME SCALING CONSIDERATIONS

The question always arises whether we could improve matters by going to a tenfold scale or a 100-cm diam hemispherical cavity. It can be shown that the required driver energy (derived from the Lawson criterion) is given by (for a D-T reaction at 10 KeV, but will be used here for convenience)

$$E_s = 1.6\mu^3 \frac{1}{\varepsilon_\ell^4} \left(\frac{n_s}{n_d} \right)^2 \qquad (A3.1)$$

where E_s is the energy generated by the (driver) source, μ is the energy multiplier for the entire process (or $\mu = E_f/E_s$, where E_f is the fusion energy), ε_ℓ is the coupling efficiency between the plasma and driver energies (or $\varepsilon_\ell = E_p/E_s$), n_s/n_d is the ratio of particles in solid deuterium to that of the final deuterium-particle density. The break-even point (no net energy production) is given by $\mu = 1$. For the present driver of D_2O + PETN explosive, E_s = 1220 k_j, $n_s = 4.5 \times 10^{22}/cm^3$, $n_d = 5.2 \times 10^{22}/cm^3$, $T = 10^7 K$ (in view of the low neutron flux). Assume a fusion reaction diameter of 10 μm, then the particle velocity is ∿ 100 km/sec [see Saito, (21)] and E_s = 0.1j, consequently $\varepsilon_\ell = 0.1j/1220\ k_j \sim 10^{-7}$ (a very low coupling efficiency). The difficulty arises from the fact that high shock velocities or temperatures are attained only close to the focus of the implosion in a very small volume. Therefore, by scaling up the facility by a factor of 10, the driver energy is increased 1000-fold, but the velocity will only go up by $10^{0.35}$ or 2.24-fold [Saito (21)]. The density will remain near the asymptotic condition and the temperature at 10 μm will increase as the pressure or as $10^{0.65}$ or only by a factor of 4.45. Consequently, the coupling efficiency, which occurs to the inverse fourth power in the above equation can be improved paradoxically enough by scaling down rather than by scaling up.

Of course the two successful runs using $2D_2 + O_2$ + PETN directly and the Voitenko-type compressor with pure deuterium indirectly [Glass and Sagie (52)] out of twenty tries using configurations shown in Fig. A1.1 are only a beginning in order to investigate the details of the neutron production and the efficiency of the process. However, the foregoing considerations do point to the conclusions that scaling up the facility is not worthwhile and that perhaps some new ideas for an indirect method may be worth pursuing.

UTIAS Technical Note No. 233

Institute for Aerospace Studies, University of Toronto (UTIAS)
4925 Dufferin Street, Downsview, Ontario, Canada, M3H 5T6

EXPLOSIVE-DRIVEN HEMISPHERICAL IMPLOSIONS FOR GENERATING FUSION PLASMAS

Sagie, D. and Glass, I. I.

1. D-D fusion 2. Implosion dynamics 3. Explosion dynamics 4. Neutrons and γ-rays
5. Fusion plasmas

I. Sagie, D., Glass, I. I. II. UTIAS Technical Note No. 233

The UTIAS explosive-driven-implosion facility was used to produce stable, centered and focussed hemispherical implosions to generate neutrons from D-D reactions. A high resolution scintillator-detection system measured the neutrons and γ-rays resulting from the fusion of deuterium. Several approaches were used to initiate fusion in deuterium. The simplest and most direct proved to be in a predetonated stoichiometric mixture of deuterium-oxygen. The other successful method was a miniature Voitenko-type compressor where a plane diaphragm was driven by the implosion wave into a secondary small spherical cavity that contained pure deuterium gas at one atmosphere. A great deal of work still remains in order to measure accurately the neutron flux and its velocity distribution as well as the precise interactions of the neutrons with the steel chamber which produced the γ-rays. Nevertheless, this is the only known work where fusion neutrons were produced by chemical energy only in a direct and indirect manner.

Available copies of this report are limited. Return this card to UTIAS, if you require a copy.

UTIAS Technical Note No. 233

Institute for Aerospace Studies, University of Toronto (UTIAS)
4925 Dufferin Street, Downsview, Ontario, Canada, M3H 5T6

EXPLOSIVE-DRIVEN HEMISPHERICAL IMPLOSIONS FOR GENERATING FUSION PLASMAS

Sagie, D. and Glass, I. I.

1. D-D fusion 2. Implosion dynamics 3. Explosion dynamics 4. Neutrons and γ-rays
5. Fusion plasmas

I. Sagie, D., Glass, I. I. II. UTIAS Technical Note No. 233

The UTIAS explosive-driven-implosion facility was used to produce stable, centered and focussed hemispherical implosions to generate neutrons from D-D reactions. A high resolution scintillator-detection system measured the neutrons and γ-rays resulting from the fusion of deuterium. Several approaches were used to initiate fusion in deuterium. The simplest and most direct proved to be in a predetonated stoichiometric mixture of deuterium-oxygen. The other successful method was a miniature Voitenko-type compressor where a plane diaphragm was driven by the implosion wave into a secondary small spherical cavity that contained pure deuterium gas at one atmosphere. A great deal of work still remains in order to measure accurately the neutron flux and its velocity distribution as well as the precise interactions of the neutrons with the steel chamber which produced the γ-rays. Nevertheless, this is the only known work where fusion neutrons were produced by chemical energy only in a direct and indirect manner.

Available copies of this report are limited. Return this card to UTIAS, if you require a copy.

UTIAS Technical Note No. 233

Institute for Aerospace Studies, University of Toronto (UTIAS)
4925 Dufferin Street, Downsview, Ontario, Canada, M3H 5T6

EXPLOSIVE-DRIVEN HEMISPHERICAL IMPLOSIONS FOR GENERATING FUSION PLASMAS

Sagie, D. and Glass, I. I.

1. D-D fusion 2. Implosion dynamics 3. Explosion dynamics 4. Neutrons and γ-rays
5. Fusion plasmas

I. Sagie, D., Glass, I. I. II. UTIAS Technical Note No. 233

The UTIAS explosive-driven-implosion facility was used to produce stable, centered and focussed hemispherical implosions to generate neutrons from D-D reactions. A high resolution scintillator-detection system measured the neutrons and γ-rays resulting from the fusion of deuterium. Several approaches were used to initiate fusion in deuterium. The simplest and most direct proved to be in a predetonated stoichiometric mixture of deuterium-oxygen. The other successful method was a miniature Voitenko-type compressor where a plane diaphragm was driven by the implosion wave into a secondary small spherical cavity that contained pure deuterium gas at one atmosphere. A great deal of work still remains in order to measure accurately the neutron flux and its velocity distribution as well as the precise interactions of the neutrons with the steel chamber which produced the γ-rays. Nevertheless, this is the only known work where fusion neutrons were produced by chemical energy only in a direct and indirect manner.

Available copies of this report are limited. Return this card to UTIAS, if you require a copy.

UTIAS Technical Note No. 233

Institute for Aerospace Studies, University of Toronto (UTIAS)
4925 Dufferin Street, Downsview, Ontario, Canada, M3H 5T6

EXPLOSIVE-DRIVEN HEMISPHERICAL IMPLOSIONS FOR GENERATING FUSION PLASMAS

Sagie, D. and Glass, I. I.

1. D-D fusion 2. Implosion dynamics 3. Explosion dynamics 4. Neutrons and γ-rays
5. Fusion plasmas

I. Sagie, D., Glass, I. I. II. UTIAS Technical Note No. 233

The UTIAS explosive-driven-implosion facility was used to produce stable, centered and focussed hemispherical implosions to generate neutrons from D-D reactions. A high resolution scintillator-detection system measured the neutrons and γ-rays resulting from the fusion of deuterium. Several approaches were used to initiate fusion in deuterium. The simplest and most direct proved to be in a predetonated stoichiometric mixture of deuterium-oxygen. The other successful method was a miniature Voitenko-type compressor where a plane diaphragm was driven by the implosion wave into a secondary small spherical cavity that contained pure deuterium gas at one atmosphere. A great deal of work still remains in order to measure accurately the neutron flux and its velocity distribution as well as the precise interactions of the neutrons with the steel chamber which produced the γ-rays. Nevertheless, this is the only known work where fusion neutrons were produced by chemical energy only in a direct and indirect manner.

Available copies of this report are limited. Return this card to UTIAS, if you require a copy.